





Universitat Autònoma de Barcelona

**ADVERTIMENT.** L'accés als continguts d'aquesta tesi queda condicionat a l'acceptació de les condicions d'ús establertes per la següent llicència Creative Commons:  [http://cat.creativecommons.org/?page\\_id=184](http://cat.creativecommons.org/?page_id=184)

**ADVERTENCIA.** El acceso a los contenidos de esta tesis queda condicionado a la aceptación de las condiciones de uso establecidas por la siguiente licencia Creative Commons:  <http://es.creativecommons.org/blog/licencias/>

**WARNING.** The access to the contents of this doctoral thesis it is limited to the acceptance of the use conditions set by the following Creative Commons license:  <https://creativecommons.org/licenses/?lang=en>

Doctoral thesis

# Inhibiting Myc in cancer using Omomyc

---

From defining the fundamental  
mechanism of action to its  
pharmacological application

Toni Jauset González  
Barcelona, 2018



# **Inhibiting Myc in cancer using Omomyc: From defining the fundamental mechanism of action to its pharmacological application**

Doctoral thesis

**Toni Jauset González**

Director: Dr. Laura Soucek

Mouse Models of Cancer Therapy laboratory  
Vall d'Hebron Institute of Oncology (VHIO)

Tutor: Dr. José Miguel Lizcano de Vega

PhD program in Biochemistry, Molecular Biology and Biomedicine  
Department of Biochemistry and Molecular Biology  
Universitat Autònoma de Barcelona (UAB)  
Barcelona, 2018





The director **Dr. Laura Soucek** and the tutor **Dr. José Miguel Lizcano de Vega**,

Certify:

That the experimental work and the writing of the memory of this doctoral thesis entitled "Inhibiting Myc in cancer using Omomyc: from defining the fundamental mechanism of action to its pharmacological application" have been performed by Toni Jauset González under their supervision and consider that it is suitable to be presented for the degree of PhD in Biochemistry, Molecular Biology and Biomedicine at Universitat Autònoma de Barcelona.

Barcelona 16<sup>th</sup> of April of 2018.

Director:

Dr. Laura Soucek

Tutor:

Dr. José Miguel Lizcano de Vega

PhD student:

Toni Jauset Gonzalez



# Acknowledgments

---

No puc imaginar millor manera de començar que agraint a totes aquelles persones que han fet d'aquests anys una experiència inoblidable. Disculpeu-me si em quedo curt, però difícilment podré expressar en poques línies la meva immensa gratitud a cada un de vosaltres.

First of all to you, Laura, for accepting me as part of this big family that you have created, always guiding me toward the right direction and offering me a priceless opportunity for a personal and professional growth. You have been, as much as a boss, a friend.

Marie-Eve, you have been the greatest unexpected surprise of all these years. I did not think that someone like you could appear and act as an endless source of inspiration, knowledge and ideas. You have helped me a lot and I hope I can continue learning from you for a long time.

Dani, vam començar això junts, i ho hem acabat junts. He tingut la sort de poder compartir l'experiència del doctorat amb algú proper que no solament m'ha donat el suport científic, si no també l'emocional, sempre que ho he necessitat. Has estat un amic i company de viatge genial.

Silvia, Sandra; des de que vaig tornar de Boston heu estat les millors companyes de passadís que podria imaginar. Hem fet molt feina, però sempre hem trobat el moment per riure, gaudir i compartir idees entre experiment i experiment. M'heu ajudat i donat molt quan més ho he necessitat.

Jony, besides Laura, you have been the person that saw me arriving to the lab as a young unexperienced scientist, took my hand and helped me growing. You have corrected virtually all my scientific writings and I hope you are proud of my progress (if there has been any... xD). Thank you for having always good words for me.

Mariano, todavía recuerdo lo feliz que me sentí cuando me dijeron que serías parte de nuestro laboratorio. Ya des de antes he admirado tu paciencia, comprensión y potencial. También espero poder seguir aprendiendo de ti. Y gracias por organizar esos asados inolvidables!



A la resta del laboratori: Virginia, Laia, Erika, Génesis, Meri; de totes vosaltres també he après i m'emporto bons records. Gràcies per crear moments que m'acompanyaran sempre.

Albert, Oriol, Faiz; heu fet el viatge molt més divertit. Tenir amics com vosaltres als que inevitablement havia de veure pràcticament cada dia només podia resultar en coses bones.

A la resta d'amics i companys del VHIO, als que em vaig trobar al arribar i encara hi són, als que he vist marxar i als que han arribat nous: Ada, Irene, Lorena, AnnC, Gerard, Àgueda, Cristina, Isabel, Anna, Elena, Nello, Esther(s), Isma, Gemma, Estefania...; hem disculpo per no escriure tots els vostres noms, però gràcies per contribuir d'una manera o altra en fer de la tesi una experiència tan positiva.

Mireia, ho vam intentar. Llàstima que no sortís res millor d'aquells experiments. Però haver pogut retrobar-me amb tu per crear un potencial fàrmac junts ha estat genial. Ho tornaria a fer, fins i tot sabent que no ho podríem tirar endavant.

Dr. Torchilin, you accepted me in your lab and the experience I lived in Boston thanks to that has been huge. I am extremely grateful for that. Thank you also for you time and guidance.

To the rest of people I met in Boston: Livia, Can, Jiayi, Edcar, Rachit, Prabarna, Jin, among the many others. You took a piece of me that will always stay there. If the experience was great it was not just because of the science, but most importantly because of you.

To the rest of collaborators and people that contributed to this thesis and made it possible: Jun, Francesco, Enriqueta, Peter, Arianna. You have my gratitude.

Als amics, que sempre estan allí quan et fan falta, sigui quan sigui, pel motiu que sigui, especialment a vosaltres, Alex, Miquel; fa casi 25 anys que formeu part de la meva vida. Què més us puc dir. Fran, has sido compañero de piso y amigo durante estos años de tesi. Tú has sido quien se ha encontrado de cara la persona que volvía cabreada del lab, y has sabido lidiado muy bien con ella. Gracias!

Ernest, de tu també he après. La teva energia positiva contagiosa m'ha fet tirar endavant en molts moments durs.

Mare, pare; sempre heu estat allà per ajudar en el que sigui sense condicions, no solament aquests anys de tesi sinó sempre. L'única manera de tornar-vos tant és fent que us sentiu orgullosos del que sóc, i desitjos estar-ho fent bé.

Cristina, no podria tenir millor germana. Gràcies per mostrar sempre interès per com van les coses al laboratori i per haver escollit seguir el camí de la tesi. Ho creguis o no, també ets una font d'inspiració.

laia, padrí (encara que ja no hi siguis), tot el que m'heu ensenyat des de petit m'ha acompanyat durant aquests anys. També sóc qui sóc gràcies a vosaltres.

Semblarà una conya, però gràcies a tu, Swing. Et vaig descobrir i la teva música, el teu ritme i el teu ball em van donar energia en moment de debilitat. I gràcies a les múltiples hores de tren Lleida-Barcelona; Barcelona-Lleida, sense vosaltres potser mai hagués trobat el moment per seure i escriure la tesi.

I finalment, gràcies a tu, Iris. Possiblement tu has estat l'única que sap tot el que ha suposat la tesi per a mi. Amb tu ho he pogut parlar tot i sempre m'has escoltat. Hi ha hagut moments bons i dolent, i has demostrat ser capaç de gaudir el bons amb mi i ser comprensiva i pacient en els dolents. Estar al costat d'algú que fa la tesi pot ser fins i tot més dur que fer-la, i per tot el que m'has donat aquests anys tindràs sempre la meva gratitud. Solament em queda disculpar-me per aquells moments en els quals la tesi hagi resultat massa pesada.

A tots vosaltres, MIL GRÀCIES!

# Table of Contents

---

|   |    |
|---|----|
| Abbreviations .....   | 1  |
| Summary .....   | 5  |
| 1. Introduction.....  | 9  |
| 1.1. The problem of cancer .....                                | 9  |
| 1.2. Heterogeneity in cancer .....                              | 9  |
| 1.3. Precision medicine in cancer therapies.....                | 11 |
| 1.4. Primary or acquired resistance to targeted therapies ..... | 13 |
| 1.5. The ideal cancer target.....                               | 14 |
| 1.6. The Myc oncogene .....                                     | 16 |
| 1.7. Modelling Myc inhibition using Omomyc .....                | 20 |
| 1.8. Pharmacological Myc inhibition .....                       | 22 |
| 1.8.1. Direct Myc inhibitors.....                               | 22 |
| 1.8.2. Indirect Myc inhibitors .....                            | 23 |
| 1.8.3. Polypeptide Myc inhibitors .....                         | 25 |
| 1.9. Omomyc mechanism of action .....                           | 27 |
| 1.10. Omomyc-derived peptide-based drugs.....                   | 31 |
| 1.10.1. Cell-penetrating peptides.....                          | 32 |
| 1.10.2. Liposomal nanoparticles .....                           | 33 |
| 2. Research Objectives .....                                    | 37 |
| 3. Materials and Methods.....                                   | 39 |
| 3.1. Cloning strategy of expression vectors .....               | 39 |
| 3.2. PCR conditions.....  | 40 |
| 3.3. Restriction enzyme digestion .....                         | 41 |
| 3.4. CIP phosphatase and ligation .....                         | 41 |
| 3.5. Bacterial transformation .....                             | 41 |
| 3.6. Plasmid purification.....                                  | 42 |
| 3.7. Cell lines .....   | 43 |

|  |    |
|--|----|
| 3.8. Lentiviral production and transduction of target cells.....   | 43 |
| 3.9. Induction of Omomyc expression .....  | 44 |
| 3.10. Quantification of cell number, RFP intensity and cell size .....   | 44 |
| 3.11. BrdU and cell cycle .....  | 45 |
| 3.12. Cycloheximide treatment.....   | 45 |
| 3.13. Immunofluorescence of cells and tissues .....  | 46 |
| 3.14. Cell synchronization with nocodazole.....  | 47 |
| 3.15. Western Blot .....   | 48 |
| 3.16. Co-immunoprecipitation .....   | 49 |
| 3.17. Production, purification and labelling of Omomyc <sup>CPP</sup> .....  | 50 |
| 3.18. Liposomal production and treatment .....   | 50 |
| 3.19. Endocytosis and entrance inhibition.....   | 51 |
| 3.20. Treatment with modified-mRNA.....  | 52 |
| 3.21. CHIP-qPCR and ChIP-sequencing .....  | 53 |
| 3.22. Animal studies .....   | 53 |
| 3.23. In vivo biodistribution .....  | 55 |
| 4. Results .....   | 57 |
| Section 1: Investigating Omomyc’s fundamental mechanism of action in lung cancer .....                               | 57 |
| 4.1.1. Design and characterization of an Omomyc-RFP inducible vector .....   | 58 |
| 4.1.2. Anti-tumorigenic efficacy of Omomyc-RFP expression in A549... 59  |    |
| 4.1.3. Myc inhibition in A549 upon Omomyc-RFP expression .....   | 60 |
| 4.1.4. Evaluation of Omomyc-RFP’s efficacy in different lung cancer cell lines .....                                 | 61 |
| 4.1.5. Omomyc-RFP’s dependent macroscopic change .....   | 65 |
| 4.1.6. Characterization of the effect of Omomyc expression on Myc and Max levels and their subcellular location..... | 67 |
| 4.1.7. Characterization of genome-wide changes in Myc and Max DNA-binding upon Omomyc expression.....                | 70 |

|  |     |
|--|-----|
| 4.1.8. Evaluation of the efficacy of OmoHER and $\Delta$ Myc compared to Omomyc .....                        | 73  |
| Section 2: Transforming Omomyc from proof of principle to therapeutic strategy.....                          | 79  |
| 4.2.1. Setting up of suitable experimental models for the preclinical evaluation of Omomyc-based drugs ..... | 80  |
| 4.2.2. Validation of Omomyc as cell-penetrating peptide that inhibits Myc.....                               | 84  |
| 4.2.3. Biodistribution of Omomyc <sup>CPP</sup> in vivo.....   | 87  |
| 4.2.4. In vivo efficacy of Omomyc <sup>CPP</sup> .....   | 88  |
| 4.2.5. Dose increase of Omomyc <sup>CPP</sup> and combination with paclitaxel... ..                          | 90  |
| 4.2.6. Formulation and in vitro validation of the first Omomyc-based liposomal nanoparticles .....           | 92  |
| 4.2.7. Optimization of Omomyc <sup>CPP</sup> -liposomes .....  | 97  |
| 4.2.8. Proof-of-principle validation of Omomyc-derived mRNA delivery .....                                   | 102 |
| 5. Discussion.....   | 105 |
| Section 1: Investigating Omomyc’s fundamental mechanism of action in lung cancer .....                       | 105 |
| Section 2: Transforming Omomyc from proof of principle to therapeutic strategy.....                          | 110 |
| 6. Conclusions.....  | 115 |
| 7. References.....   | 117 |

# Abbreviations

---

**ADB:** Agarose Dissolving Buffer  
**adeno-CRE:** CRE recombinase adenoviruses  
**ALK:** Anaplastic Lymphoma Kinase  
**AM:** Agarose Magnetic  
**ARRIVE:** Animals in Research: Reporting In Vivo Experiments  
**Balb/c:** BALB/cAnNRj-Foxn1nu  
**BET:** Bromodomain and Extraterminal Bromodomain  
**b-HLH-LZ:** Basic Helix-loop-helix Leucine Zipper  
**Bis-Tris:** Bis(2-hydroxyethyl) aminotris (hydroxymethyl) methane  
**BRD4:** Bromodomain-containing Protein 4  
**BRG1:** ATP-dependent Chromatin Remodeler SMARCA4  
**BSA:** Bovine Serum Albumin  
**CDK7:** Cell Division Protein Kinase 7  
**CDKN2B:** Cyclin-dependent Kinase 4 inhibitor B  
**CEEA:** Ethical Committee for the Use of Experimental Animals  
**CHEMS:** Cholesteryl Hemisuccinate  
**ChIP:** Chromatin Immunoprecipitation  
**Chol:** Cholesterol  
**CHX:** Cycloheximide  
**CIEMAT:** Centro de Investigaciones Energéticas, Medioambientales y Tecnológicas  
**CMV:** Human Cytomegalovirus  
**CPP:** Cell-penetrating Peptide  
**CT:** Computed Tomography  
**DAPI:** 4',6-diamino-2-phenylindole  
**DE:** Depleted Fraction  
**DFO:** Deferoxamine  
**DMEM:** Dulbecco's Modified Eagle Medium  
**DNA:** Deoxyribonucleic acid  
**DOPE:** 1,2-dioleoyl-sn-glycero-3-phosphoethanolamine  
**DOPS:** 1,2-dioleoyl-sn-glycero-3-phospho-L-serine  
**DOTAP:** 1,2-dioleoyl-3-trimethylammonium-propane  
**Dox:** Doxycycline  
**DPPC:** 1,2-dipalmitoyl-sn-glycero-3-phosphocholine  
**DSPE:** 1,2-Distearoyl-sn-glycero-3-phosphoethanolamine

**E.coli:** Escherichia coli  
**E-box:** Enhancer box consensus DNA sequence  
**EDTA:** Ethylenediaminetetra acetic acid  
**EE:** Encapsulation Efficacy  
**EGF:** Epidermal Growth Factor  
**EGFR:** Epidermal Growth Factor Receptor  
**EGTA:** Ethylene Glycol-bis( $\beta$ -aminoethyl ether)-N,N,N',N'-tetraacetic acid  
**ER:** Estrogen Receptor  
**FBS:** Fetal Bovine Serum  
**FDA:** Food and Drug Administration  
**FITC:** Fluorescein Isothiocyanate  
**HDAC:** Histone Deacetylases  
**HEK293T:** Human Embryonic Kidney cells 293  
**HEPES:** 4-(2-hydroxyethyl)-1-piperazineethanesulfonic acid  
**HER2:** Human Epidermal Growth Factor Receptor 2  
**HIF-1 $\alpha$ :** Hypoxia-inducible Factor 1, alpha subunit  
**HPLC:** High-performance Liquid Chromatography  
**HRP:** Horseradish Peroxidase  
**i.v.:** Intravenous  
**ID:** Injected Dose  
**IFN- $\gamma$ :** Interferon gamma  
**IL-2:** Interleukin 2  
**IN:** Input fraction  
**IP:** Immunoprecipitation  
**ITLC:** Instant Thin Layer Chromatography  
**IVIS:** In Vivo Imaging System  
**LB:** Lysogeny broth  
**LBA:** Lysogeny Broth containing Ampicillin  
**LKB1:** Liver Kinase B1  
**LSL:** Lox-Stop-Lox cassette  
**MAPK:** Mitogen-activated Protein Kinase  
**MB:** Myc Box  
**MG:** Malignant Glioma  
**miRNA/miR:** microRNA  
**MQ:** Milli-Q  
**mRNA:** Messenger RNA  
**mTOR:** Mammalian Target of Rapamycin  
**NCL:** Nuclear Localization Signal

**NEB:** New England Biolabs  
**NEU:** Northeastern University  
**NOCO:** Nocodazole  
**NPM1:** Nucleophosmin 1  
**NSCLC:** Non-small cell lung cancer  
**Omo:** Omomyc  
**PAGE:** Polyacrylamide Gel Electrophoresis  
**PBS:** Phosphate Buffered Saline  
**PBS-T:** PBS+0.1%Tween20  
**PCR:** Polymerase Chain Reaction  
**PEG:** Polyethylene Glycol  
**PES:** Polyethersulfone  
**PET:** Positron Emission Tomography  
**PI:** Propidium Iodide  
**PI3K:** Phosphoinositide 3-kinase:  
**PVDF:** Polyvinylidene Fluoride  
**qPCR:** Quantitative Real-time Polymerase Chain Reaction  
**RFP:** Red Fluorescent Protein  
**RIP1:** Rat Insulin 1 gene Promoter  
**RIPA:** Radioimmunoprecipitation assay  
**RNA pol II:** RNA polymerase II  
**RNA:** Ribonucleic acid  
**RNAi:** RNA interference  
**ROI:** Region of Interest  
**Rpm:** Revolutions per minute  
**RPMI:** Roswell Park Memorial Institute  
**rtTA:** Reverse Tetracycline-controlled Transactivator  
**S.O.B:** Super Optimal Broth  
**S.O.C.:** S.O.B + 20mM glucose  
**SCLC:** Small Cell Lung Cancer  
**SD:** Standard Deviation  
**SDS:** Sodium Dodecyl Sulfate  
**Seq:** Sequencing  
**siRNA:** Small-interference RNA  
**SKP2:** S-phase Kinase-associated Protein 2  
**SP HP:** Sepharose High Performance  
**Suc:** Sucrose  
**TAD:** Transcriptional Activation Domain



## Abbreviations

**TAT:** Transactivator of Transcription

**TFIIH:** Transcription factor II Human

**TKI:** Tyrosine Kinase Inhibitor

**TRE:** Tetracycline Response Element

**TRRAP:** Transformation/transcription Domain-associated Protein

**TSS:** Transcription Starting Site

**USA:** United State of America

**USP:** Ubiquitin-specific Proteases

**UV:** Ultraviolet

**VHIO:** Vall d'Hebron Institute of Oncology

**ZP:** Z-potential

# Summary

---

Identifying and targeting cancer cell components that play non-degenerate and non-redundant functions within cancers could lead to the development of more effective therapies. Myc is considered a prime example of such a target, and has been characterized as a downstream effector of multiple oncogenic pathways. Indeed, several studies have shown that inhibiting Myc displays notable therapeutic potential against different types of cancer. However, targeting Myc pharmacologically – directly or indirectly – is still considered challenging.

Use of the Myc dominant negative mutant termed Omomyc provided the first evidence of the efficacy and safety of targeting Myc and displayed one of the most outstanding anti-tumorigenic potentials to date.

This thesis project is divided into two major tasks: firstly, we aimed to better determine the source of Omomyc's therapeutic effect, which could provide clues on how to develop better Myc inhibitors; Secondly, despite the claims that Omomyc itself could not be used as a drug, we assessed different ways in which it could be effectively delivered to cancer cells to validate the first Omomyc-based drugs.

In the context of our first task, by expressing Omomyc in a panel of lung cancer cells lines, we showed for the first time a gain-of-function of Omomyc, which intriguingly re-locates endogenous Max on Myc-unrelated DNA regions, thus potentially acting not only as a Myc inhibitor but also producing additional effects within cancer cells. Moreover, its dimerization with endogenous Max and the occupancy of DNA were identified as key effectors of Omomyc's anti-tumorigenic efficacy.

In the context of generating the first Omomyc-based pharmacological approaches, Omomyc was first produced as a polypeptide. Remarkably, we determined that its systemic administration is safe and effective against subcutaneously implanted lung cancer cells, both as monotherapy and in combination with standard chemotherapy. Second, we generated Omomyc-encapsulating liposomes, which are able to improve the cellular uptake of the polypeptide and its nuclear localization. Finally, we provided the first evidence that Omomyc could be delivered as mRNA into cells that will translate it into a functional nuclear peptide product.

Together, our results provide insights into Omomyc's mechanism of action that might be used to develop new therapeutic approaches, including more effective Omomyc-derived drugs. Furthermore, we show that these could be delivered to cancer cells as cell-penetrating peptides (CPPs), liposomes and/or mRNA, providing an arsenal of tools to effectively and safely inhibit the Myc oncogene in the clinic.

“Twenty years from now you will be more disappointed by the things that you didn't do than by the ones you did do. So throw off the bowlines. Sail away from the safe harbor. Catch the trade winds in your sails. Explore. Dream. Discover.”

- *MARK TWAIN*



# 1. Introduction

---

## 1.1. The problem of cancer

In medicine, cancer refers to a group of related diseases, which are characterized by an abnormal and uncontrollable proliferation of the body's cells and their spread to other tissues. These diseases are the second leading cause of mortality worldwide, accounting for approximately 14.1 million new cases, 32.6 million people living with cancer (within 5 years of diagnosis) and 8.2 million deaths in 2012 [1, 2]. According to the American Cancer Society, the average lifetime risk of developing or dying from cancer in the US population is 1 in 3 and 1 in 5 respectively [3]. The economic burden of cancer is also significant and increasing. In 2010, the annual costs of cancer worldwide were estimated around US\$ 1.16 trillion [4]. Thus, cancer remains a major health, social and economic problem.

## 1.2. Heterogeneity in cancer

Cancer arises from changes in genes that regulate the functions of cells, especially how they divide and how they die. These changes are usually acquired during a person's lifetime, when errors during cell division occur or due to DNA damage produced by specific environmental exposures. A total of 294,881 mutations in 20,000 protein-coding genes from 3,284 tumors have been reported [5]. The number of genes that can drive cancer is highly variable across cancer types (Figure 1). In common solid tumors such as colorectal, breast, brain or pancreatic cancers, an average of 33 to 66 genes show somatic mutations that affect their protein product. However, other types of cancer such as lung cancer and melanoma display around 200 of those type of mutations per tumor [5]. These alterations trigger multiple newly acquired capabilities in tumors, known as hallmarks of cancer, that contribute to its initiation, growth and survival: promoting proliferation signaling, replicative immortality, angiogenesis, genomic instability, inflammation, invasion and metastasis, avoidance of cell death and immune destruction, and reprogramming of cell metabolism (Figure 2) [6]. These multiple driving mutations and different altered cellular functions exemplify the complexity

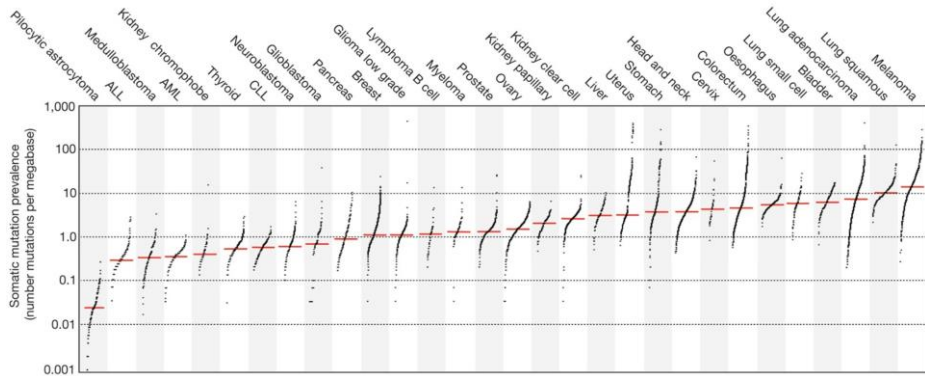


**Figure 1: Prevalence of somatic mutations in different cancers.** Every black dot represent a sample, while red lines represent the median number of mutations. Y axis (log scale) shows the number of mutations per megabase, while X axis shows the cancer type ordered by the median number of mutations. Obtained from [7].

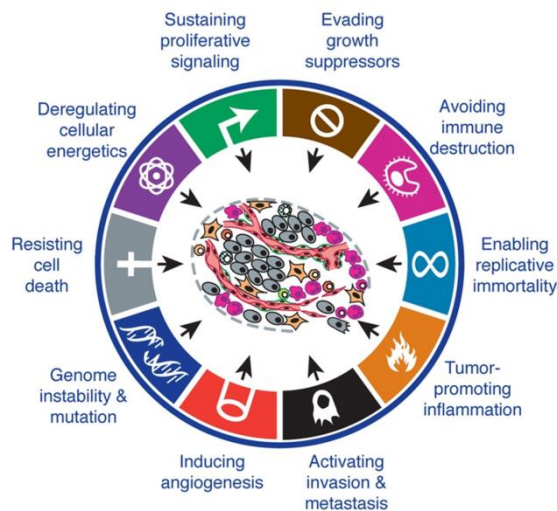


**Figure 2: Acquired capabilities necessary for tumor growth and progression known as hallmarks of cancer.** Adapted from [6].

and heterogeneity of human cancers. Indeed, while all cancers have been traditionally gathered as one disease and treated similarly, nowadays it is well-established, thanks to the developments in genomic techniques, that every cancer might be different, even if originating from the same tissue [8]. On the basis of this heterogeneity, a novel therapeutic strategy has emerged called “precision medicine”, which uses personalized treatments according

to the specific alterations present in the tumor of each patient. In combination with regular chemotherapy, radiotherapy and surgery, personalized therapies have opened a new era in cancer therapeutics [9].

### 1.3. Precision medicine in cancer therapies

Precision, personalized and individualized medicine are often used as synonyms. However, some physicians claim that patients have always been treated on the personalized/individualized level. Therefore, precision medicine is the preferred term to emphasize the new aspects of this field: while the personalized approach in the relationship doctor-patient is still a central aspect of precision medicine, the term refers to the use of new biomedical information beyond visible disease signs and symptoms, and implies the incorporation of broad arrays of individual data such as clinical, lifestyle, genetic, immunohistologic and biomarker information that distinguish a given patient from others with similar disease presentation [10, 11].

An example of this novel strategy is found in lung cancer diagnosis, where the traditional classification based on the histology of the tumors (large-cell carcinoma, squamous cell carcinoma, adenocarcinoma and small-cell lung cancer) is complemented by the molecular testing of genetic markers such as EGFR, MET, RAS and ALK among others (Figure 3). For instance, the few lung cancer patients (<5%) harboring tumors driven by an ALK rearrangement can benefit from a dramatic clinical response if they are treated with the targeted inhibitor crizotinib. Conversely, patients without ALK fusion will not be treated with this drug, avoiding a likely ineffective and costly treatment that could even trigger toxic side effects [12].

Another clear example of a revolutionary step achieved by precision medicine in lung cancer therapy was made with the discovery of mutations and the targeting of EGFR. Ligands of EGFR (such as EGF) can bind to the extracellular domain of the transmembrane receptor, which will form dimers with other EGFR molecules or HER family members, undergoing the phosphorylation of key residues and triggering the activation of different downstream signaling pathways. Mutations or amplifications in EGFR can constitutively activate this receptor and the downstream effector pathways and have been described as oncogenic alterations that can initiate and sustain tumor progression. Only 2 types of alterations in EGFR account for



90% of the known activating mutations: deletions in exon 19 and an L858R substitution in exon 21. The treatment of patients harboring these 2 molecular alterations using tyrosine kinase inhibitors (TKI) has resulted in an improved clinical outcome. The 12-month progression-free survival of 6.7% with chemotherapy was increased to 24.9% with the TKI gefitinib in EGFR-mutated lung cancer patients [13]. Erlotinib and afatinib also demonstrated that first-line EGFR-TKI offered improved objective response rate, progression-free survival and better quality of life compared to chemotherapy [14, 15]. However, none of these studies demonstrated a clear benefit in overall survival of EGFR-targeted therapies [16, 17]. On the other hand, more recent retrospective analysis of several studies show that those patients with EGFR-activating mutations can benefit from a significantly longer survival advantage (13.5 months) when treated with EGFR-TKIs [18], or at least in a subgroup of those patients with deletion in exon

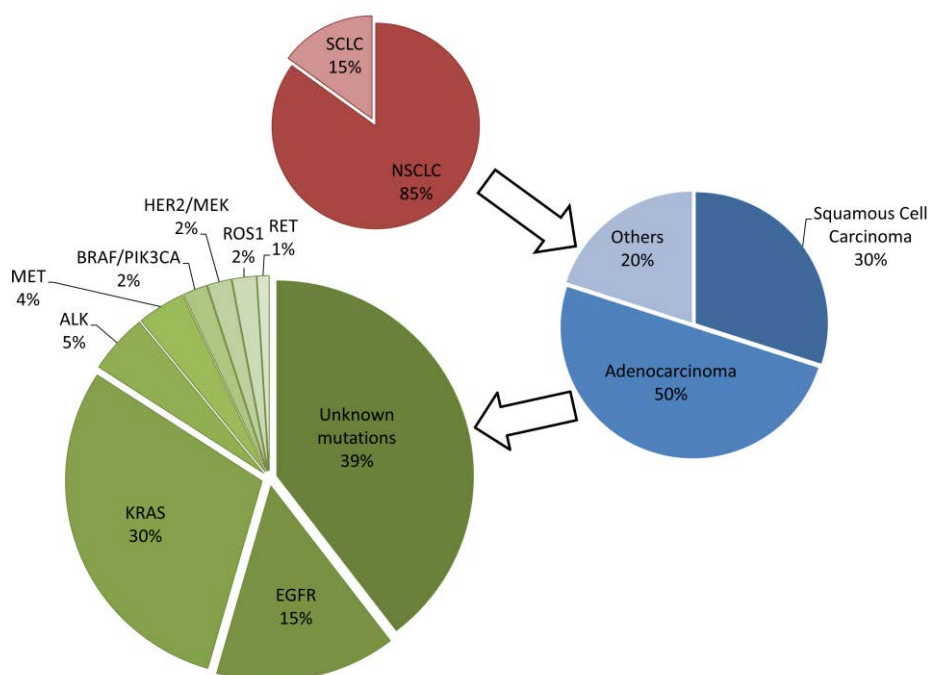


**Figure 3: Distinction of NSCLC by histology and adenocarcinoma by mutated genetic markers.** Adapted from [16]. SCLC: Small-cell lung cancer; NSCLC: Non-small cell lung cancer.

19 [19]. This later study suggested, in addition, that the different responses observed in patients presenting the different activating EGFR mutations (deletion in exon 19 vs. L858R mutation) might be distinct and therefore these 2 groups of patients should be differentiated in future trials, illustrating new degrees of complexity in the stratification of patients with lung cancer, and possibly, other types of cancer as well.

#### 1.4. Primary or acquired resistance to targeted therapies

Cancer patients have benefited from precision medicine and will continue doing so even further given the rapid technological developments in next-generation sequencing and fierce competition of pharmacological companies to provide novel and more potent molecular targeted drugs. This medical approach, while harboring promising prospects, is currently at its infancy and must overcome a number of problems and deficiencies [20]. To start, intra-tumoral genetic heterogeneity has important implications for precision medicine and is one of the key factors that limit its therapeutic efficacy. In fact, it is now well established that, within each tumor, there are multiple subpopulations of cancer cells presenting different molecular alterations. Studies in advanced colorectal [21] and breast cancers [22], for example, suggest that treating patients with drugs matching certain molecular targets might not always produce an improved outcome, because, even if the tumor responds initially to the targeted therapy, the intra-tumoral genetic heterogeneity and the selective pressure of the treatment might trigger the emergence of resistance. For instance, the previously mentioned EGFR-mutated tumors that initially respond to EGFR-TKIs might develop acquired resistance by the uprising of cells presenting secondary mutations in EGFR (T790M), phenotypic transformation (from adenocarcinoma to small cell lung cancer) or the activation of alternative pathways (amplification of MET and HER2) [23]. Hence, continued investigation needs to be undertaken to understand how tumors circumvent targeted therapeutic strategies and evolve into resistant clones in order to rationally design more effective treatment combinations or drugs.

A strategy to counteract resistance has been implemented, for instance, in BRAF-mutated melanoma treated with the BRAF inhibitor vemurafenib. This inhibitor has displayed an initial outstanding efficacy in these types of tumors, which however develop resistance by activation of EGFR. Because of that, this type of resistance can be targeted by the combination of

vemurafenib with EGFR-TKIs [24, 25]. Other potential solutions to effectively implement precision medicine are the use of targeted therapies at earlier stages of the diseases, when likely fewer molecular alterations have accumulated, and the monitoring of the cancer genotype progression to re-adjust therapeutic regimens as needed [26].

The problem of primary or acquired resistance of tumors to targeted therapies is in part a consequence of the redundancy of their molecular targets in cancer cell function. Resistances often emerge because the molecular target has a function within cancer cells that becomes dispensable for tumor progression because it can be easily compensated by alternative molecular pathways. Thus, the therapeutic intervention produces no significant effect in the global outcome, resulting in modest or no overall survival increase [27]. Indeed, the efficacy of cancer drugs does not only depend on how well they can reach the cancer cell and effectively inhibit the target, but in the nature of the target itself.

### 1.5. The ideal cancer target

Nowadays, more than 34,000 drugs allow us to target more than 3,000 molecules [28]. Drugs used in the clinic are able to target a variety of cellular components, most of which are relatively easy to inhibit, such as G protein-coupled receptors, ion channels, kinases and proteases [29]. There is currently an arsenal of drugs that target some of the molecules found mutated or deregulated in cancer (Figure 4). However, other more complex molecular targets might hold the key for more effective and broader responses compared to current targeted therapies. There are some features that may constitute the ideal cancer target. First, the target should be a molecule whose function is central to many types of cancer and, consequently, whose inhibition could display efficacy in a variety of tumor types. Second, to avoid the problem of resistance, the target should be part of a functionally non-degenerate and non-redundant node, indispensable for the maintenance and survival of the tumors. Third, while the target's function should be essential for cancer cell survival, it must be dispensable for normal cells, thus displaying minimal or, preferentially, no side effects. Finally, the molecule must be effectively druggable and mechanistically well characterized, allowing the development of compounds that could totally

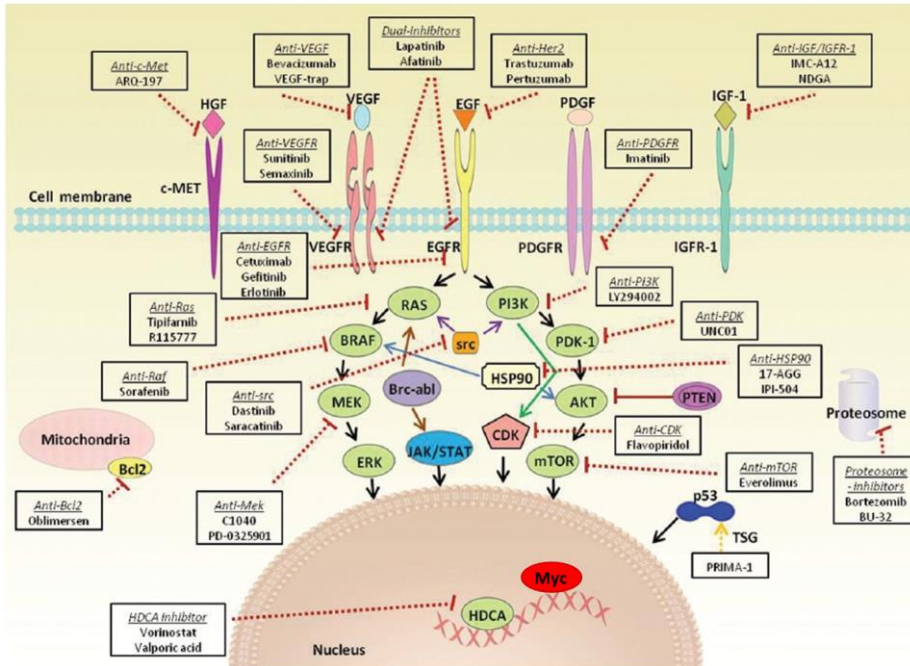


**Figure 4: Representation of the main signaling pathways involved in proliferation and progression of cancer and some of the targeted therapy agents against them.** EGF: Epidermal growth factor; EGFR: EGF receptor; HGF: hepatocyte growth factor; c-MET: mesenchymal– epithelial transition factor; PDGF: Platelet-derived growth factor; PDGFR: PDGF receptor; IGF-1: insulin-like growth factor-I; IGF-1R: IGF-1 receptor; PI3K: phosphatidylinositol 3-kinase; Ras: Rat sarcoma subfamily of GTPases; AKT: protein kinases B; PDK1: pyruvate dehydrogenase kinase isozyme 1; mTOR: mammalian target of rapamycin; MEK: mitogen-activated protein kinase kinase; VEGF: vascular endothelial growth factor; VEGFR: VEGF receptor; BRAF: B-type RAF kinase; src: v-Src (Rous sarcoma virus) tyrosine kinase; BCRABL: Philadelphia chromosome; JAK/STAT: Janus kinases/signal transducers and activators of transcription; PTEN: phosphatase and tensin homolog; HDAC: histone deacetylases. Image adapted from [30].

neutralize its deregulated function and downstream effects [31, 32]. Among the few molecules and pathways that could potentially match these features, we have focused on the Myc oncogene. Myc was discovered in 1979 as responsible for inducing myelocytomatosis in birds [33] and 3 years later it was implicated for the first time in a human malignancy [34]. Today, almost 40 years later, Myc is considered one of the most frequently deregulated

oncogenes in many different types of cancer and one of the most attractive therapeutic targets [35, 36].

### 1.6. The Myc oncogene

The Myc family is composed of c-Myc (hereinafter Myc), N-Myc and L-Myc, which act as transcription factors that form dimers with Max and regulate the expression of multiple genes across the genome [37].

The many pathways transducing growth signals that converge on Myc show the central role of this transcription factor in regulating cell proliferation (Figure) [38-45]. The importance of Myc's function in normal cells and its pathological potential are also mirrored by its tightly controlled regulation. Beyond gene expression, multiple mechanisms regulate Myc at both the mRNA and protein levels. Myc's mRNA stability and translation can be controlled by microRNAs and RNA-binding proteins [46, 47]. At the protein level, Myc's translational activity, stability and degradation are controlled by kinases, ubiquitin ligases, acetyl transferases, long non-coding RNAs and other partnering proteins within its network [38, 48-52]. The various upstream proliferative signals use these mechanisms to regulate the expression of Myc and its short-lived mRNA and protein levels, ensuring Myc presence only when it is required. Hence, in the absence of such sustained stimuli, Myc expression is switched off, the mRNA and protein levels rapidly fall and the cell undergoes growth arrest. Additional check-points within normal cells also protect the organism against Myc deregulation, so that abnormal Myc expression causes cell growth arrest or even cell death [53]. Indeed, Myc-induced apoptosis in the absence of other oncogenic lesions might be a reason why Myc is rarely the driving alteration in cancers at early stages [54]. However, loss of these check-points or obstruction of apoptosis is able to synergize and cooperate with Myc deregulation to promote proliferation and tumorigenesis [55-58]. In this context, Myc deregulation is typically the result of oncogenic mutations in the various upstream signaling pathways that control its expression and/or stability [35].

Once it is expressed, Myc is able to develop its function through its different domains: a nuclear localization sequence, that directs Myc to the nuclei of cells where it performs its function; a helix-loop-helix leucine-zipper (HLH-LZ) dimerization domain that interacts with Myc's partner Max to form functional dimers; a basic DNA-binding domain that selectively recognizes

target gene promoters; a transactivation domain (TAD) harboring Myc boxes I and II that controls the transcriptional activity of the target genes through the recruitment of co-activator proteins; and a central domain that harbors Myc boxes III and IV, which contribute to transcription repression and induction of apoptosis among other functions (Figure 5) [59]. These domains are distributed among all the protein length: the unstructured N-terminal transcriptional regulatory domain contains the highly conserved boxes I and II, followed by III and IV and one nuclear localization sequence [60-62]; the C-terminal region contains the b-HLH-LZ dimerization domain, which harbors a second nuclear localization sequence, heterodimerizes with Max to bind mainly to consensus DNA regions called E-boxes (CACGTG) and regulate the expression of thousands of genes across the genome [63].

The basic principle of equilibrium behind the specific heterodimerization of Myc and Max relies on the formation of more stable heterodimers compared to the formation of respective homodimers. The b-HLH-LZ of Myc (Myc'SH) is intrinsically disordered and presents low solubility. Only in the presence of Max b-HLH-LZ (Max'SH), Myc'SH is able to form stable secondary, tertiary and quaternary structures upon binding with Max'SH [64]. The heterodimers bind to DNA through specific recognition of E-boxes, while the N-terminal domain forms complexes with co-factors such as TFIID, TRRAP and GCN5 that regulate gene expression through chromatin modification [65, 66]. Transactivating activity by Myc/Max is regulated and counteracted by Mad/Max heterodimers and Max/Max homodimers, which reduce the Max monomers available for Myc heterodimerization and compete to bind E-box DNA sequences [67].

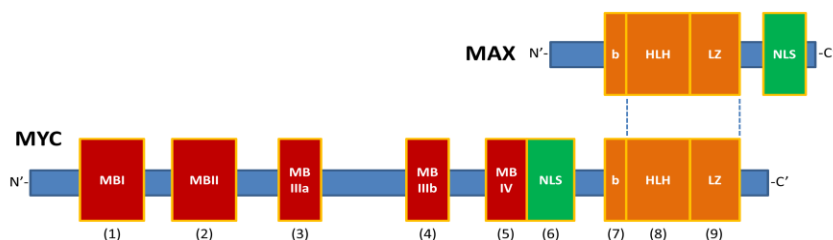


**Figure 5: Topology of Myc and Max proteins.** (1) Myc box-I: located between amino acids 45 and 63 and contains T58 and S62 phosphorylation sites, which regulate Myc stability [68, 69]. (2) Myc box-II: located between amino acids 128 and 143, this is most studied region within the TAD and responsible of the binding to multiple key interactors including histone acetyltransferases

*complexes such as TRRAP [70]. The MBI-II TAD region is also associated to effectors of Myc activity such as BRD4 and P-TEFb [71, 72]. (3) Myc box-IIIa: located between amino acids 188 and 199, represses transcription by interacting with HDAC3 [73]. (4) Myc box-IIIb: located between amino acids 259 and 270, this region facilitates Myc recruitment on target gene promoters through WDR5 [74]. (5) Myc box-IV: located between amino acids 304 and 324, has been associated to regulation of DNA binding, apoptosis, transformation and G2 arrest [62]. (6) Nuclear localization signal: this region, from amino acids 320 to 328 (PAAKRVKLD), is the main responsible for Myc's nuclear localization [60]. (7) Basic region: located between amino acids 355 and 369, it mediates DNA recognition and binding to E-boxes, and harbors a second nuclear localization signal within residues 364 to 374 (RQRNRELKRSP) [60, 63]. (8-9) Helix-loop-Helix leucine zipper: from amino acid 370 to 439, this region mediates the dimerization of Myc with its principal partner Max, and others such as Miz-1 and SKP2 [59].*

Besides acting as transactivator, Myc can also repress genes implicated in cell cycle arrest by less well-characterized mechanisms, mainly through binding to Miz-1 and other co-regulators and activation of miRNAs [75, 76]. For instance, Myc represses CDKN2B (p15INK4b) by binding to Miz-1 and displacing its transcriptional co-factors [77]. Similarly, E2F1, a key Myc effector of cell cycle control, can also be attenuated by Myc-mediated activation of miR-17-92 cluster of miRNAs [78].

Although Max has been described as Myc's obligate partner, in some contexts Myc function remains active even in the absence of a functional Max protein [79, 80], although it is not clear to what extent. In fact, some recent studies suggest that Max inactivation is implicated in the initiation and progression of some tumors [81, 82].

The pleiotropic role of Myc is illustrated by its broad range of target genes [83, 84], controlling processes such as proliferation, cell death, metabolism, senescence, angiogenesis, immune response, microenvironment remodeling and differentiation [85-87]. The pivotal role of Myc in integrating the various upstream growth signals to coordinate these multiple processes through the expression of thousands of genes makes it functionally non-redundant. Indeed, developmental plasticity is not able to circumvent the absence of Myc since its deficiency is embryonically lethal in mice [88] and ablation of Myc in Rat1 fibroblasts (that, in addition, express neither N-Myc nor L-Myc)

causes multiple defects in cell cycle that notably slow down cell proliferation [89]. Both observations illustrate the unique function that Myc serves within the complex cellular pathway network.

The same programs that Myc controls during normal somatic cell expansion become pathological when Myc is deregulated, as observed in the majority of cancers. There, Myc deregulation contributes to autonomous proliferation and growth, relentless DNA replication, increased protein biogenesis, global changes in cellular metabolism, activation of the angiogenic switch, suppression of the response to autocrine and paracrine regulatory programs and a restraint of host immune response (Figure 6) [90]. Various switchable in vivo models show how Myc's pathological activation can trigger tumorigenesis in different tissues and fuel the survival and progression of tumors, as evidenced by the fact that Myc de-activation causes tumor regression [91-94]. Thus, many published studies suggest that reverting a single oncogenic lesion such as Myc deregulation, to which cancers may be addicted, could represent a specific and effective treatment approach for different types of cancer [95, 96].

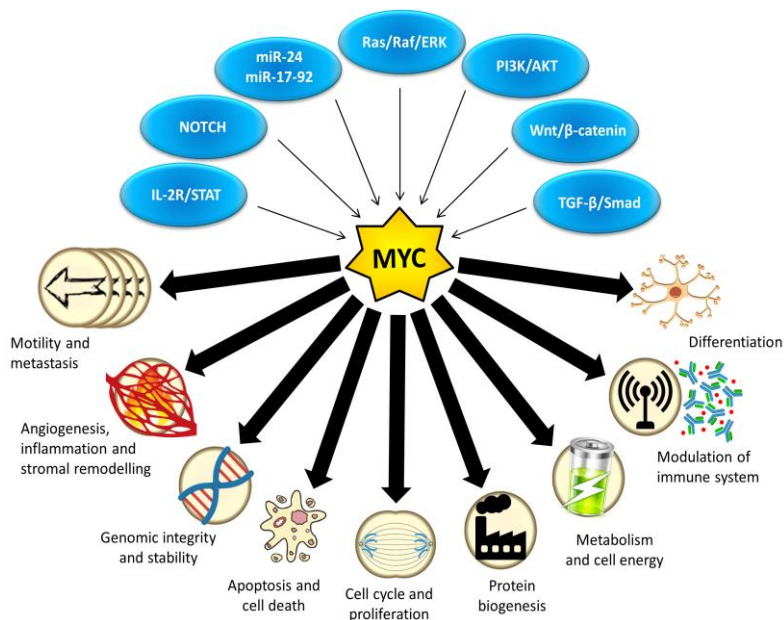


**Figure 6: Myc is a central conduit of tumorigenesis.** Myc acts as a key cellular node that couples various upstream signaling pathways to multiple functions and processes within cells, both in physiological and pathological conditions.



### 1.7. Modelling Myc inhibition using Omomyc

Although many studies placed Myc as an interesting therapeutic target, 2 important issues still remained to be clarified. Firstly, as described before, many human cancers are not induced by direct Myc overexpression. Rather, other upstream alterations are responsible for the deregulation of endogenous Myc, which might not be exactly recapitulated by ectopic and acute Myc overexpression. Thus, the role of endogenous Myc in tumor survival when deregulated by other oncogenic lesions remained unclear. Secondly, Myc is essential for normal cell proliferation. Therefore, potential catastrophic side effects of its inactivation in normal proliferating tissues could counteract the use of Myc inhibition as an effective therapeutic approach against cancer.

To address both concerns, Soucek et al. tested the effects of systemic Myc inhibition in a KRAS-driven model of lung cancer [97] using the Myc dominant negative called Omomyc [98-100]. In this study, the Omomyc transgene was placed under the control of the TRE promoter (TRE-Omomyc) together with the constitutive expression of the reverse tetracyclin-dependent transactivator (rtTA) driven by the CMV promoter [101]. In this model, upon the addition of doxycycline to the drinking water, Omomyc expression was systemically induced in virtually all tissues of the mouse. Surprisingly, systemic Myc inhibition did not produce any general toxicity measured by weight loss. Animals only exhibited mild and well-tolerated side effects in proliferating tissues when they were analyzed by tissue histology. For instance, the intestine villi presented a certain degree of atrophy, but blood tests revealed that nutrient absorption was not affected by Myc inhibition. Testis and skin tissues showed a reduction in proliferative rate as well, but no cell death was observed. Importantly, all these effects observed in normal tissues were fully reversible upon Omomyc repression and restoration of endogenous Myc function.

In order to assess the therapeutic effect of systemic Myc inhibition in cancer, the Omomyc transgenic mouse model was crossed with the widely used LSL-KRas mouse model [97], which develops adenocarcinomas in the lungs within 16 weeks following adeno-CRE intranasal administration. Unexpectedly, while Omomyc expression displayed lack of toxicity in normal tissues, not only had a cytostatic effect on established tumors, but also

caused potent cytotoxicity that triggered their complete regression after only 7 days of expression [101].

Later on, this same model was also crossed with a functionally inactive p53 (p53-ER) to allow the development of more aggressive and heterogeneous tumors [102], in order to better mimic their human counterpart. In this new model, metronomic Omomyc expression (4 weeks on and 4 weeks off) was enough to indefinitely extend the survival of the animals (Figure 7). After every cycle of induction, histology revealed that fewer tumors emerged, until they were completely eradicated. Only those rare tumors that spontaneously lost Omomyc expression were present at the endpoint. These results demonstrated that endogenous Myc is required for tumor maintenance in KRAS-driven tumors and that its inhibition could represent a safe and effective therapeutic approach without the emergence of resistance even after long term treatment.

Importantly, Omomyc expression proved to be effective in various other mouse models that develop tumors in different tissues driven by different genetic alterations, including direct Myc overexpression in the skin [98]. For instance, in the RIP1-Tag2 model of pancreatic insulinomas driven by SV40 T/t antigens (which develops tumors through the simultaneous alteration of p53 and Rb functions [103]), Myc inhibition by Omomyc expression in tumorigenic  $\beta$  cells triggered shrinkage of the tumors through the collapse of their microenvironment [104]. Similarly, in a Harvey-RAS-driven glioma model, Omomyc expression triggered cancer cell death by mitotic catastrophe [105]. Again in glioma, Omomyc expression in an orthotopic xenograft model of glioma patient-derived cells extended mouse survival [105, 106]. Finally, in 2 different breast cancer models driven by either WNT or HER signaling pathways and in a KRAS-driven model of pancreatic ductal adenocarcinoma, Omomyc expression also caused tumor regression (unpublished data, personal communication with the Evan laboratory).

Together, all these studies confirm the lack of compensatory mechanisms that could overtake the unique and essentially non-redundant function of Myc in cancer cell survival. Coupled with the broad anti-tumorigenic efficacy of Myc inhibition, the lack of severe side effects position Myc as a therapeutic target to treat many, perhaps all, cancers. However, pharmacological Myc inhibition has been considered a pipe dream for a long

time, since transcription factors have been generally seen as “undruggable” [107].

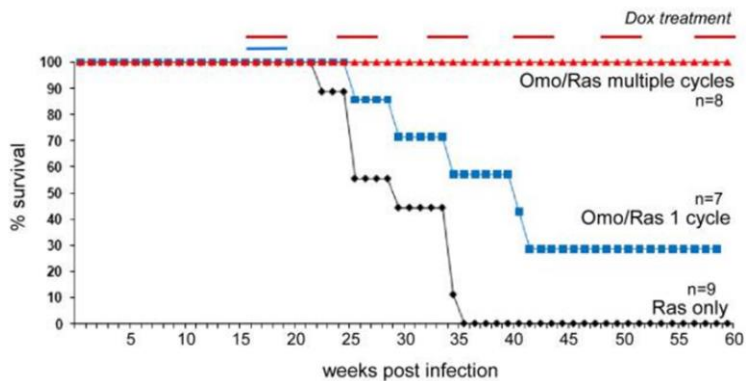


**Figure 7: Omomyc confers survival advantage to animals bearing lung adenocarcinomas.** Survival curve of mice subjected to metronomic Omomyc expression (4 weeks on, 4 weeks off) (Red) compare to mice expressing a single cycle of Omomyc (blue) and no-Omomyc control mice (black). Image obtained from [102].

## 1.8. Pharmacological Myc inhibition

Despite the identification of Myc as a potentially effective and safe therapeutic target, today there is still no Myc inhibitor in the clinic. Indeed, Myc has been shown challenging to target with classical small molecules, at least in part because, in order to inhibit Myc, the drug must travel to the nuclei of cells and interfere with large protein-protein interactions, a more complex task than classical inhibition of enzymes [36, 108]. However, various scientists have come up with different pharmacological approaches to target Myc, either directly or indirectly (Figure 8) [109].

### 1.8.1. Direct Myc inhibitors

Several approaches have been tested to directly inhibit Myc:

1. G-quadruplexes stabilization: G- quadruplexes are guanine-rich DNA regions that form tertiary structures, like the one present in the control region of the Myc promoter. Some studies have shown that stabilization

of the Myc G-quadruplex leads to downregulation of the oncogene [110, 111].

2. Myc mRNA inhibition: antisense nucleotides as a tool to inhibit the translation of the targeted mRNAs by promoting their degradation [112, 113] were also used to downregulate Myc protein levels. However, no such drug has so far reached the market [114]. Similarly, lentiviral delivery of small-interference RNA (RNAi) has been used to inhibit Myc translation in vitro [115] and a lipid nanoparticle delivering Myc RNAi (DCR-MYC) even entered clinical trials. Unfortunately, the efficacy results did not match the expectations of the company and Dicerna stopped any further development to focus on its other promising compounds.
3. Oncolytic viruses: a relatively new approach that is starting to show great promise in the treatment of cancer is the use of oncolytic viruses [116]. This therapeutic strategy has also been tested to deliver siRNA against N-Myc and inhibit neuroblastoma tumor growth in vivo [117].
4. Inhibition of Max/DNA binding: although Myc is an intrinsically disordered protein that does not present an active site or binding pocket, its binding to Max and DNA have been considered good targets for specific inhibitors. Thus, drugs aimed at inhibiting Myc protein interactions and DNA binding have also been tested, but their poor selectivity has mainly limited their use in vivo [118]. Another therapeutic strategy to achieve Myc inhibition, as mentioned above, is inhibiting the DNA binding of the Myc/Max dimers required to modulate the expression of target genes.

### 1.8.2. Indirect Myc inhibitors

Myc has proven difficult to target directly. Small molecules have in general displayed low affinity and specificity towards Myc and poor bioavailability. Thus, other more tractable targets around Myc have been proposed to affect Myc's transcriptional regulation, stability and activity. Various approaches to indirectly target Myc has been tested:

1. Inhibition of bromodomain and extra-terminal domain (BET): one of the most widely used BET inhibitors, JQ1, was found to downregulate Myc by interfering with the chromatin-dependent signal transduction to RNA polymerase mediated by BET proteins [119, 120]. However, the capacity of BET inhibitors to downregulate Myc seems very context-dependent, since BET inhibition has displayed anti-tumorigenic potential

independently of Myc regulation in other tumor types, such as non-small cell lung cancer [121] and pancreatic ductal adenocarcinoma [122], among others [123-127]. Concerns about the accelerated progression of BET inhibitors toward clinical trials, without an appropriate biological knowledge of their properties and molecular mechanisms, have also been discussed [128]. BET bromodomain inhibitors with different chemical scaffolds are currently being tested in the clinic for various haematological and solid tumor types, including pancreatic ductal adenocarcinoma and NSCLC. The most advanced ones include CPI-0610, GS-5829, GSK525762, INCB054329, INCB057643 and BMS-986158, which are currently being evaluated in Phase I/II or Phase II studies.

2. Inhibition of CDK7: in addition to the BET inhibition strategy, Myc transcription has also been inhibited by targeting CDK7, a catalytic subunit involved in the transcriptional initiation complex that phosphorylates serine-5 of RNA pol II [129]. This approach has recently been tested in preclinical mouse model [130, 131]. However, to our knowledge, information of the efficacy of this strategy in patients is not yet available.
3. Inhibition of mTOR: besides Myc transcription, its mRNA translation can also be blocked. In this context, mTOR seems to act as a key element in mediating the translation of Myc's mRNA [132]. Thus, targeting mTOR or upstream molecular pathways, such as PI3K or MAPK, for which there are various drugs already approved, represents a feasible strategy [133]. However, in a mouse model of colorectal cancer, direct inhibition of mTOR failed to inhibit Myc translation, while inhibiting eIF4A using silvestrol did [134]. In addition, more recent data demonstrated that double targeting of HDAC and PI3K displays therapeutic impact in various mouse models of Myc-driven tumors [135] and the first preliminary data of this drug, CUDC-907, in clinical trials is encouraging and a phase II study is currently ongoing [136].
4. Increase of Myc degradation: various E3 ligases, such as FBW7, are able to ubiquitinate Myc to promote its degradation. Some ubiquitin-specific proteases (USPs) on the other hand are able to deubiquitinate Myc and stabilize it. Therefore, either induction of FBW7 or inhibition of USPs could downregulate Myc due to proteasomal degradation [137, 138].

### 1.8.3. Polypeptide Myc inhibitors

Most small molecules and targeting upstream pathways to inhibit Myc are likely to display low selectivity for Myc, either because the drug is not specific enough and may target other molecules, or because the molecular pathways are involved in other cellular processes besides Myc regulation. In this regard, peptides and miniproteins directly targeting Myc might provide higher selectivity due to the larger interaction surface they enable with the target [139].

Therapeutic peptides are a novel and promising approach for the development of anti-cancer agents [140]. Peptide and miniproteins aimed to inhibit Myc comprise mainly a group of structurally-related molecules based on regions and domains of the proteins within the Myc network. To our knowledge, 2 peptides have been used pharmacologically to inhibit Myc so far:

1. A modified Myc peptide of 14 aminoacids based on the H1 region of Myc was used: this region bears 2 substitutions at non-conserved residues (S6A and F8A) that confer greater helicity and increase its heterodimeric interaction with Myc'SH interfering with its DNA binding [141, 142]. This peptide was fused to an internalization sequence [143] to translocate the fusion product through biological membranes and inhibit Myc transcriptional activity in vitro [144]. Initial results showed poor in vivo efficacy, in part due to an ineffective nuclear translocation that could be improved by fusion proteins that direct the drug to the nucleus [145]. More recently, docetaxel was used to arrest cells in G2/M and prolong the disassembly of the nuclear envelop prior to the treatment with the H1 peptide. The strategy slowed down tumor growth and improved animal survival [146]. Its efficacy against brain tumors was also improved by thermally targeted delivery of a H1-fused thermally responsive biopolymer, elastin-like polypeptide, and Bac cell-penetrating peptide, Bac [147].
2. The b-HLH-LZ domain of Max (Max\*) has shown to behave as protein transduction domain, spontaneously transducing cells, entering into the nucleus and inhibiting Myc transcriptional activity in HeLa cells [148]. The efficacy of this strategy is based on the formation of Max\*/Max\*

homodimers that could compete with endogenous Myc/Max dimers for DNA-binding sites.

Other peptide-based approaches have been used as well to interfere with Myc/Max DNA binding [149, 150]. Although the results are encouraging, further investigation will reveal if these approaches represent valid pharmacological strategies.

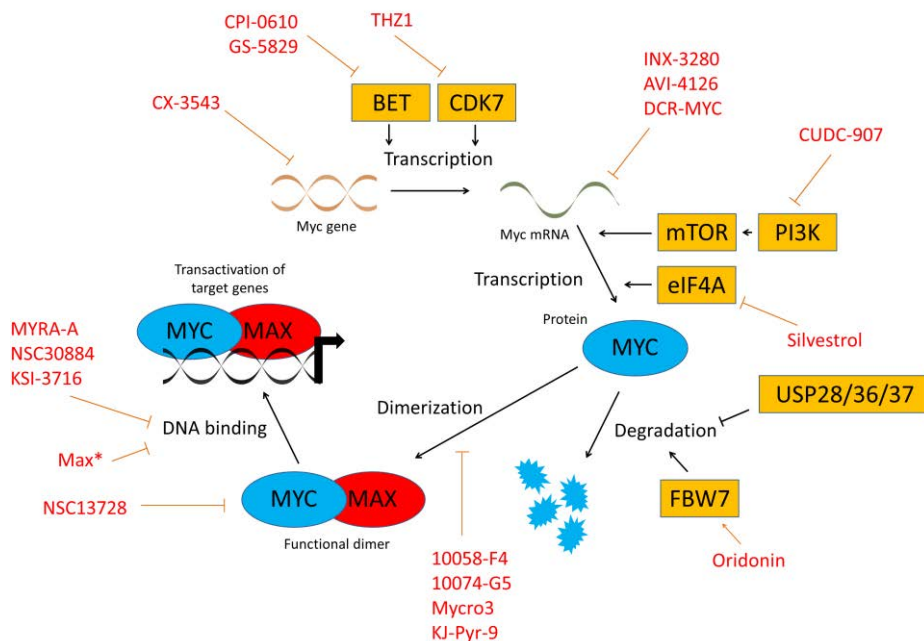


**Figure 8: Myc have been inhibited using a variety of drugs that target the oncogene at different levels. Some examples of drugs that can target Myc either directly or indirectly are represented.**

Thus, during the last years, an arsenal of drugs that inhibit Myc in various ways and at different levels has been tested. However, despite the efforts, unfortunately, no Myc inhibitor has reached the clinic. While some therapies failed, others might have been discontinued and we hope that the most promising ones are still under development. Looking at the future, we clearly need to keep trying to effectively inhibit Myc pharmacologically by refining the current drugs and/or creating new ones more specific and potent. Although Myc can be inhibited in many different ways, not all the strategies might be equally effective. Thus, to create these new drugs, we must also

examine in depth the features of the best Myc inhibitors shown to date to find out the best place and the best way in which Myc can be knocked out.

### 1.9. Omomyc mechanism of action

Among the various pharmacological and genetic approaches that have proven to inhibit Myc, Omomyc has been one of the most effective and the one providing the first proof of concept for the feasibility of systemic Myc inhibition. Unfortunately, to date, Omomyc itself has not been used as a pharmacological approach. However, as a proof of principle, Omomyc could provide valuable insights to guide future development of cancer therapies against Myc.

As mentioned above, Max is considered to be Myc's obligate partner to trigger activation of target genes. Both Myc and Max must form dimers to bind DNA, which is mediated mainly by their Leucine Zipper (LZ) domain and their basic region respectively (Figure 9A). Interactions with other partners and cofactors might take place also through the TAD or/and HLH domains [59]. The LZ domain that mediates the dimerization is present in other transcription factors as well [151]. This region is formed by an amphipathic helix that harbors repetitions of 7 residues called heptad repeats  $((\text{abcdefg})_n(\text{abcdefg})_{n+1}(\text{abcdefg})_{n+2}\dots(\text{abcdefg})_{n+n})$  [152]. LZs interact with each other and are stabilized by the presence of interfacial hydrophobic aminoacids residues at "a" and "d" positions of each LZ. In fact, the high incidence of leucines at positions "d" gave the name to this domain. In addition, electrostatic interactions between the residues "g" and "e" of the different LZ further stabilize the structure. The remaining residues at positions "b", "c" and "f" are less well conserved and are thought to contribute little to the formation of stable dimers.

Exceptions to this canonical structure of LZs exist however within the LZ structure of Myc and Max that explain their specific dimerization properties. Instead of nonpolar aminoacids at positions "a", Myc presents several charged aminoacids (E410, E417 and R424) (Figure 9B). The repulsive forces that act when these residues from 2 different Myc molecules face each other prevent the stable homodimerization of Myc [99, 153]. Max also presents polar residues at "a" N78 and "d" H81 positions, which in certain conditions can be positively charged. In contrast to Myc, Max is able to form homodimers despite the presence of these interfacial polar residues,



although the formation of heterodimers with Myc is favored by the presence of a buried salt bridge between the interfacial residues E410-E417 of Myc and H81 of Max [154].

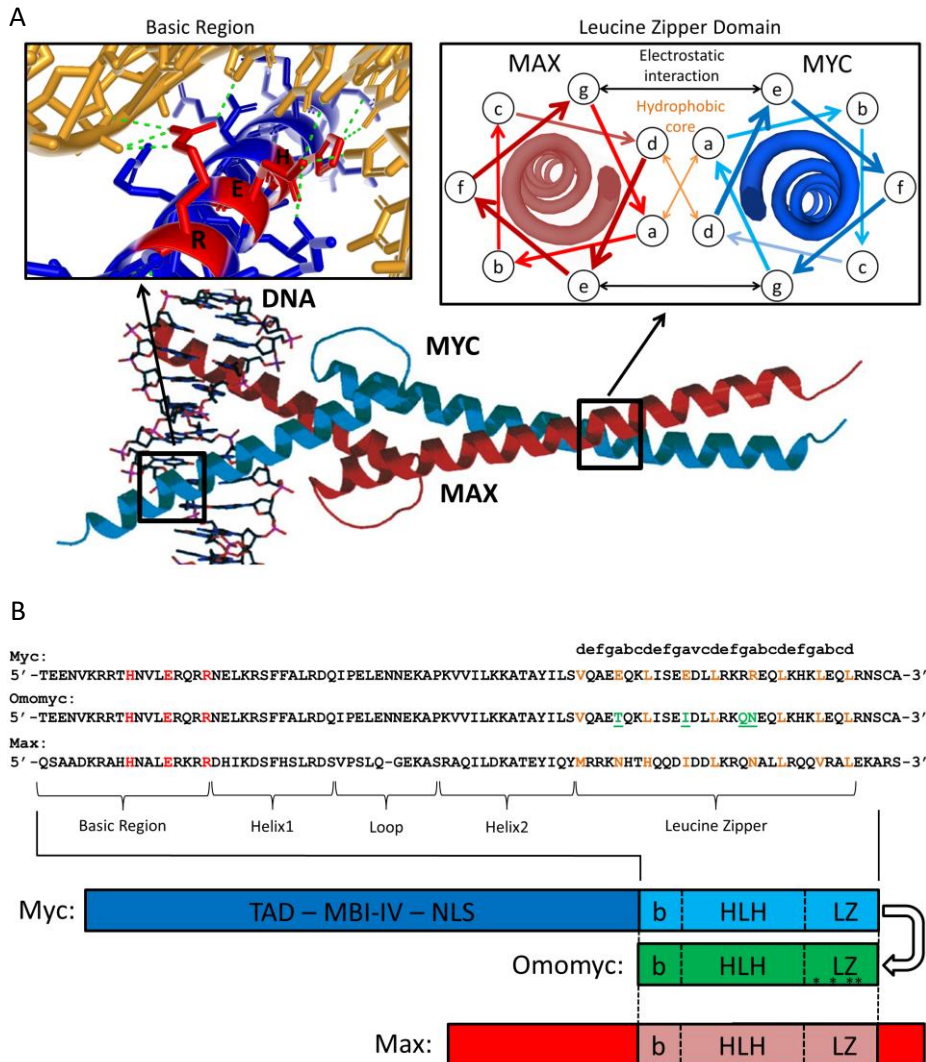


**Figure 9: The interactions that promote specific dimerization take place in the leucine zipper (LZ) interface of Myc and Max, while the residues that mediate binding to DNA are located in the basic region. (A) Crystal structure of a Myc'SH/Max'SH heterodimer bound to DNA. Left panel shows the interaction of H-E-R between the basic region and DNA (in yellow). Residues are highlighted in red and polar contacts are labelled in green dotted lines. Right panel shows a schematic helical wheel representation of the LZ region**

*of both Myc and Max and the interaction of residues at positions from “a” to “g”. Electrostatic interactions “g-e” and hydrophobic core “a-d” that can stabilize the interaction are indicated. Arrows indicate the direction of the helix (from N-terminal to C-terminal). (B) Myc (in blue), Omomyc (in green) and Max (in red) are represented. Arrow from Myc to Omomyc indicate that Omomyc was derived from the Myc b-HLH-LZ. The 4 “\*” represent the 4 amino acid substitutions that differentiate the 2 LZ domains. The amino acid sequences forming the b-HLH-LZ of the 3 peptides are shown. The residues that mediate the specific interaction of the basic region with DNA bases are colored in red, the residues forming the hydrophobic core of the LZs are colored in yellow and the 4 amino acids of Omomyc that differ from Myc are colored in green. In addition, the “a-g” nomenclature is indicated.*

Once Myc/Max heterodimers are formed, they are able to recognize and bind DNA, preferentially to canonical E-boxes (5'-CACGTG-3') but also independently of the nucleotide sequences with lower affinity [155]. The DNA binding occurs via the basic regions of both Myc and Max. The specific contacts with DNA are mostly mediated by residues H359, E363 and R367 of Myc and the corresponding H-E-R residues of Max [156, 157]. Other positively charged residues present at the basic and H1 regions also contribute to the non-specific interaction of the transcription factors with the DNA backbone phosphate groups [156].

Omomyc was conceived as a tool to inhibit Myc through interference with Myc/Max dimerization. Based on the b-HLH-LZ domain of Myc, Omomyc bears 4 amino acid substitutions (E410>T, E417>I, R423>Q and R424>N) which abolish the net electrostatic repulsion that destabilizes the Myc homodimer [99]. Thus, Omomyc was shown to homodimerize, heterodimerize with Myc, while still retaining the ability to heterodimerize with Max, thereby interfering with Myc/Max dimerization. In fact, Omomyc is able to dimerize with all Myc family members [158, 159]. The mutations of Omomyc also allow it to homodimerize. The weak DNA binding affinity of the Myc/Omomyc dimers contributes to prevent the transactivation of Myc target genes [99]. In addition, Omomyc is also able to directly compete with Myc DNA-binding through Omomyc/Omomyc and Omomyc/Max dimers. Indeed, while it has been shown that Myc/Omomyc does not bind DNA, Omomyc/Omomyc and Omomyc/Max dimers are still able to occupy DNA

with high efficiency and compete with transcriptionally active Myc/Max heterodimers for DNA-target regions [99, 158].

Overall, Omomyc has been described to interfere with Myc transactivation in 4 ways: sequestering Myc away from DNA, breaking Myc/Max dimers by binding to Max, competing for DNA binding sites as transcriptionally inactive Omomyc/Max heterodimers and as Omomyc/Omomyc homodimers (Figure 10). Importantly, Omomyc selectively affects Myc/Max dimerization since structurally similar transcription factors such as HEB, ID1 and HIF-1 $\alpha$  did not bind Omomyc or, in the case of MAD, bound it very inefficiently [158]. While further experiments confirmed that Omomyc inhibited Myc transcriptional activation, surprisingly, Omomyc also enhanced transcriptional repression and potentiated Myc-induced apoptosis presumably through Miz-1, which was shown to co-precipitate with Omomyc [100, 158]. Thus, Omomyc-based Myc inhibition did not simply ablate all Myc functions as direct Myc depletion would do. Instead, Omomyc inhibits Myc-mediated transactivation while it enhances transrepression.

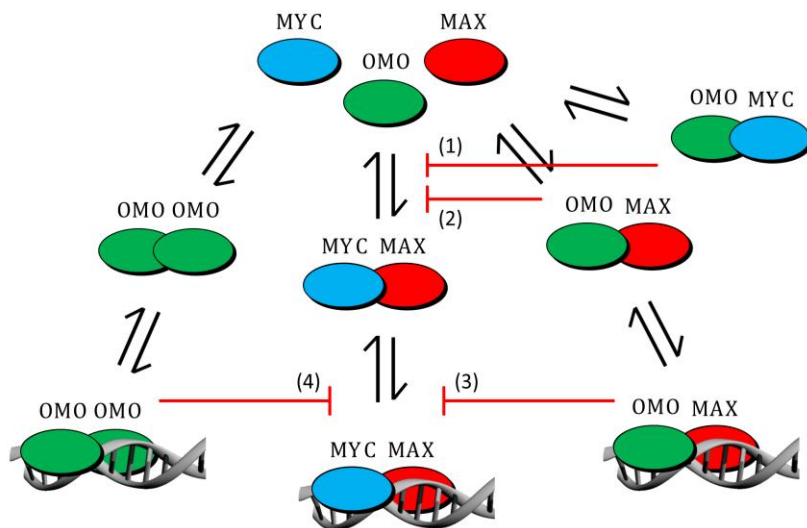


**Figure 10: Schematic representation of Omomyc's proposed mode of action.**

The described mechanisms by which Omomyc might be able to inhibit Myc are: (1) binding to Myc and sequestering it away from Max and from DNA; (2) binding to Max and (3) occupying Myc-target DNA regions; and (4) forming homodimers that bind Myc-target DNA sites. Omomyc would act in (1) and (2) by competing with the formation of Myc/Max dimers and in (3) and (4) by competing with the binding of Myc/Max on its target genes.

The relative contribution of these different events on Omomyc's anti-tumorigenic effect is still not clear. However, a recent study provided some new insights. Jung et al. hypothesized that Omomyc forms more stable homodimers (Omomyc/Omomyc) than Myc/Omomyc and Omomyc/Max heterodimers, due to the existence of putative repulsive interactions and/or lack of stabilizing interactions between Omomyc and Myc and Max [160]. Moreover, the electrophoretic mobility shift assay (curiously performed at 12°C) using b-HLH-LZ constructs suggested that Omomyc/Omomyc homodimers are able to bind DNA with an affinity even higher than Myc/Max complexes. Thus, Omomyc/Omomyc would be able to inhibit Myc mainly by competing for its DNA-binding sites. Indeed, the same study demonstrated that mutating the H-E-R aminoacids of Omomyc's basic region responsible for base-specific interactions impaired DNA binding and partially suppressed Omomyc's capability of inhibiting Myc occupancy from its DNA-target regions. An independent study also supported the importance of Omomyc homodimers during Omomyc-based Myc inhibition [106]. In this case, through ChIP-sequencing/qPCR analysis, a reciprocal DNA binding pattern of Myc and Omomyc was observed. In addition, the inhibition of Max binding when Omomyc was expressed indicated that Omomyc occupies Myc-target DNA regions mainly as homodimers, the most abundant state within cells.

These studies are in contrast with previous evidence that defined a potential key role of the ability of Omomyc to effectively dimerize to Myc and Max and the competition of Omomyc/Max dimers with Myc/Max on DNA occupancy [99, 158]. Thus, more investigation is required to fully understand the relative contribution of the different events that Omomyc triggers inside cancer cells to inhibit Myc. Elucidating Omomyc's precise molecular mechanism could lead to the rational design of more effective Myc inhibitors.

### 1.10. Omomyc-derived peptide-based drugs as therapeutic agents

To date, Omomyc has demonstrated an extraordinary potential in inhibiting tumorigenesis and triggering cancer eradication, and it is not clear whether a different molecule could gather all the features that currently make Omomyc an excellent anti-cancer prototype. Therefore, besides investigating new drugs that mimic the mechanism of action of Omomyc, a complementary

strategy would be to create a drug from Omomyc itself. Some reports have claimed that Omomyc cannot be used as a drug since its polypeptide would be too bulky to reach the desired cellular compartment [148, 158, 161]. However, an Omomyc therapeutic peptide could represent an invaluable tool against cancer, since, as previously noted in this thesis, peptides are recognized for providing a potential high selectivity and efficacy, while being at the same time relatively safe, as it is mirrored by the increased interest in peptides in pharmaceutical research and development [162].

#### 1.10.1. Cell-penetrating peptides

As described before, Max\* showed to act as a cell-penetrating peptide (CPP) [148]. Importantly, Omomyc shares a similar structure and properties compared to Max\*, which is formed by a b-HLH-LZ of around 10KDa and a predominant amount of positive charges in the N-terminus basic region. Hence, we posit that if Omomyc harbored an intrinsically CPP potential similarly to Max\*, the peptide could be directly used as a CPP drug.

In fact, CPPs have been successfully applied for intracellular delivery of a variety of cargo molecules, including peptides and proteins [163]. Cationic CPPs, in particular, have shown great potential for intracellular delivery and cross epithelial barriers [164]. Moreover, the so-called “dual-acting CPP” is an emerging concept that refers to those peptides harboring both membrane-permeating and bioactive properties [165] such as neuroprotectant or anti-tumorigenic [166, 167]. Indeed, CPPs have already been tested against oncological pathologies in preclinical models. For example, a TAT-mediated transducible peptide based on the C-terminal regulatory domain of p53 was developed to restore the endogenous proapoptotic activity of the tumor suppressor p53, the most frequently mutated gene in cancer [168]. Systemic administration of the peptide inhibited the growth of subcutaneous tumors, extended the survival of mice harboring terminal peritoneal carcinomatosis and resulted in the generation of disease-free animals that were initially bearing in peritoneal lymphoma. CPPs have been also used to improve the pharmacokinetics and the efficacy of chemotherapeutic agents and siRNAs in preclinical models [169, 170].

All these achievements of CPPs in various preclinical models have encouraged their clinical application. Pharmaceutical companies have thus undertaken clinical development of CPPs against different diseases including

cancer [171]. A recent example of such application is a 28-amino-acid peptide derived from the bacterial protein azurin, p28, which enters cells and inhibits degradation of p53 [172]. The drug entered a Phase I clinical trial to test for potential side effects in patients with p53-positive solid tumors resistant to the standard therapies (NCT00914914). The compound was well-tolerated and effective in patients with disease refractory to prior treatments [173].

Given the number of CPPs that have reached the clinical stage for several diseases, a potential CPP based on Omomyc could be a good candidate for its use in patients. Further, in the case-scenario in which an Omomyc peptide could not be directly delivered as a therapeutic agent itself, various strategies have been proposed to effectively deliver proteins into cells [174]. Among them, lipid drug delivery has shown great promise for use with therapeutic peptides.

#### 1.10.2. Liposomal nanoparticles

Nanotechnology has been used to facilitate the cell-entrance and improve the in vivo biodistribution of several compounds, potentially reducing the side-effects and increasing the efficacy [175]. In particular, liposomes have been successfully used to deliver peptides and proteins such as enzymes, peptide hormones and cytokines such as insulin, IL-2, EGF and IFN- $\gamma$  [176-180].

Liposomes are composed of phospholipids which self-assemble to form spheres of lipid bilayers around an aqueous core, thanks to their amphiphilic nature [181]. Because of the presence of both an aqueous core and a lipid bilayer, liposomes can incorporate hydrophilic and/or hydrophobic drugs, providing a very flexible system for drug encapsulation. A level of versatility is also brought by the possibility of decorating the surface of liposomes with distinct molecules, ligands or antibodies (Figure 11). For instance, the coating of insulin-containing liposomes with polyethylene glycol (PEG) or mucin resulted in long-lasting lowering of glucose levels following oral administration [182]. Intravenous administration of PEG-insulin-liposomes also provided the strongest and longest decrease in glucose, supporting the hypothesis that the concentration in blood is maintained for a longer time thanks to the coating [177]. Especially in cancer, liposomes can also be coated with antibodies or ligands to achieve improved pharmacokinetics by a

high accumulation of the drug in the tumor site. Long-circulating liposomes loaded with doxorubicine and linked to an anti-HER2 monoclonal antibody (trastuzumab) provided targeted drug delivery to HER2-overexpressing cells. Higher efficacy compared to any other combination was observed [183]. Similarly, transferrin-PEG-liposomes displayed specific receptor binding and receptor-mediated endocytosis to target cells expressing transferrin receptor in vivo [184].

The intrinsic characteristics of a pathological zone can also be used to increase the accumulation of drugs in certain tissues. For instance, intratumoral pH is slightly more acidic than blood pH, around 6.5 and 7.4 respectively, due to hypoxia and cell death [185]. Interestingly within cells, pH also varies from cytosol and endosomal vesicles, where it can reach values lower than 5.5. Liposomes sensitive to changes in pH would destabilize and release their content upon a decrease of pH, thus in the tumor tissue or within lysosomes to favor endosomal escape [186]. pH-sensitive liposomes are usually composed of a surfactant with pH-titratable carboxylate groups and fusogenic, conical shaped lipids such as DOPE and weakly acidic amphiphilic such as CHEMS [187]. Cisplatin-containing liposomes for the treatment of peritoneal carcinomatosis displayed longer circulation time and increased tumor uptake compared to the free drug. The lack of efficacy observed in phase I-II clinical trials was attributed to low bioavailability and slow release [188, 189]. The liposomes were then reformulated as pH-sensitive using DOPE, CHEMS and DSPE-PEG and showed higher drug retention by the tumor, higher efficacy and lower toxicity than free cisplatin [190, 191]. External stimuli can also be applied to direct liposomal delivery to targeted tissues, such as used of sterically stabilized magnetoliposomes which can be controlled by magnetic fields [192]. Importantly, the use of liposomes has already been approved by the FDA and Doxil®, a PEG-liposome-encapsulated form of doxorubicin whose use was granted in 1995, represents a good example of it [193].

Hence, liposomal encapsulation of a potential Omomyc-based peptide could be used to improve its solubility, prevent degradation during storage or after administration, avoid recognition by the immune system extending circulating time, and improve pharmacokinetics by passive or active targeting and increase the therapeutic index, all using biodegradable and nontoxic materials.

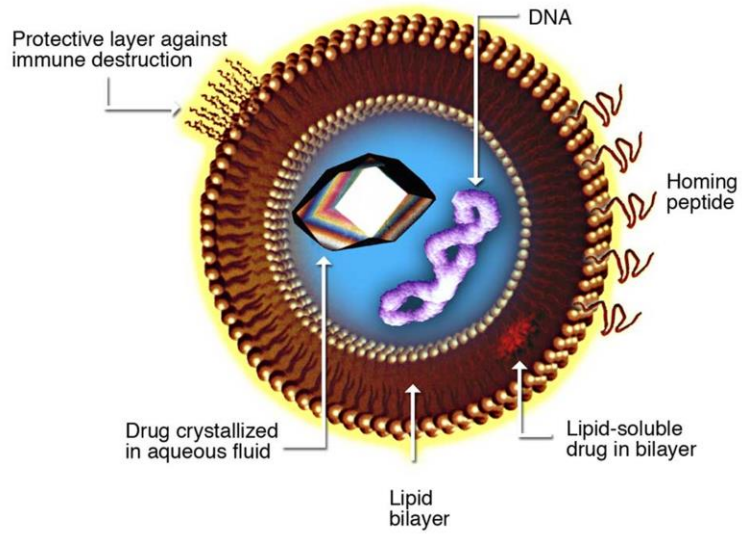


**Figure 11: Schematic representation of a liposome.** Principal features of liposomes, including potential cargos and surface-decorations, are shown.



## Objectives

## 2. Research Objectives

---

The results of this thesis are divided into 2 different sections. Each section is conceived to address specific questions and therefore is formed by its own hypothesis and objectives.

### Section 1:

Investigating Omomyc's fundamental mechanism of action in lung cancer

#### Background

Myc has been described as a common non-redundant node indispensable for cancer cell survival in different cancers. Omomyc, a Myc dominant negative that inhibits Myc's transactivation, has shown dramatic therapeutic potential in various mouse models of cancer. Thus, unravelling the mechanism by which Omomyc produces this effect could lead to the design of more effective Myc inhibitors.

#### Hypothesis

We hypothesize that Omomyc expression in various lung cancer cell lines, which represent one of the most heterogenic types of cancer, will be effective regardless of their diverse mutational profile. In addition, we predict that the different cell lines will show communalities in their response that might underpin Omomyc's anti-tumorigenic action.

#### Objectives:

- Create a lentiviral Omomyc expression vector to generate stable lung cancer cell lines that inducibly express Omomyc.
- Characterize the effects of Omomyc expression in the various cell lines and determine common responses across them.
- Further investigate the common responses that could explain Omomyc's effect on cancer cells and use Omomyc variants to confirm its putative mechanism of action.

### Section 2:

Transforming Omomyc from proof of principle to a clinically viable therapeutic strategy

#### Background

Omomyc has shown dramatic therapeutic potential in various mouse models of cancer. However, Omomyc has been conceived as proof of concept to model Myc inhibition, but not as a potential therapeutic agent itself. Unfortunately, to date, no Myc inhibitor has matched the expectations generated by Omomyc and none has been approved for clinical application.

#### Hypothesis

We hypothesize that an Omomyc peptide could be used as a pharmacological therapeutic approach, either by direct delivery - due to its potential cell-penetrating properties - or by delivering it using liposomal nanoparticles.

#### Objectives

- Use in vivo models derived from human lung cancer cell lines to determine the biodistribution and the therapeutic index of intravenously administered Omomyc-based pharmacological approaches.
- Determine the cell-penetrating potential of an Omomyc peptide and characterize its efficacy in vitro and in vivo
- Engineer other pharmacological strategies to overcome the potential limitations of delivering a “naked” Omomyc peptide.

### 3. Materials and Methods

#### 3.1. Cloning strategy of expression vectors

The original Inducible Dharmacon™ TRIPZ™ Lentiviral shRNA (GE Healthcare) (Figure 12) was kindly donated by Joan Seoane's laboratory (VHIO, Barcelona, Spain). The shRNAmir insertion site was removed from the original vector by ClaI/MluI double digestion and the resulting plasmid was re-circularized to obtain a pTRIPZ-RFP vector. Both the amplicon and the pTRIPZ-RFP vector were digested using AgeI and purified. The Omomyc amplicon was inserted into the AgeI-linearized vector by ligation, upstream the RFP sequence. The ligation product was transformed in competent cells, selected with ampicillin and surviving colonies expanded. DNA was purified by Miniprep (Qiagen) to assess the right orientation of the insert by sequencing. The colony harboring such vector was further expanded and a Maxiprep (Invitrogen) performed to purify the vector.

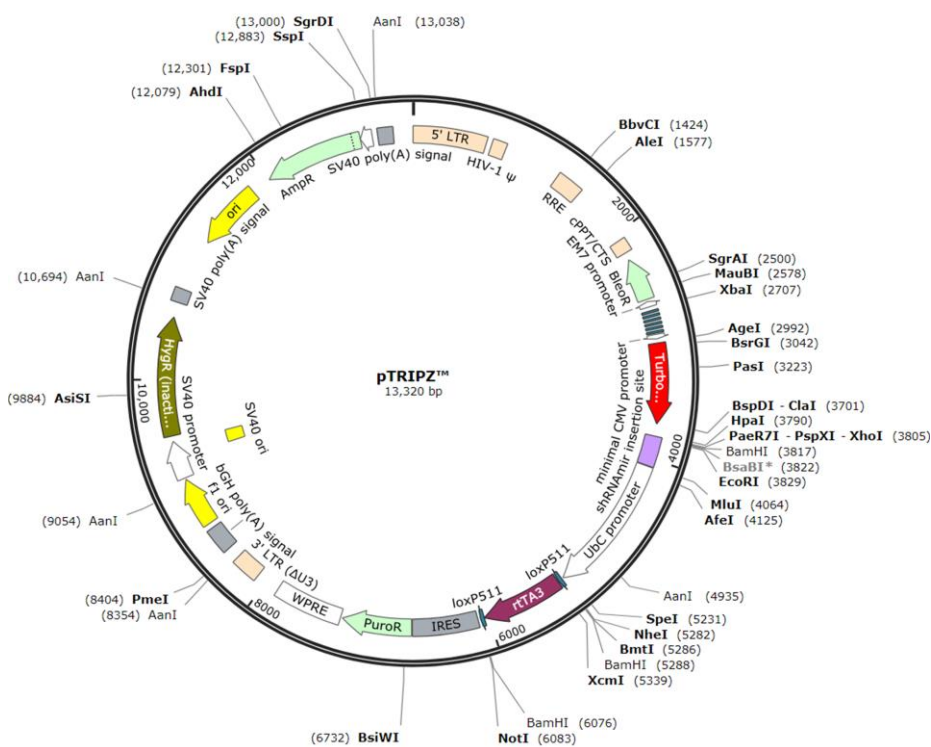


**Figure 12: Schematic representation of the commercial pTRIPZ-RFP lentiviral vector.** Obtained from [www.snapgene.com](http://www.snapgene.com).

OmoHER and  $\Delta$ Myc sequences (provided by the laboratories of Martin Eilers' and Gerard Evan respectively) from unidentified vectors were amplified using the same conditions (see below section). Omomyc sequence was cut out from the new pTRIPZ Omomyc-RFP by Agel digestion. OmoHER and  $\Delta$ Myc amplicons were also digested using Agel and a ligation reaction was performed for both sequences with the Agel-linearized pTRIPZ RFP.

### 3.2. PCR conditions

An Omomyc amplicon was generated by PCR using primers harboring Agel restriction sites at both 3' and 5' extremes. The 3' primer was design to maintain RFP in frame with the Omomyc sequence, to finally express an Omomyc-RFP fusion protein.

The Omomyc sequence was amplified from the pBP-Omomyc vector using the following 5'-Plus and the 3'-Agel primers (5'-GCGCACCGGTACCATGGAGACCGAGGAGAATGTCAAGAGGCGAACACACA-3' and 5'-GCGCACCGGTGAATTCTTCGCACAAGAGTTCCGTAGCTG-3' respectively). The PCR mixture was as follows: 10 $\mu$ L of PCR buffer (Sigma) + 1 $\mu$ L of dNTPs (Sigma) + 1 $\mu$ L of each of the primers (from stocks at 25 $\mu$ M) + 10ng of pBP-Omomyc vector + 0.5 $\mu$ L of Taq DNA polymerase (Sigma) + ddH<sub>2</sub>O to 50 $\mu$ L. A vector-free negative control was included. PCR amplification was initiated at 98°C for 30 seconds followed by 35 cycles of: 98°C for 7 seconds, 55°C for 30 seconds and 72°C for 30 seconds. After the completion of the cycles, an additional elongation step was set at 72°C for 10 minutes. Samples were loaded in an agarose gel and, after confirming the absence of amplified bands in the negative control, the bands that appeared at 300bp were cut in a UV transilluminator and were placed in a 1.5mL tube. The Gel DNA Recovery Kit (Zymoclean) was used to recuperate the DNA from the gel following the manufacturer's protocol. Each gel piece was weighed, 3 volumes of ADB to each volume of agarose were added into the tube and incubated at 50°C until gel slices were completely dissolved (10-15 minutes approximately). The melted agarose was transferred into the Zymo-Spin columns in side collection tubes. Columns were then centrifuged for 1 minute at maximum speed and the flow-through was discarded. 200 $\mu$ L of DNA Wash Buffer were added into the columns and centrifuged for 30 seconds. The washing step was repeated once again. Finally, columns were placed in clean 1.5mL tubes and 30 $\mu$ L of ddH<sub>2</sub>O were added into each to

recover the DNA. All DNA concentrations were quantified using NanoDrop (Thermo).

### 3.3. Restriction enzyme digestion

All enzymes were purchased at New England Biolabs (NEB). Digestions were performed using the recommended buffers for each restriction enzyme according to NEB's website. The components were mixed as follows: 3µg of DNA + 2µL of recommended buffer (10x) + 0.5µL of restriction enzyme + ddH<sub>2</sub>O to 20µL. The digestion was incubated at 37°C for 2 hours.

### 3.4. CIP phosphatase and ligation

Before ligating the Omomyc amplicons inside the pTRIPZ-RFP vector, the Agel-digested pTRIPZ was treated with CIP (Calf Intestine Phosphatase, Roche) to prevent re-circularization. A maximum of 4µg of DNA were incubated with 4µL of phosphatase in 40µL of total volume (4µL of 10x Dephosphorylation Buffer and remaining volume of H<sub>2</sub>O). The mixture was incubated at 50°C for 1 hour. After that, the enzyme was inactivated by adding EGTA to a final concentration of 20mM and heated to 65°C for 15 minutes.

To ligate the Agel-digested Omomyc amplicons and the CIP-treated pTRIPZ-RFP vector, the T4 DNA ligase (NEB) was used. The mixture was as follow: 2µL of T4 DNA Ligase Buffer (10x) + 100ng of vector + 1µL T4 DNA ligase + ddH<sub>2</sub>O to 20µL. To insert Omomyc in the pTRIPZ-RFP vector, the Agel-digested Omomyc amplicons were added into the mixture in different insert:vector DNA mass ratios (for 3:1, 5:1 and 7:1, 6.5ng, 11ng and 15ng respectively). The mixture was incubated 1 hour at room temperature and then left at 4°C overnight.

### 3.5. Bacterial transformation

To transform vectors in competent cells, Max Efficiency® DH5α™ Competent Cells (Thermo) were thawed on ice. The first time, aliquots of 50µL of competent cells in polypropylene tubes were prepared and refrozen in dry ice. 2µL of the ligation product or 10ng of purified DNA were added into 50µL of competent cells and incubated in ice for 30 minutes, gently mixing every 10 minutes. Cells receive then a heat-shock pulse at 42°C for 45 seconds using a thermoblock and placed again in ice for at least 2 minutes. 450µL of S.O.C. (or S.O.B) medium stored at room temperature were added to the

competent cells and shaken at 200 rpm at 37°C for 1 hour. If purified DNA was used to transform, 20µL of cells were spread in LB plates containing ampicillin 100µg/mL (LBA). In case of transforming a ligation, cells were centrifuged at 600rcf, 450µL of supernatant removed and the pellet resuspended in the remaining volume (approx. 50µl) and spread in the LBA plate. The plates were then incubated overnight at 37°C.

### 3.6. Plasmid purification

Colonies from transformation plates were picked using a 100µL-tip and transferred into tubes containing 5mL of LBA. The tubes were then placed in a shaker at 200rpm/37°C and incubated overnight. 1mL of LBA with grown bacteria (LBA should be more opaque than the previous day) was transferred into a 1.5mL tube and centrifuged at 6.000rpm for 10 minutes. The remaining volume was maintained at 4°C to be used as a pre-culture for a Maxiprep (see next paragraph). To extract DNA from the pellet of bacteria, QIAprep® Miniprep (Qiagen) was used applying the manufacturer's protocol. The pellet was resuspended in 100µµof resuspension buffer. 200µL of lysis buffer were then added to the cells and incubated in ice for 5 minutes. 150µL of precipitation buffer were added and incubated for 5 minutes at 4°C. The mixture was centrifuged at 4°C for 10 minutes at maximum speed (13.000rpm) and supernatant transferred to a new tube. 300µL of isopropanol were added and the solution was mixed by inversion and immediately centrifuged at 4°C for 10 minutes at maximum speed (13.000rpm). Pellet was finally resuspended in 100µL of ddH<sub>2</sub>O after letting it dry for 20 minutes at room temperature.

To purify a larger amount of DNA, 500µL of the overnight culture were added in an Erlenmeyer flask containing 300mL of LBA. The flask was left incubating overnight at 200rpm and 37°C. Bacteria were centrifuged at 4.000g for 10 minutes. The MaxiPrep PureLink® HiPurePlasmid Filter Purification kit (Qiagen) was used to extract the DNA according to manufacturer's protocol. The pellet was resuspended in 10mL of resuspension buffer (R3). 10mL of lysis buffer (L7) were then added and incubated for 5 minutes. 10mL of precipitation buffer (N3) were added and mixed by gently inverting the tube. The filter previously equilibrated with 30mL of equilibration buffer (EQ1) was loaded with the bacterial lysate. The filter was removed from the column and 50mL of wash buffer (W8) were added. To elute the DNA, the column was placed in a clean 50mL tube and 15mL of elution buffer (E4) added until

complete elution of the column after 30 minutes. 10.5mL of isopropanol were added into the eluted DNA and centrifuged at 4.000rpm. The pellet was gently washed with 5mL of 70% ethanol, centrifuged again and pellet left drying for 20 minutes before resuspending it in ddH<sub>2</sub>O.

### 3.7. Cell lines

NSCLC cells lines were provided by the laboratories of Jun Yokota (A549, H441, H23, H1975, PC-9, HCC193, N417, PC-14 and H1299), Joaquin Arribas (H292 and HCC827) and Joan Seoane (Hop62). All these cells were grown in RPMI (Life Technologies) supplemented with 10% of FBS and 1% of glutamine. Classification of cancer subtype and EGFR/KRAS status was done according to literature. Experiments with U87-MG cells were performed at Vladimir Torchilin's laboratory (NEU, Boston, USA). U87-MG were grown in DMEM supplemented with 10% FBS. HEK293 cells (a gift from the Arribas laboratory, VHIO) were cultured in DMEM supplemented with 10% FBS and 1% glutamine.

All cells were maintained in a humidified incubator at 37°C and 5% CO<sub>2</sub>. To freeze cells, 10% DMSO was added to the respective complete medium, cell vials were placed in a Mr. Frosty container (Thermo) with isopropanol and maintained at -80°C for at least 48 hours. Then cells were transferred to liquid nitrogen. To thaw cells, vials were placed in contact with water at 37°C for 2 minutes and then all the contents plated in a 10cm dish with 20mL of complete medium. 24 hours later, the medium containing the DMSO was replaced by complete medium.

All cell lines were tested mycoplasma free or cleaned using Plasmocin (Invivogen).

### 3.8. Lentiviral production and transduction of target cells

The same protocol was used to transduce cells with pTRIPZ (Omomyc/OmoHER/ $\Delta$ Myc)-RFP. 5 million HEK293 cells (kindly provided by Joaquin Arribas' laboratory) were seeded in 15-cm dishes in DMEM 10% FBS. 8 hours after cells were treated for 2 hours with chloroquine at a final concentration of 25mM. Cells were then transfected with the DNA using calcium phosphate: 125 $\mu$ L of CaCl<sub>2</sub> were mixed with 1.25mL of 2xHBS (NaCl 280mM + HEPES 100mM + Na<sub>2</sub>HPO<sub>4</sub> 1.5mM; pH 7.12) with the pTRIPZ



vectors (25µg) along with the pMD2G (8.75µg) and psPAX2 (16.5µg) vectors and 1.125µL of sterile water. 24 hours later the medium was replaced by fresh medium containing 5% FBS and 5mM of sodium butyrate. 24 hours later the medium containing viral particles was harvested and filtered through a PES 0.45µM filter. Polybrene and FBS were added to a final concentration of 8mg/mL and 5% respectively to the filtered-medium containing viruses and added to the target cells (first round of infection). HEK293 cells were refed with DMEM 5%FBS + 5mM of sodium butyrate and the same process repeated after 24 hours (second round of infection). At this point, HEK293 plates were discarded. Between the first and the second round of infection, RPMI 10% FBS was added to the target cells for 4 hours. After the second round, cells were allowed to recover for 48 hours in complete RPMI. Then, puromycin was added to transduced cells at a final concentration of 2µg/mL until the non-transduced control was dead. Once the selection was complete, all cells were maintained in 1µg/mL of puromycin.

### 3.9. Induction of Omomyc expression

Either Omomyc-RFP or RFP only were induced in all cell lines by adding a final amount of doxycycline of 0.6µg/mL in the culture media.

### 3.10. Quantification of cell number, RFP intensity and cell size

To directly quantify the number of cells, cell size and RFP expression, cells were trypsinized, centrifuged and resuspended in either medium or PBS and counted with the TALI Image Cytometer (Thermo). 20µL of cell suspension at a concentration between  $5 \times 10^5$  and  $3 \times 10^6$  cells/mL were introduced in R Cellular Analysis Slides and cell number, cell size and RFP intensity were measured.

To estimate cell viability, either AlamarBlue (Thermo) or Cell Titer-Blue (Promega) was used. After treating cells in 96-well plates, medium was removed from the wells. Either of the reagents was diluted 1:10 in complete medium and 50µL of the mixture was added to cells. The plate was incubated at 37°C to allow cells to metabolize the medium until control wells lose the blue intensity (from 1 to 2 hours, depending on the cell line). Fluorescence signal was measured at excitation/emission of 530/590nm.

To measure cell density in 96-well plates, medium was removed after the treatment and cells were fixed with 4% formaldehyde for 20 minutes. Cells were then stained using a solution of crystal violet (Sigma) at 0.5% for 20 minutes. Staining was removed and wells washed twice with tap water. Cells were left to dry up-side-down overnight at room temperature before diluting the dye in 10% acetic acid for 20 minutes in agitation. Crystal violet intensity was measured at 590nm with a spectrophotometer.

### 3.11. BrdU and cell cycle

Cells were plated in 6-cm dishes and treated with doxycycline or untreated for 3 days. BrdU (Sigma) was diluted in water at 20mM and added to cells at a final concentration of 10 $\mu$ M for 2 hours. Cells were then trypsinized, collected and centrifuged (1.500rpm at 4°C). The pellet was washed with cold PBS and centrifuged again. The pellet was resuspended this time in 1mL of cold PBS and then 3mL of cold 100% ethanol was added dropwise while gently vortexing. Cells were stored in the fridge for 2-3 days. Fixed cells were centrifuged and resuspended in cold washing buffer (0.5% BSA in PBS) twice and then incubated for 20 minutes at room temperature in 300 $\mu$ L of denaturing buffer (HCl 2M in ddH<sub>2</sub>O). 1mL of washing buffer was added; cells were centrifuged, resuspended in 500 $\mu$ L of neutralizing buffer (0.5M borate pH 8.5) and incubated 2 minutes at room temperature. Cells were washed with washing buffer and pellet was incubated for 1 hour with 100 $\mu$ L of anti-BrdU-FITC (BD Pharmingen) dilution: washing buffer + 0.5% Tween+ 20% anti-BrdU. Cells were washed and incubated for 30 minutes with propidium-iodide (PI) solution: 25mg/L of PI + Triton X-100 1:1000 in PBS. Alternatively, 2mg/L of DAPI could also be used. FITC and PI intensity were measured by cell cytometry (Navios, Beckman). Analysis and representation of the cytometry results was done either using Cyflogic or FCS Express.

### 3.12. Cycloheximide treatment

To determine the relative protein stability of Max, cells either uninduced or expressing Omomyc-RFP for 2 days were treated with 20  $\mu$ g/mL of cycloheximide (Sigma) for 0, 18, 36 and 45 hours. Cells were then harvested to perform Western Blots.

### 3.13. Immunofluorescence of cells and tissues

To perform immunofluorescence in cultured cells, 13mm-tissue culture coverslips were placed inside 12-well plates and cells were plated on top. Treatments were applied accordingly. Medium was then aspirated, wells washed with PBS and cells fixed using 4% formaldehyde for 15 minutes. Cells were then washed twice with PBS and plates stored in the fridge up to 1 week. In case of storing the cells at 4°C, PBS was warmed at room temperature before proceeding. Cells were then permeabilized with 0.5% of Triton X-100 for 5 minutes. After washing the wells with PBS, blocking solution (PBS 0.2% Triton X-100 + 2% BSA) was added and cells were incubated at room temperature for 1 hour. Primary were diluted in blocking buffer antibodies (1:100 for all of them; anti-Myc N-262 (SantaCruz), anti-Max C-17 (SantaCruz) and anti-Omomyc (primary rabbit polyclonal anti-Omomyc antibody affinity purified and selected against the MYC b-HLH-LZ) and, for each coverslip, 100µL were added in a parafilm placed in a wet chamber. Coverslips were placed upside-down on top of each 100µL. The wet chamber was closed and placed at 4°C overnight. The following day, coverslips were acclimated at room temperature before washing them twice with PBS. Secondary antibodies (either mouse or rabbit) conjugated to Alexa488 were 1:500 diluted in Triton-free blocking solution (to co-visualize Myc or Max with Omomyc-RFP, secondary antibodies conjugated to Alexa488 were used. 100µL of the dilution were placed on parafilm, coverslips placed up-side-down on to each drop of antibody and incubated at room temperature for 1 hour. Cells were incubated with DAPI 1µg/mL for 10 minutes and washed 3 times with PBS. Coverslips were mounted with Dako Fluorescent Mounting Medium (Agilent) on microscope slides. Slides were dried overnight and the next day confocal images were acquired.

To perform immunofluorescence on tissue sections, either lungs or subcutaneous tumors were introduced in tissue cassettes and fixed in a beaker containing 4% formaldehyde for 24 hours. Cassettes were transferred into 70% ethanol and kept in the fridge. Samples were paraffin-embedded, cut and placed on microscope slides. Slides were heated at 65°C overnight and let cool down before proceeding with the deparaffinization. To deparaffinate, samples went through the following washes, during 5 minutes each: xylene (x2), ethanol 100%, ethanol 90%, ethanol 70% and H<sub>2</sub>O. To retrieve the antigens, slides were introduced in Citrate buffer (10mM sodium

citrate, 0.05% Tween 20, pH 6.0) and boiled in a microwave (20 minutes at 400 watts). Buffer and samples were left to recover room temperature around 30 minutes. Slides were washed with PBS twice, permeabilized using PBS-Tween 2% during 30 minutes and washed again. Primary antibodies anti-Ki67 (clone MIB-1, SantaCruz) and anti-Omomyc were mixed in blocking solution (PBS + 3% of BSA) at 1:100 and 1:250 respectively. Slides were placed in a wet chamber. Approximately 120 $\mu$ L of the solution were placed on top of each section and parafilm used to extend the solution across the tissue. Samples were incubated with the mixture of antibodies overnight at 4°C. Samples were brought up to room temperature before washing them with PBS. The secondary antibodies anti-mouse Alexa488 and anti-rabbit Alexa568 (Invitrogen) were mixed 1:500 in Dako REAL Antibody Diluent (Agilent) and DAPI diluted at 1 $\mu$ g/mL. Microscope slides were placed in a wet chamber. Approximately 150 $\mu$ L were added on each tissue section and spread by covering them with parafilm. Samples were incubated for 1-2 hours at room temperature and protected from light. Slides were then washed and tissue sections totally covered by coverslips using Fluorescent Mounting Medium (Agilent). Mounting medium was dried at room temperature for at least 5 hours and fluorescent signal was analyzed in the confocal microscope.

Confocal microscopy images were captured using a Nikon C2+ confocal microscope and NIS-elements software.

### 3.14. Cell synchronization with nocodazole

To synchronize cells in G2/M, H1299 pTRIPZ-Omomyc-RFP cells were plated in 44 15-cm dish at 3x10<sup>6</sup> cells/dish. Doxycycline was added to 22 plates to express Omomyc-RFP. After 2 days, nocodazole (Sigma), previously diluted in DMSO at 10mg/mL, was added into 11 plates both expressing and not expressing Omomyc at a final concentration of 5 $\mu$ g/mL. One dish of each group (-Omomyc-nocodazole; +Omomyc-nocodazole; -Omomyc+nocodazole; +Omomyc+nocodazole) was trypsinized, cells were counted to determine number of cells per plate and cell cycle analyzed by flow cytometry to determine enrichment of G2/M populations. The remaining 10 dishes were prepared for CHIP analysis as described below.

### 3.15. Western Blot

Cells were either treated with doxycycline or untreated for 3 days. After removing the medium, cells were collected using a cell scraper and harvested in 10mL of cold 1mM EDTA in PBS. Cells were first added in a 15mL tube and centrifuged at 1.500rpm. The pellet was resuspended in 1mL of cold PBS, transferred into a 1.5mL tube and centrifuged at 3.000rpm. The supernatant was removed and the pellet was quickly frozen using dry ice and stored at -80°C.

The frozen pellet was resuspended in 100µL of cold RIPA buffer complemented with a Halt Protease Inhibitor Cocktail (Thermo). Samples were incubated in ice for 30 minutes, vortexing them every 10 minutes to help disrupting the cell membrane. Samples were centrifuged at 4°C at maximum speed (13.000rpm) to separate unsolubilised cell debris from soluble components. The pellet was discarded and supernatant kept in ice. Protein concentration was quantified with DC™ Protein Assay (Bio-Rad). For each 980µL of RA reagent, 20µL of RS was added to make up the AS mixture. A BSA standard curve (ranging from 5µg/mL to 0.15µg/mL) was prepared fresh. 5µL of each sample or standard was added into the wells of a 96-well plate. 25µL of the AS mixture and 200µL of the RB reagent were consecutively added into each well. Samples were protected from light and incubated in mild agitation for 15 minutes. Absorbance was measured at 650nm to determine protein quantification. Protein concentrations were diluted to the most diluted sample of the group of samples using RIPA. Laemmli buffer 4x (+15% 2-mercaptoethanol) was added to the samples.

Equivalent protein amounts of each samples or 12µL of molecular marker (Precision Plus Protein™ Dual Color Standards, Bio-Rad) were loaded in 10% or 12%, 15- or 10-well respectively, NuPAGE Bis-Tris Precast gels (Thermo). For electrophoresis, XCell SureLock Electrophoresis Cell (Thermo) was used and gels were run at 125 volts for 3 hours in Running Buffer. Gel cassettes were disassembled and incubated in Transfer Buffer. The PVDF membrane was activated using methanol for 20 seconds, then washed with ddH<sub>2</sub>O and incubated in Transfer Buffer together with the blotting papers and pads. For the transfer, the XCell II Blot Module was used and components placed as sandwich in the following order: pad-pad-paper-gel-membrane-paper-pad-pad. Transfer Buffer was added in the sandwich structure up to until the sandwich was totally covered. DdH<sub>2</sub>O water was added to the outer chamber. The structure was placed in a box with ice to maintain the low

temperature and voltage set at 25-30 for 2 hours. The structure was disassembled and membranes stained with Ponceau S (Bio-Rad). The staining was scanned and used as a protein loading control. Membranes were then washed with PBS-Tween 0.1% (PBS-T) until the staining is gone and blocked for 1 hour in PBS-T + 5% milk (v/w). Membranes were washed 3 times before overnight incubation with the primary antibody. Antibodies were diluted in red solution (5% BSA + azide 0.02%+phenol red) 1:1000 for anti-Myc (9E10, SantaCruz), 1:500 for anti-Max (C-17, SantaCruz). The next day membranes were washed 3 times and incubated for 1 hour with either mouse (for 9E10) or rabbit (for C-17) secondary antibodies conjugated to horseradish peroxidase (HRP) diluted 1:5.000 in PBS-T + 5% milk. Membranes were washed again 3 times before detection using Pierce™ ECL Western Blot Substrate (Thermo). Chemiluminescent signal was revealed using Fuji Medical X-Ray films (FujiFilm).

### 3.16. Co-immunoprecipitation

Once the cell pellets were collected as previously described for Western Blot, they were resuspended in 200µL ice-cold lysis buffer (20mM HEPES pH 7.5, 200mM NaCl, 0.2% NP-40, 0.5 mM EDTA and 10% glycerol). Resuspended cells were placed in ice for 30 minutes and mixed by pipetting every 10 minutes. Cell lysates were centrifuged at maximum speed (13.000rpm) for 10 minutes at 4°C. Supernatant was transferred to a clean pre-cooled tube and 300µL of dilution buffer (20mM HEPES pH 7.5, 200mM NaCl and 0.5mM EDTA) were added. To equilibrate the RFP-Trap®\_MA beads (Chromotek) used to immunoprecipitate RFP, beads were vortexed and 25µL (for each 500µg of protein) diluted in 475µL of ice-cold dilution buffer. Beads were magnetically separated and supernatant removed. Dilution buffer was added and discarded again following the same procedure. Cell lysate was added to the beads, saving 50µL for a parallel Western Blot analysis (input). The bead-lysate mixture was incubated at 4°C for 2 hours in mild agitation. Then, magnetically separate the beads until the supernatant is clear. Save 50µL of the supernatant for parallel Western Blot analysis (depleted fraction). After removing the supernatant, wash the beads twice as previously described. To dissociate the immunocomplexes, resuspend beads in 2x SDS buffer (120 mM Tris/Cl pH 6.8, 20% glycerol, 4% SDS, 0.04% bromophenol blue and 10% β-mercaptoethanol) and incubate the mixture at 95°C for 10 minutes. After

separating the beads, the sample is ready to be loaded, along with the other 2 fractions previously separated.

### 3.17. Production, purification and labelling of Omomyc<sup>CPP</sup>

The Omomyc peptide sequence was reverse transcribed, codon optimized for expression in *E.coli*, cloned in a pET3a expression vector (Novagen) and purified from BL21 (DE3) Arabinose-Inducible (Invitrogen®) bacterial strain using protocols adapted from the Max° purification protocol [194]. Identification of the purified construct was confirmed by mass spectrometry and by western blot analysis. Maleimide conjugation with AlexaFluor488- (Invitrogen), FITC- or DFO- (Macrocylics) moieties to the unique C-terminal cysteine residue of Omomyc was performed according to the manufacturers' indications. The covalently modified peptides were purified from the free labelling agent by cationic exchange followed by size exclusion chromatography, and the complete labelling and purity were confirmed by mass spectrometry analysis, SDS-PAGE and UV spectroscopy. A diagram of the complete process is represented in Figure 13.

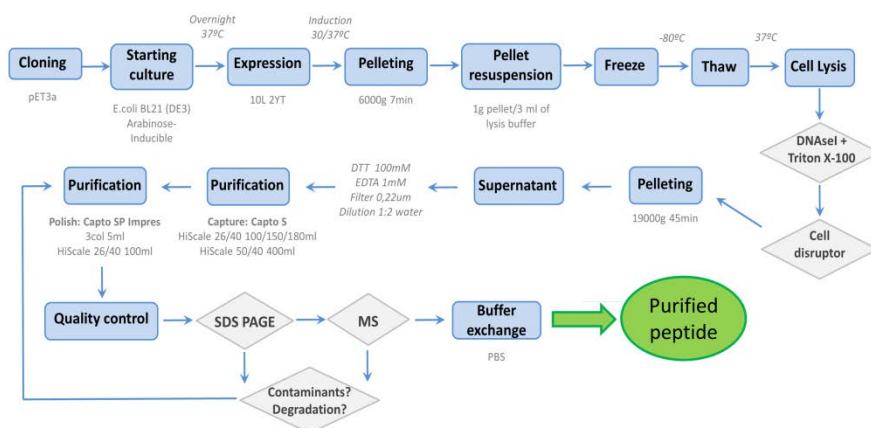


**Figure 13: Schematic representation of the Omomyc<sup>CPP</sup> production procedure.**

### 3.18. Liposomal production and treatment

1,2-dipalmitoyl-sn-glycero-3-phosphocholine (DPPC, Corden), 1,2-dioleoyl-sn-glycero-3-phosphoethanolamine (DOPE, Avanti), 1,2-dioleoyl-sn-glycero-3-phospho-L-serine (DOPS, Avanti), 1,2-dioleoyl-3-trimethylammonium-

propane (DOTAP, Avanti), cholesterol (Sigma) and cholesteryl hemisuccinate (CHEMS, Avanti) dissolved in chloroform were mixed in a round-bottom flask to obtain the desired formulation. Chloroform was evaporated in a rotary evaporator creating lipid films at the bottom of the flasks, which were left overnight in a vacuum chamber. 100 $\mu$ M of purified Omomyc<sup>CPP</sup> (or 90 $\mu$ M of Omomyc<sup>CPP</sup>+ 10 $\mu$ M of Omomyc<sup>CPP</sup>-FITC when specified) were dissolved in encapsulation buffer (10mM HEPES + 9% sucrose) and solutions were used to hydrate the lipid films. The flasks were gently agitated and sonicated to completely dissolve the lipids. Resulting liposomes went through 5 cycle of freeze-thaw and then were extruded through 100nm-membranes. 1,2-Distearoyl-sn-glycero-3-phosphoethanolamine-N-(methoxy(polyethylene glycol)-2000) (PEG2000-PE, Corden) corresponding to 2% of the total amount of lipids was added in a round-bottom glass tube, chloroform was evaporated using nitrogen gas and the tube was placed in a vacuum chamber for 2 hours. Extruded liposomes were added into the tubes containing PEG2000-PE and incubated overnight at 4°C in agitation. Non-encapsulated Omomyc<sup>CPP</sup> was separated from the PEGylated liposomes by injecting the mixture in HiTrap SP HP columns (GE Healthcare Life Science) according to manufacturer's instructions. Encapsulation efficacy and final concentration of Omomyc<sup>CPP</sup> was determined by DC Protein Assay (Bio-Rad) and Omomyc<sup>CPP</sup>-FITC by fluorescent HPLC. Reverse-phase chromatography was used to detect Omomyc<sup>CPP</sup> by UV/Vis absorbance or Omomyc<sup>CPP</sup>-FITC by fluorescence detection. Liposomes were dissolved 1:100 in acetonitrile:water 70:30 and loaded into a C18 column. Size of liposomes was determined using a Zetasizer (Malvern). A diagram of the complete process is represented in Figure 14.

### 3.19. Endocytosis and entrance inhibition

Rhodamine-PE (0.25% molar ratio) was included in the liposomal formulation to produce labelled-liposomes. A549 and U87-MG were plated in 12-well plates at 100.000 cells per well. The following day, cells were pretreated for 1 hour with endocytosis inhibitors: 5.25 $\mu$ M of chlorpromazine (Sigma) was used as inhibitor of clathrin inhibitor; 150 $\mu$ M of genistein (Sigma) as caveolae inhibitor; and 5 $\mu$ M of cytochalasin D (Sigma) as macropinocytosis inhibitor. Cells were then treated with 1mg/mL of rhodamine-labelled liposomes (1:10 dilution of the final production) for another hour.



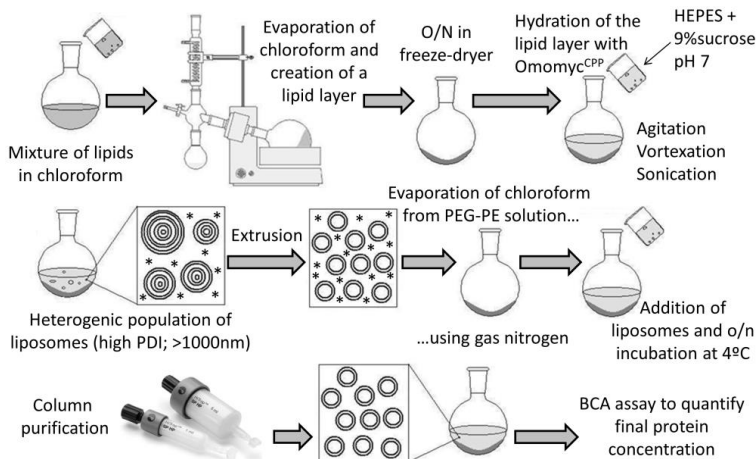


**Figure 14: Schematic representation of the Omomyc<sup>CPP</sup>-encapsulation procedure.** Adapted from [195].

### 3.20. Treatment with modified-mRNA

Omomyc modified-mRNA (Omomyc<sup>mRNA</sup>) sequence was purchased from TriLink BioTechnologies. MessengerMax Lipofectamine (Thermo) was used to transfect the mRNA into cells following the manufacturer's procedure.

To perform efficacy tests, A549 and U87-MG cells were plated in 96-well plates. 24 hours after, medium was removed from the wells and replaced by 50 $\mu$ L/well of serum-free media. Omomyc<sup>mRNA</sup> and lipofectamine were separately diluted in different eppendorfs containing serum-free media. For each 4 $\mu$ g of mRNA in 50 $\mu$ L of media, 3 $\mu$ L of lipofectamine were diluted in 50 $\mu$ L of media. mRNA and lipofectamine were then mixed (in a final volume of 100 $\mu$ L) and incubated for 10 minutes. Media was removed from the first well and the 100 $\mu$ L of lipofectamine+mRNA added. 50 $\mu$ L were then removed and 1:2 serial dilutions were done in the following wells. Therefore, the maximum concentration was 2 $\mu$ g of mRNA in 50 $\mu$ L serum-free media (approximately 200nM) and 1.5 $\mu$ L of lipofectamine. Cells were transfected during 4 hours at 37°C and then transfecting medium was replaced by complete medium. Cells were then incubated for 3 days and cell density determined by crystal violet.

To perform immunofluorescence, cells were plated on coverslips in 12-well plates. In 500 $\mu$ L of FBS-free medium, cells were treated at approximately 200nM (20 $\mu$ g of Omomyc<sup>mRNA</sup> and 15 $\mu$ L of lipofectamine). The cells were maintained in transfecting medium for 4 hours at 37°C and then refed with

complete medium. Cells were fixed 24 hours after refeed and immunofluorescence using the Omomyc antibody was performed as previously described.

### 3.21. ChIP-qPCR and ChIP-sequencing

ChIP experiments were performed in collaboration with Pete Rahl (Syros Pharmaceuticals Inc., Massachusetts, USA) and Bruno Amati (Istituto Italiano di Tecnologia, Milan, Italy). For ChIP-qPCR of Omomyc-RFP expression in A549, approximately  $1 \times 10^8$  A549 cells were treated with doxycycline for 72 hours or untreated. For ChIP-sequencing of Omomyc-RFP expression in H1299,  $1 \times 10^8$  cells were treated/synchronized with doxycycline/nocodazole or untreated as previously described. For ChIP-sequencing of A549 treated with the Omomyc<sup>CPP</sup>,  $1 \times 10^8$  A549 cells were plated; 24 hours later cells were treated with the peptide at 20  $\mu$ M or untreated for 48 hours. After the respective times, medium was removed and cells were cross-linked with 1% formaldehyde solution in PBS for 20 minutes (15mL for 15cm dishes). Glycine was added to the formaldehyde and incubated for 15 minutes. Then cells were washed twice with PBS. Cells were scraped, harvested and frozen in liquid nitrogen. Frozen cells were then shipped to our collaborators for analysis.

Briefly, whole cell extracts were sonicated to solubilize the chromatin. The chromatin extracts containing DNA fragments with an average size of 500 base pairs were immunoprecipitated using an antibody recognizing the N-terminus of Myc (N-262) or Max (C-17).

### 3.22. Animal studies

All the animal studies were performed in accordance with the ARRIVE guidelines and the 3 Rs rule of Replacement, Reduction and Refinement principles. Mice were maintained and treated following the protocols approved by the CEEA (Ethical Committee for the Use of Experimental Animals) at the Vall d'Hebron Institute of Oncology, Barcelona, Spain. All the mice from these studies are immunocompromised females BALB/cAnNRj-Foxn1nu (Balb/c) purchased at Janvier Labs.

To express Omomyc-RFP *in vivo*, H1975 and A549 cell lines were inoculated intrapleurally (Figure 15) as previously described [196] to a total of 32

animals (16 animals for each cell lines). In short, animals were anesthetized with 2.5% of isoflurane, placed with the chest -up and 3/4 of a 27G needle introduced from the lateral between the ribs in an angle of 20-30°C.  $1 \times 10^6$  cells in 100 $\mu$ L of serum-free medium were inoculated to each animal.



**Figure 15: Intrapleural injection of cancer cells in anesthetized mice.**

The progression of the tumors was monitored weekly by IVIS imaging. (IVIS procedure). Images of the thoracic cavity were acquired and quantified. Mice showing 2 consecutive weeks of tumor growth were included in the study and treated with either sucrose (5%) or doxycycline (2g/L in 5% of sucrose) in the drinking water. Both sucrose and doxycycline were replaced by fresh solution twice a week. Luciferase signal from the thorax relative to the day of the treatment was calculated for each week. Weight was recorded twice a week and general health monitored by physical appearance and respiratory distress. Weight-loss of 15% relative to the maximum weight of the animal or severe respiratory distress was established as end-point criteria. The day of euthanasia was recorded to perform survival curves of treated vs. untreated animals. The study was finished at 90 days, when all remaining animals were euthanized.

To initially assess the effect of systemic (i.v.) administration of the Omomyc<sup>CPP</sup>,  $2 \times 10^6$  of were injected subcutaneously to nude mice. For H1975, 15 animals were inoculated with one tumor in each right and left back flank (2 tumors per mouse, 30 tumors in total). Tumor volume ( $\text{mm}^3$ ) was measured according to the following:  $(D \times d^2)/2$ , where “D” represents the larger diameter of the tumor measured with a caliper and “d” the smaller diameter. Tumors were allowed to develop until they reached 100-300 $\text{mm}^3$ . Animals were then randomized in 2 groups (treated and untreated) with

similar means and deviation. Either 93.75mg/kg of Omomyc peptide or sterile PBS were injected intravenously 4 times a week, with resting days every 2 consecutive injections (1101100). Measures were recorded every 3-4 days until a total of 26 days. Weight of the animals was recorded as a measure of their general health the day after the first treatment administration and every 3-4 days later on until day 26. At day 26, 24 hours after the last administration, animals were euthanized, tumors fixed and paraffin-embedded for histological and immunofluorescent analysis.

To determine the efficacy of an increased dose of Omomyc<sup>CPP</sup> and the potential synergy with standard chemotherapy, 2x10<sup>6</sup> H1975 were injected subcutaneously to 50 nude mice in both right and left back flanks (2 tumors per mouse, 100 tumors in total). Tumor volume was measured as described above and when 100-300mm<sup>3</sup> were reached, animals were randomized in 4 different groups (vehicle, Omomyc<sup>CPP</sup> only, paclitaxel only, and combination). Vehicle group was treated with PBS and Omomyc<sup>CPP</sup> group with 187.5mg/kg of Omomyc<sup>CPP</sup> following the same regimen previously described (1101100). Paclitaxel, alone or in combination, was administered at 5mg/kg twice weekly leaving resting days between the treatments (1001000). Weight and tumor size were recorded every 3-4 days until day 29.

### 3.23. In vivo biodistribution

In vivo biodistribution was performed in collaboration with Miguel Angel Morcillo (CIEMAT, Madrid, Spain).

Omomyc<sup>CPP</sup>, Omomyc<sup>CPP</sup>-DFO and mice subcutaneously inoculated with H1975 cells were supplied to CIEMAT. Omomyc<sup>CPP</sup>-DFO concentration was estimated by measuring the absorbance at 280nm using the relationship that an A<sub>280</sub> of 0.24 = 0.1mM (obtained from Omomyc<sup>CPP</sup>).

For radiolabelling of Omomyc-DFO, <sup>89</sup>Zr (T<sub>1/2</sub>=78.4 h, β<sup>+</sup>=22.6%; ~2.7 GBq/mL supplied in 1M oxalic acid) was obtained from BV Cyclotron VU (Amsterdam, The Netherlands). The required volume of <sup>89</sup>Zr-oxalic acid solution corresponding to 74 MBq was adjusted to a total volume of 200μL using 1M oxalic acid; 90μL of 2M Na<sub>2</sub>CO<sub>3</sub> (Sigma) were added and incubated for 3 min at room temperature. 1mL of 0.5M HEPES and 710μL of Omomyc-DFO (2.17 mg/mL) were added and incubated at room temperature for 60 min on a rotating shaker; pH was checked to be at 7.0-7.5. The reaction mixture was

loaded on a previously equilibrated PD-10 column and eluted with phosphate-buffered saline (PBS) into fractions of 500 $\mu$ L. The collected fractions were measured in a dose calibrator (IBC, Veenstra Instruments). Quality control was performed by instant thin-layer chromatography (ITLC) on ITLC strips (model 150-771, Biodex) using 0.02M citrate buffer (pH 5.0):acetonitrile (9:1) as eluent. The radiochemical yield, purity, and specific activity of the Omomyc-DFO-<sup>89</sup>Zr used in this study were >98%, >99% and 34 MBq/mg respectively, assuming virtually complete recovery of the Omomyc-DFO-<sup>89</sup>Zr conjugates after size exclusion chromatography; therefore, the compound was used with no further purification. Stability studies in HS and PBS at 37°C showed that more than 99% of the radiotracer remained intact after 24h, whereas in DTPA, more than 96% of the radiotracer remained intact after 24h at 37°C, showing that Omomyc-DFO-<sup>89</sup>Zr constitutes a suitable probe for *in vivo* studies.

4.3 mg/kg of Omomyc-DFO-<sup>89</sup>Zr were administered via tail-vein injection. Ex vivo biodistribution of Omomyc-DFO-<sup>89</sup>Zr was quantified at 3 days post-injection. Manually drawn regions of interest (ROIs) in PET images or ROIs selected from PET images using CT anatomical guidelines (such as in subcutaneous tumors) were used to determine the mean radiotracer accumulation in units of percentage injected dose per gram (%ID/g) using the decay-corrected injected dose and dividing the obtained average tracer concentration (kBq/cm<sup>3</sup>) in the region by the total ID (kBq), under the assumption that the density of tissues was 1g/cm<sup>3</sup>: %ID/g=Injected dose (kBq)/ kBq/cm<sup>3</sup> (measured in ROI). A calibration factor predetermined by scanning a cylindrical phantom containing a known activity of <sup>89</sup>Zr was used to convert counts per pixel/sec to kBq/cm<sup>3</sup>. PET imaging experiments were conducted on a small-animal Argus PET-CT scanner (SEDECAL, Madrid, Spain).

## 4. Results

---

Section 1: Investigating Omomyc's  
fundamental mechanism of action in  
lung cancer

#### 4.1.1. Design and characterization of an Omomyc-RFP inducible vector

To enable inducible expression of Omomyc *in vitro*, we cloned the Omomyc sequence into a commercial doxycycline-inducible vector, placed upstream and fused to the RFP protein at the 3' extreme (Figure 16A). Sequencing was used to assess the correct insertion of the sequence (Figure 16B).

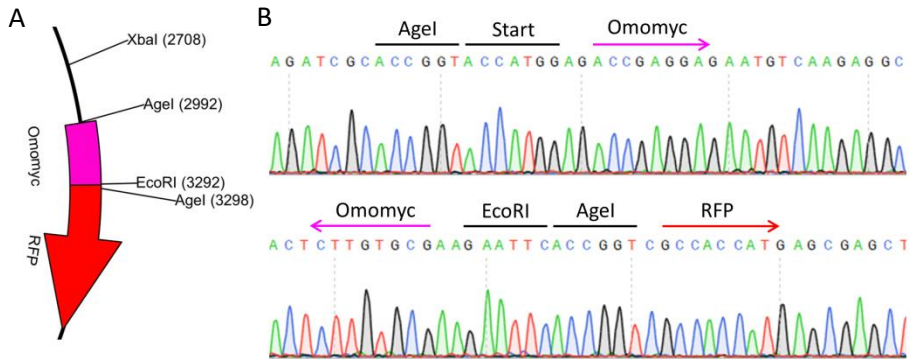


**Figure 16: Omomyc was cloned inside the AgeI site of the pTRIPZ-RFP vector.** (A) Schematic representation of the insertion is shown. Numbers in brackets indicate the position of the restriction site. The red arrow indicates the direction of the transcription. (B) Sequencing confirmed the insertion of Omomyc within AgeI sites and upstream of RFP. Upper sequence represents the 5'-extreme of Omomyc and the upstream elements (AgeI restriction site and Kozak starting site). Lower sequence represents the 3'-extreme of Omomyc and the downstream elements (EcoRI and AgeI restriction sites, and the beginning of the RFP sequence (placed in frame with Omomyc)).

To assess the expression of this newly generated Omomyc-inducible vector, the A549 NSCLC cell line was transduced with lentiviruses harboring either the Omomyc-RFP or the control RFP plasmids. The resulting cells were selected with puromycin until non-transduced cells were all dead. Omomyc-RFP was induced with doxycycline (0.6 mg/ml) and cells were analyzed and collected after 48 hours. By fluorescent microscopy, differences in the subcellular localization between the RFP products of the 2 vectors were observed: while RFP alone distributes throughout the whole cells, Omomyc-RFP accumulates mainly in the nuclei (as expected for the Omomyc protein) (Figure 17A). Cells were then trypsinized and analyzed by cell cytometry and Western Blot. Cytometry analysis showed that in both Omomyc-RFP and RFP

infected cells more than 99% of the population was red, being the control RFP-only cells the ones that displayed higher red intensity (Figure 17B). Omomyc expression and lack of leakiness in the untreated cells was confirmed by Western Blot (Figure 17C). Since Omomyc DNA sequence is around 270bp and RFP is 700bp, the resulting fusion protein appeared, as expected, around 35KDa.

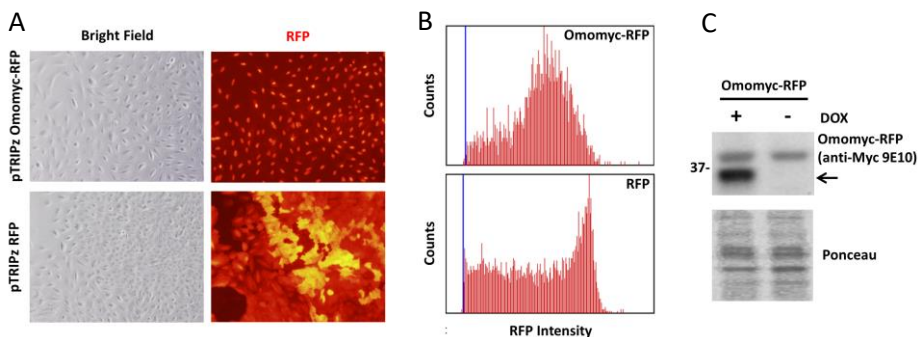


**Figure 17: Inducible expression of Omomyc-RFP in A549 using doxycycline results in a protein of predicted size (35KDa) and nuclear RFP fluorescence.** Cells transduced with either pTRIPZ Omomyc-RFP or RFP only were treated with doxycycline for 48 hours. (A) Cellular localization of Omomyc-RFP and RFP are shown by microscopy and (B) RFP intensity determined by cytometry. (C) Switchability of vector and size of the expressed construct were confirmed by Western Blot. Cells transduced with pTRIPZ Omomyc-RFP were either treated (+) with doxycycline (DOX) or left untreated (-) for 2 days. Protein extracts were then collected and immunoblot performed against Omomyc using the 9E10 anti-Myc antibody. Ponceau S is shown as protein loading control.

#### 4.1.2. Anti-tumorigenic efficacy of Omomyc-RFP expression in A549

To determine the functionality of the Omomyc-RFP product expressed from this new doxycycline-inducible vector, Omomyc-RFP and RFP expression were switched on in A549 for 3, 6 and 9 days. Cells were fixed at each time point and stained with crystal violet to look at cell density (Figure 18A). Then, the cell-bound dye was dissolved and absorbance measured. Quantification of crystal violet absorbance showed that cell growth is significantly inhibited when Omomyc-RFP is expressed (Figure 18B). In contrast, no effect was detected upon RFP expression.



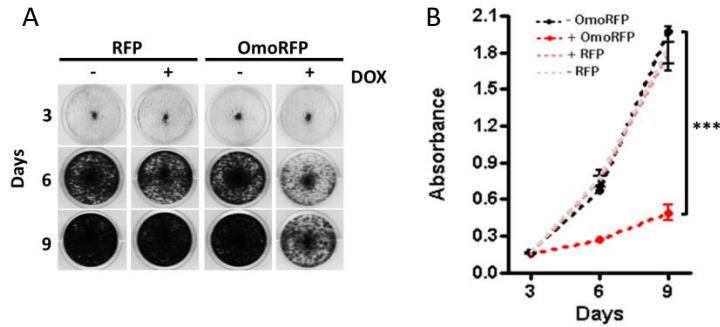


**Figure 18: Omomyc-RFP expression causes a reduction in cell growth of A549 cells.** (A) Images of fixed pTRIPZ Omomyc-RFP (OmoRFP) or RFP only (RFP) A549 cells after 3, 6 and 9 days, either doxycycline treated (+) or untreated (-), stained using crystal violet. (B) Quantification of cell density by absorbance at 560nm after dissolving the crystal violet in acid acetic. Means and standard deviations of one representative experiment out of 2 independent experiments performed are shown. Significance was determined by Student's t-test. "-OmoRFP" vs. "+OmoRFP" shows statistical significance at 6 and 9 days,  $p < 0.001$  (\*\*\*). Comparisons between the other groups show no statistical significance.

#### 4.1.3. Myc inhibition in A549 upon Omomyc-RFP expression

As previously mentioned, Omomyc is able to inhibit Myc by different mechanisms: it can sequester Myc away from DNA, sequester Max away from Myc, and/or bind DNA forming Omomyc/Max heterodimers or Omomyc/Omomyc homodimers. All of these events will trigger a common downstream effect: an impairment of Myc to occupy its target-binding sites. Therefore we started assessing whether Omomyc-RFP expression was able to inhibit Myc occupancy on DNA by ChIP-qPCR. To do so, Omomyc-RFP was expressed in A549 for 3 days; cells were then fixed, harvested and frozen. Samples were sent to Syros Pharmaceuticals, where our collaborator, Dr. Pete Rahl, performed the ChIP analysis. Myc and Omomyc-RFP were ChIPped separately in parallel experiments using anti-Myc (N-262) and anti-Omomyc, a polyclonal antibody specifically generated against Omomyc by our laboratory. Quantification of key Myc *bona fide* DNA-binding sites showed a decrease of Myc binding when cells expressed Omomyc-RFP (Figure 19A). Using our specific Omomyc polyclonal antibody, Omomyc-RFP was detected bound to Myc-target regions where Myc was displaced (Figure 19B). These

results confirm that Omomyc-RFP occupies Myc-binding sites and displaces Myc, therefore acting as an inhibitor of Myc-dependent transcription.

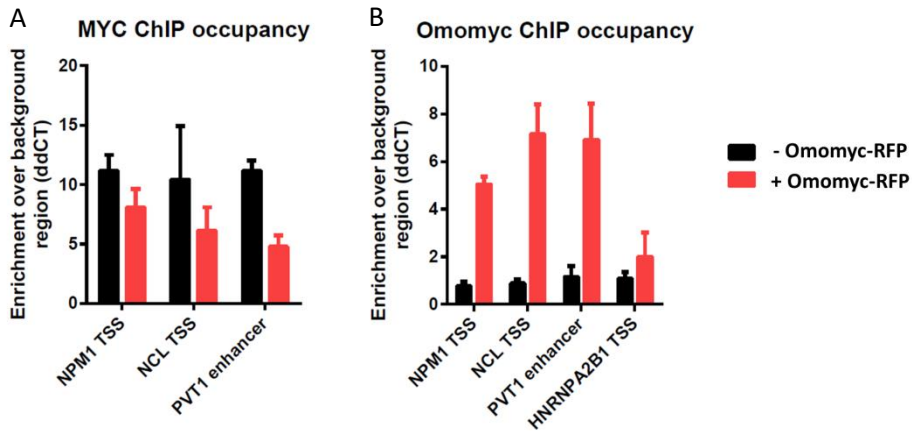


**Figure 19: Omomyc-RFP binds to specific Myc binding sites and inhibits Myc occupancy.** Quantifications by qPCR of Myc-target DNA regions (NPM1, NCL and PVT1 transcription sites) obtained from (A) Myc-ChIP and (B) Omomyc-ChIP are shown. Quantification from untreated (-Omomyc-RFP) and doxycycline treated (+Omomyc-RFP) cells are represented with black and red respectively. The Myc-unrelated HNRNPA2B1 transcription starting site (TSS) is also shown in the Omomyc-ChIP as negative control.

#### 4.1.4. Evaluation of Omomyc-RFP's efficacy in different lung cancer cell lines

Myc is one of the most frequently overexpressed and/or deregulated oncogenes in several malignancies, which makes it an interesting therapeutic target in many types of cancer. Consistently, several publications show that Myc inhibition by Omomyc is effective against different tumor models, suggesting that Omomyc might be used to treat different cancers regardless of their genetic profile. However, most of the data in literature are related to mouse tumors, not necessarily representative of human mutational heterogeneity. Hence, to determine whether Omomyc is equally effective against human cancer cells harboring different mutations, we made use of a panel of cell lines from lung cancer (one of the most heterogeneous types of cancer). The panel depicted in Table 1 is mainly divided according to the KRAS and EGFR status, the 2 most frequently mutated oncogenes in NSCLC. However, cell lines harboring mutations in other oncogenes such as NRAS,

RAF, PI3K and RET mutations, or in tumor suppressor genes like p53, LKB1, p16, BRG1, RB, FOXO3 and FOX2L, and cells resistant to tyrosine kinase targeted therapies (H1975 and HCC827) are also represented. Clearly, additional molecular alterations can also be present in the cell lines besides the ones mentioned in the table. Finally, a cell line representing another subtype of lung cancer, small-cell lung cancer (SCLC), was also included in the panel as additional control. All these cell lines showed differences in their cell size, morphology and proliferation rates, which evidences their high heterogeneity. Again, as shown before for A549, lentiviral particles were generated using the pTRIPZ Omomyc-RFP vector and used to transduce the whole panel of 12 cell lines (Table 1).

| Lung cancer cell line | Subtype | KRAS or EGFR mutation | Other mutations     |
|-----------------------|---------|-----------------------|---------------------|
| HCC193                | AD      | None                  | -                   |
| H1299                 | LCC     | None                  | NRAS;p53;FOXO3;BRG1 |
| H292                  | SCC     | None                  | p16;NF2;PI3K        |
| PC14                  | AD      | None                  | p53;p16             |
| N417                  | SCLC    | None                  | p53;RB              |
| H441                  | AD      | KRAS                  | p53;FOXL2           |
| H23                   | AD      | KRAS                  | p53;LKB1;RET        |
| A549                  | AD      | KRAS                  | p16;LKB1;BRG1       |
| Hop62                 | AD      | KRAS                  | P53;RAF             |
| HCC827                | AD      | EGFR                  | p53                 |
| H1975                 | AD      | EGFR                  | p16;PI3K;p53        |
| PC9                   | AD      | EGFR                  | p16                 |

**Table 1: Panel of 12 lung cancer cell lines selected for the study.** The name of the cell line, the lung cancer subtype (AD: adenocarcinoma; LCC: large cell carcinoma; SCC: squamous cell carcinoma; SCLC: small-cell lung cancer), the status of both KRAS and EGFR (None: wild-type for both (yellow); KRAS: only KRAS mutated (red); EGFR: only EGFR mutated (blue)) are represented. Other additional mutations in different oncogenes and tumor suppressors are also mentioned. The list of mutations was obtained from ATCC and COSMIC databases.

After inducing Omomyc-RFP for 6 days using doxycycline, cell growth and Omomyc-RFP levels were determined (Figure 20A). Cell counts of treated plates relative to the untreated counterparts demonstrated that all the cell lines responded to Omomyc by presenting fewer number of cells at the endpoint. A similar degree of response was observed in all the cell lines, leading to treated cell numbers being only 13 to 35% compared to their respective controls. These different responses did not correlate with the status of KRAS, EGFR or any other oncogene or tumor suppressor identified in Table 1. Quantification of Omomyc-RFP levels by RFP intensity revealed a high variability across the different samples, but are more likely to reflect Omomyc expression levels. However, an XY representation of the response vs. the RFP expression shows that a group of cell lines (HCC827, PC9, H292 and H1975 – all presenting alterations in EGFR) displays a similar response compared to other cell lines that express higher levels of Omomyc (PC14, A549, HCC193 and Hop62) (Figure 20B). This observation seems to indicate that, while all the cell lines responded to Omomyc regardless their mutational profile, cell lines presenting alterations in EGFR are prone to respond more effectively.

To further investigate the anti-tumorigenic effects of Omomyc on cell proliferation and cell death, representative cells from each group (KRAS mutated, EGFR mutated and KRAS/EGFR wild type) were selected. Cells were treated with doxycycline for 3 days, then exposed to BrdU for 2 hours and fixed. Incorporated BrdU was detected using an anti-BrdU antibody tagged with FITC and cell cycle analyzed by propidium iodide (Figure 21A-C). In all the 6 selected cell lines, Omomyc expression produced a reduction of BrdU incorporation (Figure 21D), indicating a decrease in proliferation, and an increase in G1 (Figure 21E). Interestingly, quantification of the subG1 fraction showed a significant increase in only 3 cell lines, one of which is KRAS mutated, and expresses the highest Omomyc levels (Hop62), and the other 2 present constitutively active EGFR (Figure 21F). Together, these results show that the response to Omomyc is mainly reflected by a reduction in cell proliferation, accompanied in some cases by an increase in cell death. Overall, Omomyc expression seems an effective anti-tumorigenic approach in all the cancer subtypes, independently of their genetic alterations.

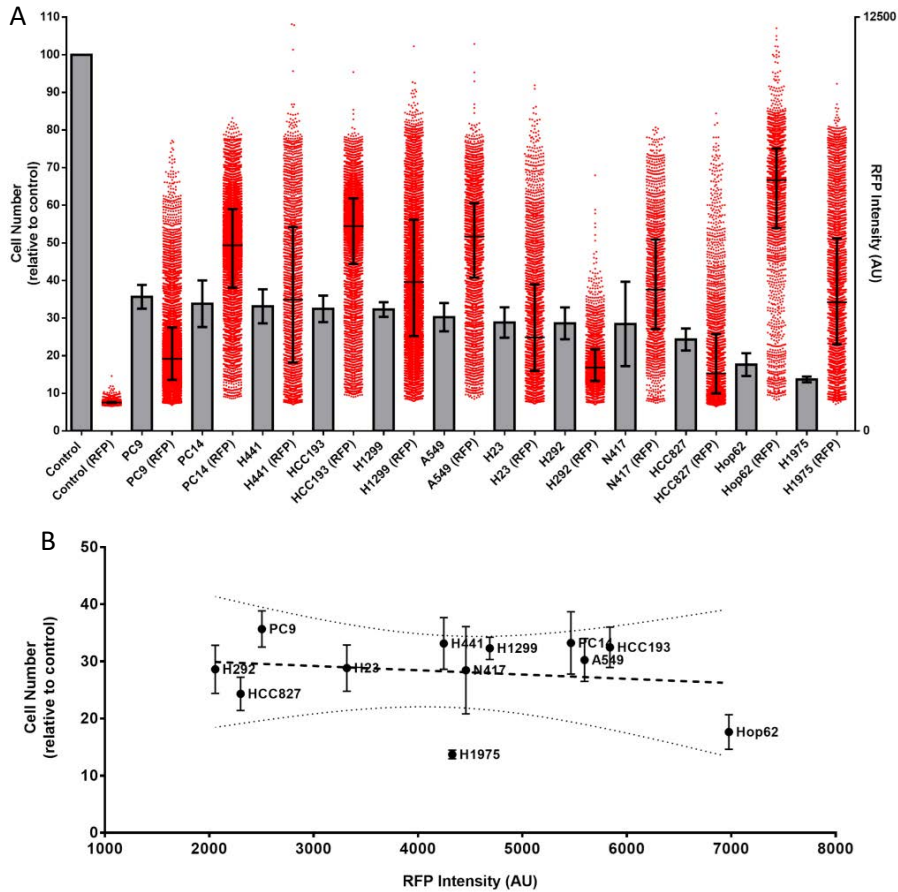


**Figure 20: Omomyc displays anti-tumorigenic efficacy in the selected panel of lung cancer cell lines.** (A) Relative cell number of cells after 6 days of Omomyc expression compared to the untreated counterparts (grey bars, left axis) and Omomyc-RFP expression levels determined by RFP-intensity (red dots, right axis). For cell counts, mean and standard deviation of 3 independent experiments are represented. Statistical significance was determined by Student's t-test. All the values show statistical significance when compared to each untreated counterpart,  $p < 0.0001$  (not represented). For RFP intensity, a representative cytometry result is shown; mean and standard deviation of the events is represented. (B) XY representation of relative cell number at 6 days and the RFP-intensity of the different cell lines. 95% confidence intervals are defined by the dotted lines.

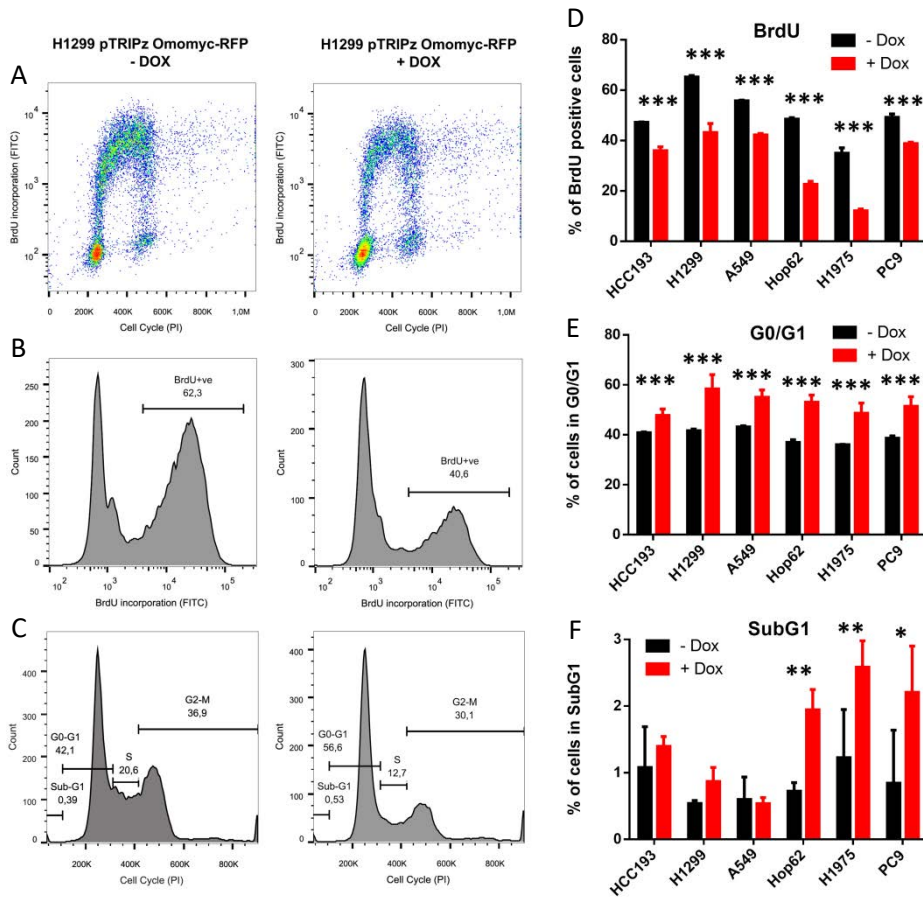


**Figure 21: Omomyc expression reduces cell proliferation, increases cells in G1 and, in some cells, increases the SubG1 population.** (A) Dot plots of cell cycle (x axis) and BrdU incorporation (y axis). (B) Histograms of BrdU incorporation and (C) cell cycle. Left panels show control cells (-DOX) and right panels correspond to Omomyc-expressing cells (+DOX). Bar graphs show (D) quantification of BrdU incorporation, (E) G0/G1 population and (F) SubG1 population. Student's T-test was used to assess statistical significance;  $p < 0.05$  (\*),  $p < 0.01$  (\*\*) and  $p < 0.001$  (\*\*\*). One representative experiment is represented out of 2 independent experiments performed.

#### 4.1.5. Omomyc-RFP's dependent macroscopic change

Given the broad efficacy of Omomyc expression in all cell lines regardless of the mutational profile, we hypothesized that Omomyc might trigger similar alterations at the molecular level as well. According to this line of thought, we aimed at finding communalities in the response of all the cell lines when

Omomyc is expressed. For example, an increase in cell size was detectable by microscopy upon Omomyc-RFP expression across a representative group of cell lines (Figure 22A). Quantification of cell size by TALI confirmed the bigger size even when cells are trypsinized, indicating that their diameter is not only dependent on their ability to adhere to plates (Figure 22B). This result was confirmed by cytometry analysis: gating cells with different levels of Omomyc-RFP expression showed that this increase in cell size is more pronounced in individual cells expressing higher levels of Omomyc (Figure 22C). Further investigation will be required to determine the source of this intriguing phenotype that is displayed by virtually all the cell lines expressing Omomyc.

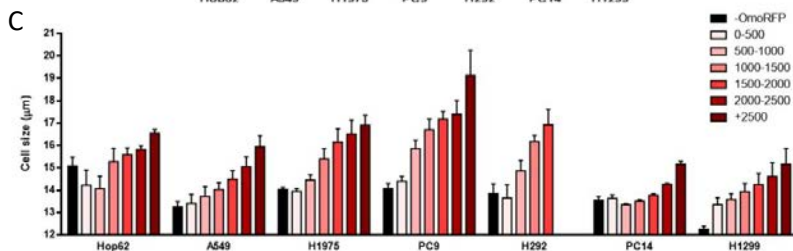
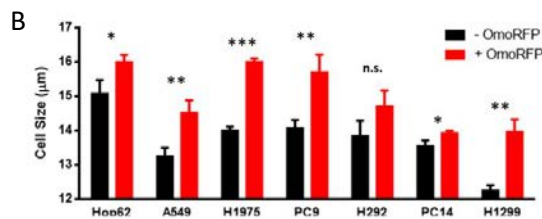
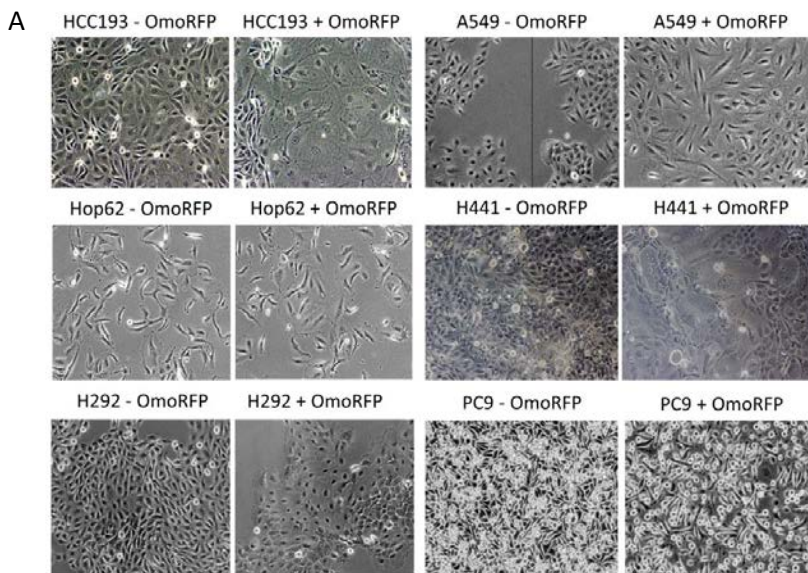


**Figure 22: Omomyc expression produces an increase in cell size in all the cell lines.** (A) Microscopy images of control cells (-OmoRFP) and Omomyc-expressing cells (+OmoRFP). (B) Average cell size determined by Tali cytometer of Omomyc expressing cells (red) and control counterparts (black). Means and standard deviations of 3 independent experiments are represented. P-values were calculated using a two-tailed Student's T-test;  $p < 0.05$  (\*),  $p < 0.01$  (\*\*) and  $p < 0.001$  (\*\*\*). (C) Cell size of a populations selected by gating increasing Omomyc-RFP intensities. Darker red indicates higher RFP intensity and black represents control cells.

#### 4.1.6. Characterization of the effect of Omomyc expression on Myc and Max levels and their subcellular location

Since Omomyc-RFP can bind to both Myc and Max, we decided to look at the protein content of both partners in several cell lines by Western Blot. Cells were collected after 3 days of Omomyc expression and lysed using RIPA buffer. Equivalent amount of total protein were loaded in the wells. The 9E10 anti-Myc antibody was used to detect both Omomyc and Myc, and the C-17 anti-Max antibody to detect Max. First, we confirmed that despite presenting different protein levels of Myc and Max, Omomyc expression was effective across the various cell lines. Second, we looked at whether Myc and Max protein levels were affected by Omomyc expression. No consistent changes in Myc levels were detected upon Omomyc treatment (Figure 23A). However, Max showed an increase in all the cell lines when Omomyc was expressed. We hypothesized that this increase could be triggered by Max forming more stable complexes with Omomyc than with other partners or in its monomeric form. Thus, protein stability was determined for Max in the presence and in the absence of Omomyc using cycloheximide to stop protein synthesis. Addition of cycloheximide to Omomyc-expressing Hop62 and PC9 showed a more pronounced stabilization of Max after 45 and 18 hours of treatment respectively (Figure 23B). Hence, Max protein increase is, at least in part, caused by its stabilization.

In parallel to Max stabilization following Omomyc expression, we observed communality in all treated cell lines. Since the Omomyc transgene is tagged with RFP, the expressed construct can be seen by epifluorescence. This allowed us to observe that Omomyc-RFP co-localizes with condensed DNA during mitosis in all cells. More in detail, to visualize both Omomyc-RFP and DNA at the same time, cells were seeded on coverslips, treated with



doxycycline and fixed after 3 days. Then, cells were permeabilized, DNA stained using DAPI, coverslips mounted and Omomyc/DNA visualized by confocal microscopy (Figure 24).

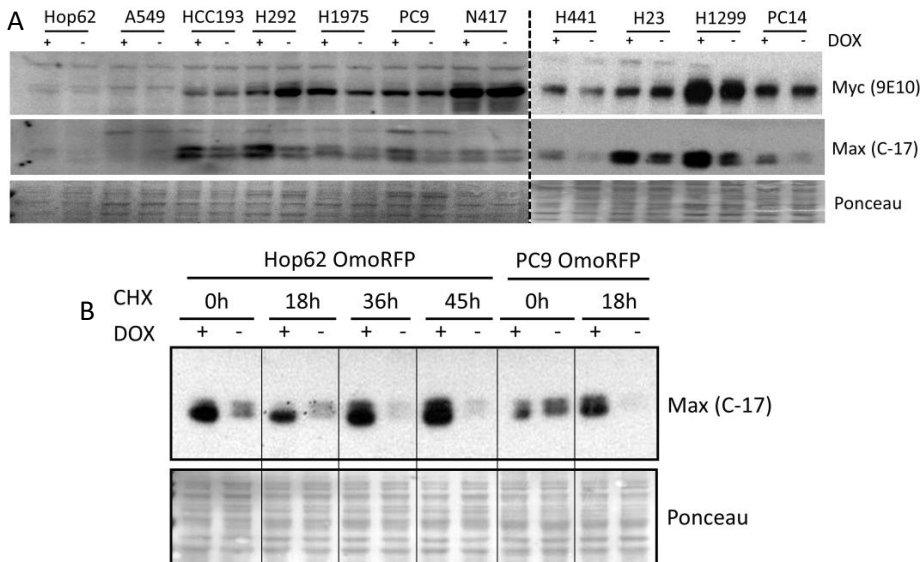


**Figure 23: Omomyc expression stabilizes Max in the different cell lines.** (A) Western Blots against Myc and Max were performed using extracts untreated (-) and treated (+) with doxycycline (DOX) from different cell lines. All the cell lines were stably transduced with the pTRIPZ Omomyc-RFP vector. A representative Western Blot out of 2 independent experiments performed is shown. (B) Hop62 cells (expressing (+) or not (-) Omomyc-RFP) were treated with cycloheximide (CHX) for 18, 36 or 45 hours before collecting the protein extracts. PC9 cells were treated for 18 hours only. Ponceau S is shown as protein loading control.

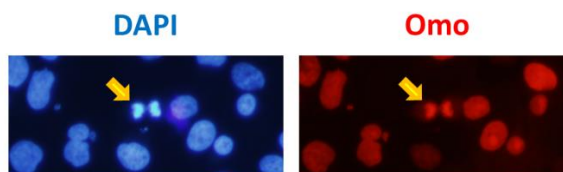


**Figure 24: Omomyc co-localizes with DNA when it condenses during mitosis.** Omomyc is tagged with RFP while DNA was stained using DAPI. Images were acquired by confocal microscopy.

To investigate whether this co-localization is a common feature of similar transcription factors and whether Omomyc is able to affect the localization of its binding partners Myc and Max during mitosis, 3-day untreated and doxycycline-treated cells were fixed, permeabilized and immunofluorescence was performed against Myc and Max as well. Confocal images of the immunofluorescence show that neither Myc nor Max displays a co-localization with mitotic DNA in normal conditions, in the absence of Omomyc (Figure 25A). However, when Omomyc is expressed, while Myc still presents poor co-localization with mitotic DNA, Max shows a different distribution and co-localizes with both Omomyc and DNA (Figure 25B). To show that this observation is independent of the molecular context, cell lines harboring different mutations and different levels of Myc/Max were stained. Regardless of the mutational profile and, importantly, the Myc and Max protein levels, all the cell lines show a Max re-localization on mitotic DNA when Omomyc was expressed (Figure 26).

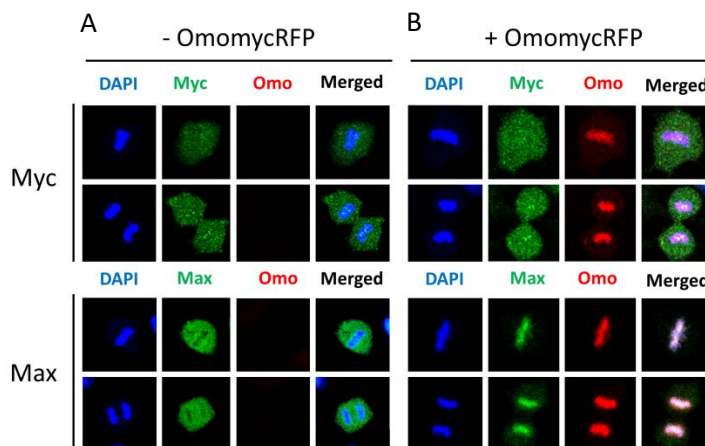


**Figure 25: Max, but not Myc, co-localize with DNA during mitosis only when Omomyc is expressed.** (A) Control cells (-OmoRFP) or (B) cells treated with doxycycline to express Omomyc (+OmoRFP) were fixed at 3 days and immunofluorescence was performed against Myc and Max. Images of cells presenting condensed DNA were acquired using confocal microscopy. Blue channels shows DNA, green channels shows either Myc or Max and red channel shows Omomyc. Images show one representative experiment out of 3 independent experiments performed.

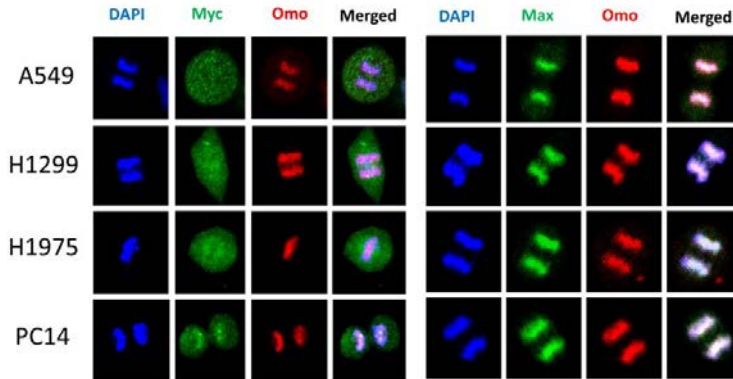


**Figure 26: Omomyc and Max co-localization with DNA is a common feature of all the cell lines analyzed.** Cells were treated with doxycycline to express Omomyc, fixed after 3 days and immunofluorescence was performed against Myc and Max. Images of cells presenting condensed DNA were acquired using confocal microscopy. Blue channels shows DNA, green channels shows either Myc or Max and red channel shows Omomyc. The experiment was performed once.

#### 4.1.7. Characterization of genome-wide changes in Myc and Max DNA-binding upon Omomyc expression

To characterize the molecular consequences of these observations during cell division more in detail, we decided to perform ChIP-sequencing analysis on actively dividing H1299 cells (G2/M) and compare the DNA-binding patterns to non-dividing cells (G1). To that end, a procedure to synchronize cells in G2/M using nocodazole was established (see materials and methods). Synchronization of cells with nocodazole is visualized in culture as an increase in rounded cells, corresponding to cells in mitosis (Figure 27A). Nocodazole, as an inhibitor of microtubule polymerization, impairs the normal arrangement of condensed DNA. Despite that, Omomyc can still be seen as co-localizing with DNA (Figure 27B). Flow cytometry analysis confirmed an increased percentage of dividing cells (G2/M) of more than 2-fold upon nocodazole treatment compared to the untreated cells (for both Omomyc expressing and non-expressing cells) (Figure 27C). As a side note, the decrease of cells in G1 as a consequence of nocodazole treatment was more dramatic in cells that did not express Omomyc (4.0-fold and 1.7-fold respectively), consistent with the role of Omomyc in promoting G1 arrest.

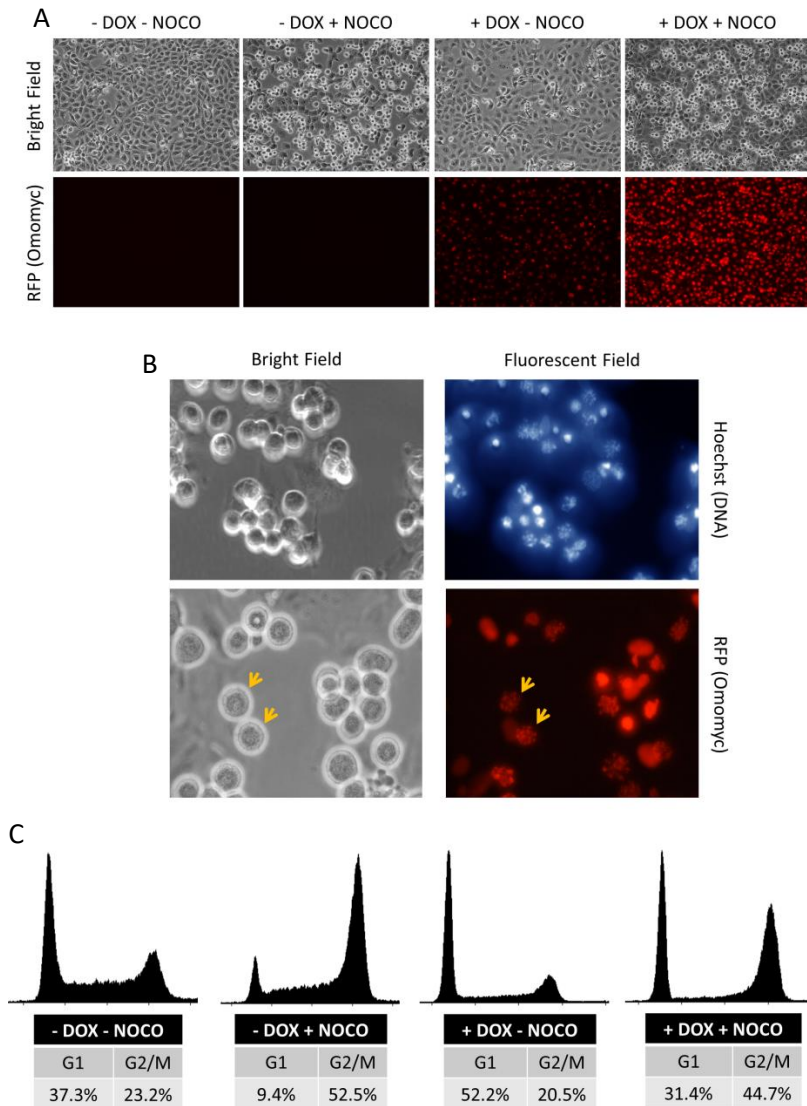


**Figure 27: Upon nocodazole treatment, cells arrest during cell division and DNA condenses without the formation of mitotic spindles.** (A) Microscopy images of cells treated with doxycycline (or without) and/or nocodazole. (B) 40x microscopy images showing condensation of DNA during mitotic arrest due to nocodazole treatment (yellow arrows). (C) Quantification of populations in G1 and G2/M after 3 days of treatment with doxycycline (or without) and/or nocodazole. Cells were trypsinized, fixed/permeabilized and incubated with propidium iodide to stain DNA. Quantification was done by flow cytometry. One representative experiment out of 3 experiments performed is shown.

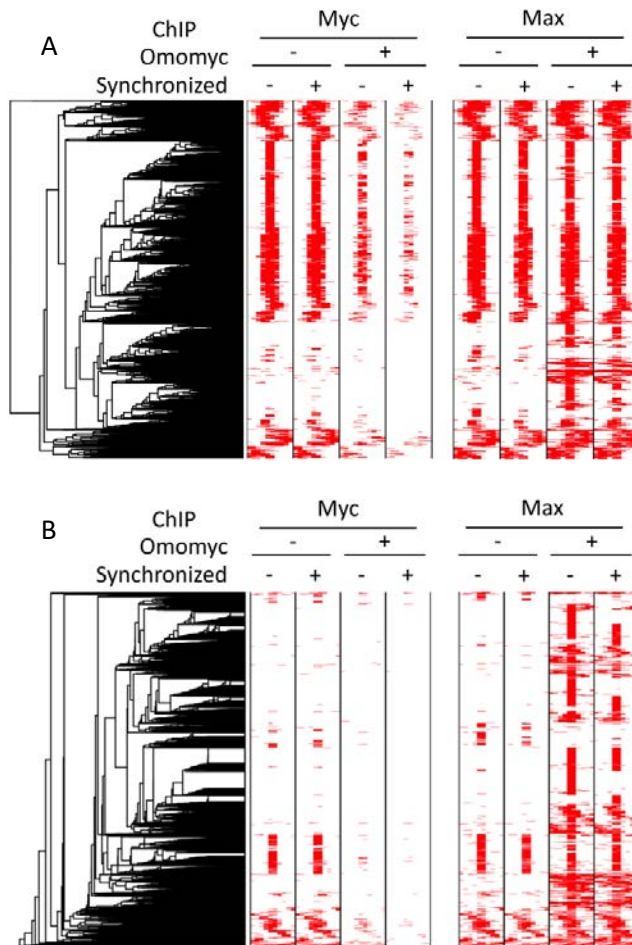


**Figure 28: Omomyc expression inhibits Myc DNA-binding across the genome and produces an invasion of Max towards new binding sites, especially in distal regions. In addition, binding profiles of both Myc and Max are largely conserved between cells synchronized in cell division and non-synchronized cells. Heatmaps of the ChIP-sequencing results for Myc and Max in synchronized and non-synchronized cells either expressing or not Omomyc are shown. Cells were either treated with doxycycline or untreated (“+” and “-” Omomyc respectively) for 2 days. Then, cells were either treated or not with nocodazole (“+” and “-” synchronized respectively) for additional 24 hours without removing the doxycycline. After that time, cells were fixed and collected. ChIP was performed with the N-262 and C-17 antibodies, to IP Myc and Max respectively. All the genomic sites where Myc or Max were detected in any of the conditions are represented. Upper panel (A) shows promoter regions and lower panel (B) shows distal regions.**

Myc and Max ChIP-sequencing analysis was then performed on synchronized and non-synchronized cells either expressing Omomyc or not (Figure 28A). The results showed, as expected, a good correlation between Myc and Max binding sites in normal conditions (-Omomyc), in both synchronized and non-synchronized cells, indicating that they bind DNA as Myc/Max heterodimers. Upon Omomyc expression (+Omomyc) there is a dramatic displacement of Myc across the genome. In contrast to Myc, though, Max DNA-binding was not only not inhibited by Omomyc but, surprisingly, even potentiated, to the point that multiple new binding sites appeared, especially in distal regions (Figure 28B). Interestingly, the binding profiles of Myc and Max between synchronized and non-synchronized cells present little differences. However, when cells are dividing, Myc displacement from DNA is more pronounced. These results, together with the immunofluorescence images in mitosis, indicate that there is an abnormal occupancy of Max on genomic regions when Omomyc is expressed. While this might be visible by immunofluorescence specifically during mitosis, the ChIP analysis indicates that it also occurs outside mitosis. Intriguingly, this increased Max binding to DNA is correlated with invasion of many distal sites.

#### 4.1.8. Evaluation of the efficacy of OmoHER and $\Delta$ Myc compared to Omomyc

To determine whether the binding of Omomyc to DNA, together with Max, is required for its anti-tumorigenic effect, we decided to clone the b-HLH-LZ domain of Myc ( $\Delta$ Myc or, as previously referred, Myc'SH) and an Omomyc mutant unable to bind DNA (OmoHER) inside the pTRIPZ-RFP vector (Figure 29).  $\Delta$ Myc, like Myc, is not able to form homodimers (nor bind Myc) but retains the ability to form dimers with Max and bind DNA. Because it lacks the transactivation domain,  $\Delta$ Myc would act as a competitor of Myc by sequestering Max and binding with it to DNA, thereby resulting in a block of Myc transcriptional activity (Figure 30A). Thus, this would mimic only 2 out of 4 of Omomyc's potential mechanisms of action (interference with Max and occupancy of Myc-target genes by forming dimers with Max). In contrast, OmoHER would still sequester either Myc or Max, disrupting the active Myc/Max heterodimers, but would not be a direct competitor for DNA-binding (Figure 30B). This mutant would mimic other 2 of Omomyc's potential mechanisms of action (interference with Myc and Max), but would not occupy Myc's target genes. OmoHER was recently described in a study

showing that, due to the mutations of H10, E14 and R18 to A, was unable to efficiently bind DNA and displace Myc from its target-genes [160]. Thus,  $\Delta$ Myc and OmoHER (kindly donated by Gerard Evan's and Martin Eilers' laboratories respectively) were cloned into the pTRIPZ-RFP vector. H1299 cells were then infected with both vectors, selected with puromycin and treated with doxycycline. RFP intensity after 3 days show a similar RFP expression of the different constructs (Figure 31A). Cell counts after 6 days of expression showed that  $\Delta$ Myc is capable of reducing cell number similarly, or even more effectively, than Omomyc, while OmoHER displayed only a mild effect (Figure 31B). In agreement with previous characterizations of both variants, the results indicate that the DNA occupancy of Omomyc/Max is a necessary event for Omomyc's potent anti-tumorigenic effect in this context.

```

1  ACCGAGGAGAATGTC AAGAGGCCGAACACACAACGTCTTGAGCGCCAG
1  -T--E--E--N--V--K--R--R--T--H--N--V--L--E--R--Q--
49  AGGAGGAACGAGCTAAAA CGGAGCTTTTTTGCCCTGCGTGACCAGATCCCGGAGTTGGAA
17  -R--R--N--E--L--K--R--S--F--F--A--L--R--D--Q--I--P--E--L--E--
109 AACAAATGAAAAGGCCCCCAAGGTAGTTATCCTTAAAAAGCCACAGCATAATCCTGTCC
37  -N--N--E--K--A--P--K--V--V--I--L--K--K--A--T--A--Y--I--L--S--
169 GTCCAAGCAGAGACGCCAAAAGCTCATTCTGAAATCGACTTGTTGCGGAAACAAAACGAA
57  -V--Q--A--E--T--Q--K--L--I--S--E--T--D--L--L--R--K--Q--N--E--
228 CAGTTGAAACACAAACTTGAACAGCTACGGAACCTTGTGCGGTAA 273
77  -Q--L--K--H--K--L--E--Q--L--R--N--S--C--A--*--

```

**Figure 29: Omomyc sequence in which the amino acids that are mutated in OmoHER and  $\Delta$ Myc are highlighted in green and red respectively.** OmoHER harbors 3 amino acidic changes in the basic region compared to Omomyc: the histidine 10, the glutamate 14 and the arginine 18 are substituted by alanines.  $\Delta$ Myc harbors the original Myc aminoacids in the leucine-zipper: threonine 61 and isoleucine 68 are replaced by glutamates and glutamine 74 and asparagine 75 are replaced by arginines.

To assess whether, despite the mutations in the basic DNA-binding region and displaying a largely reduced efficacy, OmoHER was still able to dimerize with Myc and Max, we performed co-immunoprecipitation against the RFP-fusion protein (Figure 32). The results showed that expression of both Omomyc and OmoHER reduced Max in the depleted fraction (compared to the input) and increased it in the immunoprecipitated fraction (compared to both beads only and non-induced cells). The detection of Max in the OmoHER immunoprecipitated fraction was actually even more pronounced

than in the Omomyc one. In contrast, although the result is not conclusive due to low specificity of the antibody, Myc was less present in the immunoprecipitated fraction of OmoHER compared to Omomyc. However, both Myc signals were below the background signal obtained in the non-specific precipitation using beads. Thus, in spite of displaying a notably reduced anti-tumorigenic effect compared to Omomyc, OmoHER is still able to dimerize with Max, while we could not unequivocally determine that it still dimerizes with Myc, complicating our conclusions regarding the contribution of these different aspects of Omomyc biology to its therapeutic impact.

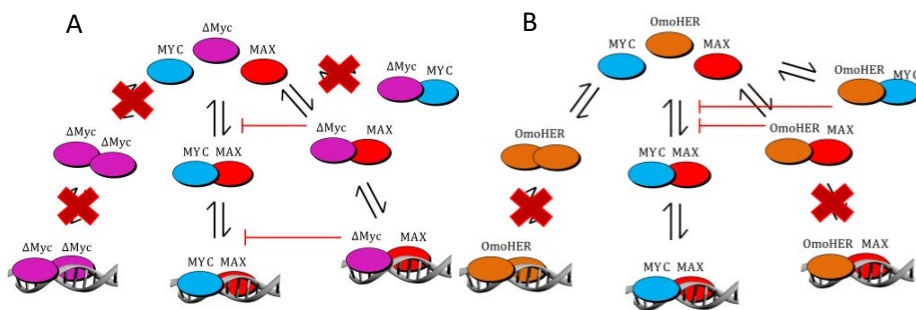


**Figure 30: Schematic representation of the postulated modes of action of  $\Delta$ Myc and OmoHER.** (A)  $\Delta$ Myc would inhibit Myc mainly by disrupting the Myc/Max dimer through dimerization with Max and competing with Myc/Max dimers to bind DNA. (B) OmoHER would inhibit Myc mainly by disrupting the Myc/Max dimer by sequestering both Myc and Max.

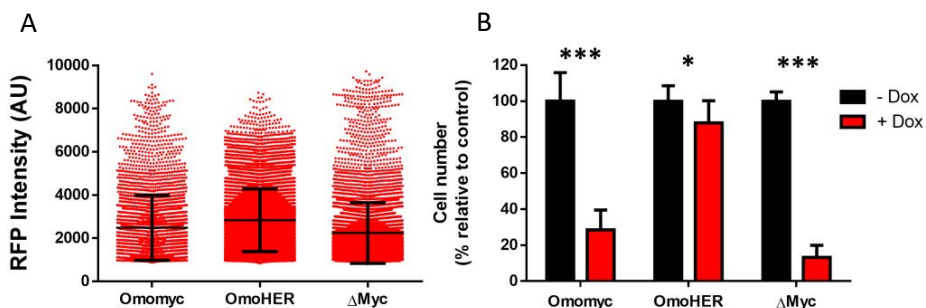


**Figure 31:  $\Delta$ Myc, like Omomyc, is able to effectively reduce the number of cells after 6 days of expression, in contrast to OmoHER which only triggers a moderate reduction.** (A) RFP intensity of the 3 constructs was assessed after 3 days of expression by cytometry. (B) Cell counts after 6 days of expression relative to the respective controls are represented. Student's T-



test was performed to evaluate statistical significance;  $p < 0.05$  (\*) and  $p < 0.001$  (\*\*\*)). Means and standard deviations of 2 independent experiments are shown.

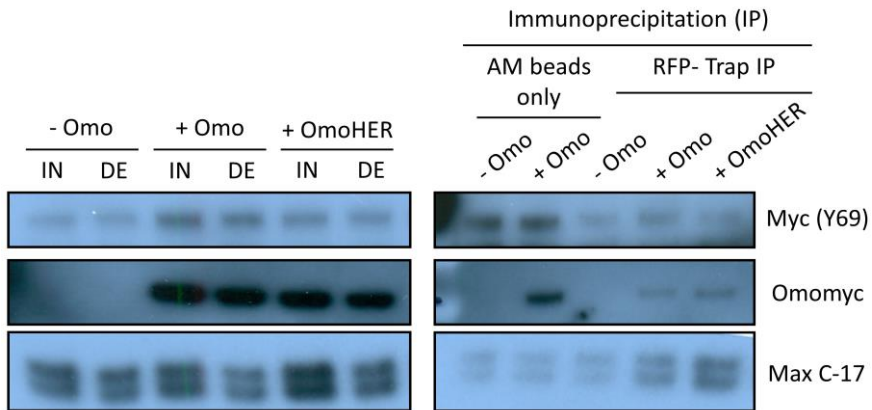


**Figure 32: OmoHER dimerizes with Max.** Input (IN) and depleted (DE, remaining protein after removing immunoprecipitated protein) fractions are shown in the left blots. Immunoprecipitated fractions are shown in the right blots. 2 fractions precipitated with agarose magnetic (AM) beads are shown as non-specific immunoprecipitation. RFP specific immunoprecipitation is shown in the last 3 lanes (-Omo, +Omo and +OmoHER). The experiment was performed once.

To determine the relevance of our observations to mitosis, we investigated the capacity of OmoHER and  $\Delta$ Myc to co-localize with mitotic DNA. Cells expressing both constructs were fixed and immunofluorescence against Max was performed. Surprisingly, OmoHER, reportedly unable to bind DNA, co-localizes with Max and DNA during mitosis (Figure 33A). In contrast,  $\Delta$ Myc, which retains the ability to bind DNA together with Max, showed a clear exclusion with condensed DNA (Figure 33B). These observations suggest that OmoHER, in contrast with what has been described in the literature, could in fact bind DNA in a way that does not impair effective cell proliferation in vitro. Moreover,  $\Delta$ Myc shows that this potential DNA-binding feature observed during mitosis is not a necessary event to, at least, reduce cell proliferation in vitro.

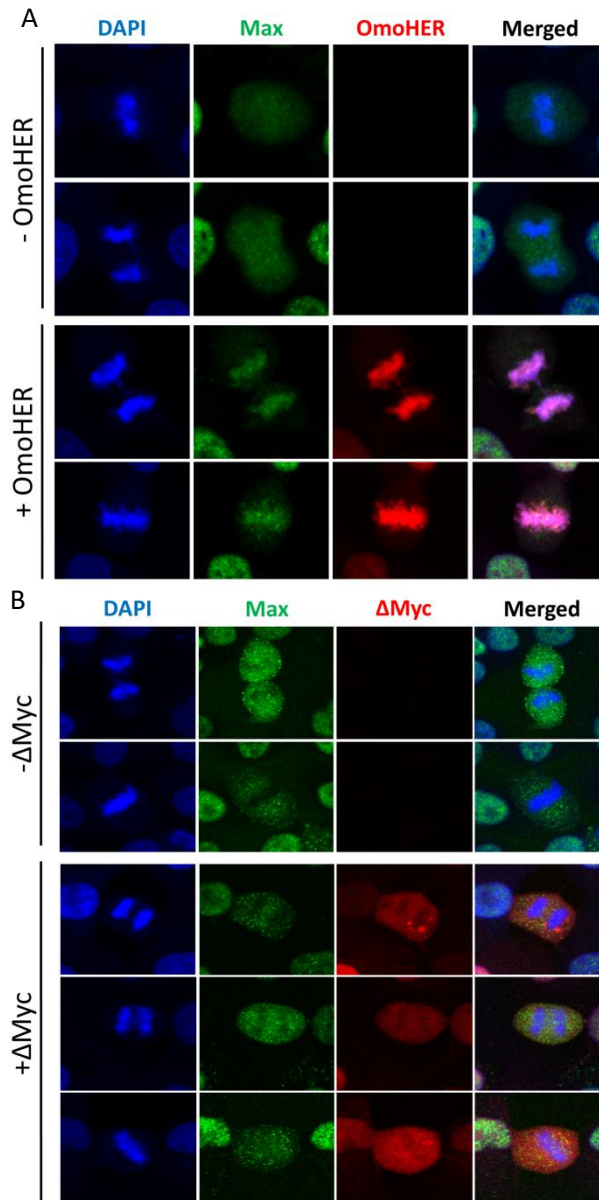


**Figure 33: OmoHER, like Omomyc, is able to co-localize with DNA during mitosis and re-localize Max, in contrast to  $\Delta$ Myc that is excluded from condensed DNA.** Cells were treated with doxycycline to express either (A) OmoHER or (B)  $\Delta$ Myc, fixed after 3 days and immunofluorescence was performed for Max. Images of cells presenting condensed DNA were acquired using confocal microscopy. Blue channels shows DNA, green channels shows Max and red channel shows OmoHER or  $\Delta$ Myc. Representative images of one out of 2 independent experiments are shown.



## 4. Results

---

Section 2: Transforming Omomyc from  
proof of principle to therapeutic  
strategy

#### 4.2.1. Setting up of suitable experimental models for the preclinical evaluation of Omomyc-based drugs

To identify suitable human cell lines to test Omomyc-derived drugs *in vivo*, we started with NSCLC lines we had already tested with the Omomyc transgene in Section 1 of this thesis. We transduced a KRAS mutated cell line (A549) and an EGFR mutated cell line (H1975) with luciferase to be able to follow their growth by IVIS imaging after inoculating them in the lungs of immunocompromised mice. After infection with a lentiviral vector, cells were selected and luciferase expression was confirmed. As a control, the Omomyc-RFP expression levels and the reduction in cell growth were re-assessed and confirmed *in vitro* (Figure 34A). Cytometry analysis of RFP intensity showed similar expression levels of Omomyc-RFP and, consistently with data already described in Section 1, a higher sensitivity of the EGFR mutant H1975 to Omomyc treatment. Each cell line was then inoculated intrapleurally in 16 mice. IVIS imaging at 16 hours after the inoculation confirmed the presence of tumor cells in the thoracic cavity of the animals (Figure 34B-C). IVIS images were recorded weekly and tumor burden determined by total luciferase intensity. Once the quantification analysis showed 2 consecutive weeks of tumor growth, mice were randomized individually in either sucrose- or doxycycline-treated groups. In total, 15 and 14 mice were included in the study, harboring A549 and H1975 cells respectively (Figure 35A-B). Tumor growth was quantified relative to the intensity at the beginning of the treatment. To perform a survival study, mice were euthanized when showing symptoms of respiratory distress and/or > 15% weight loss, according to the guidelines described in the ethical committee protocol.

After 2 weeks of Omomyc-RFP expression, quantification of luciferase intensity showed a significant and dramatic reduction of tumor burden in the H1975-treated cohort (Figure 35B), demonstrating a striking therapeutic impact by Omomyc. In contrast, no significant difference was detected in the A549 cohorts with or without treatment (Figure 35A). These differences in sensitivity to Omomyc treatment were clearly reflected by the survival of the animals: Omomyc-RFP expression conferred a clear survival advantage in the mice harboring tumors from the H1975 cells expressing Omomyc, but not in the A549 (Figure 36A-B). Notably, at experimental end-point (i.e. when a 15% weight loss was recorded -always accompanied by respiratory distress- or

when severe respiratory problems were observed), all animals presented tumors in the lungs and other regions of the peritoneal cavity, while animals that did not show symptoms did not present any macroscopic tumor (90 days post-inoculation) (Figure 36C-F).

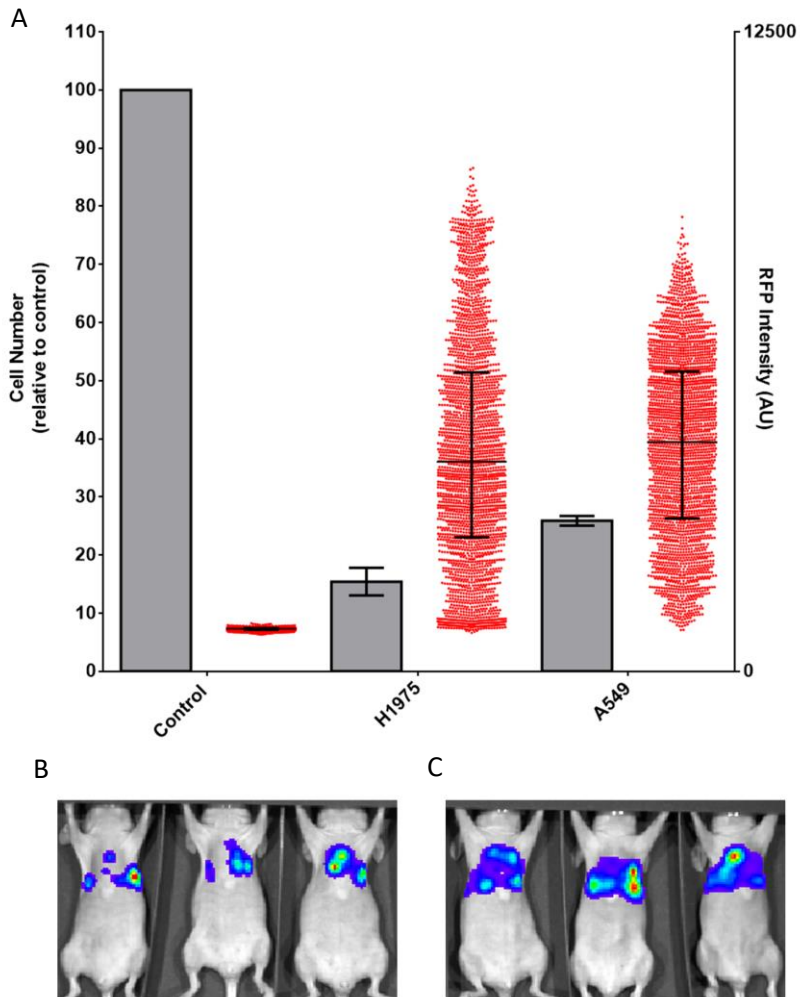


**Figure 34: H1975 and A549 transduced with a lentiviral vector expressing luciferase show similar Omomyc-RFP expression and response in vitro before the inoculation into mice, and express detectable luciferase in vivo. (A) Relative number of cells after 6 days of Omomyc expression compared to the untreated counterparts (grey bars, left axis) and Omomyc-RFP expression levels determined by RFP-intensity of each cells (red dots representing 10,000 cells, right axis). Luciferase expression detected by IVIS imaging 16 hours after intrapleural inoculation of (B) H1975 and (C) A549 cell lines.**

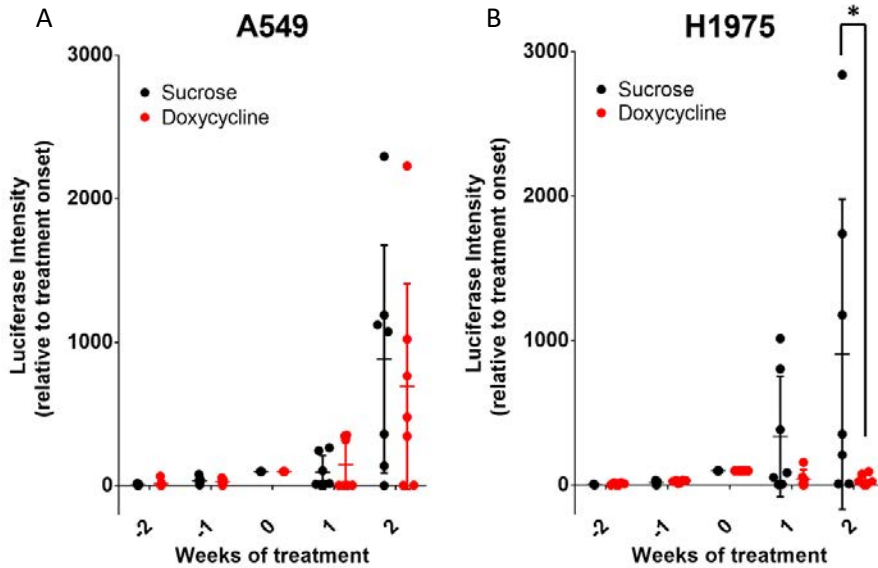


**Figure 35: Omomyc expression reduced tumor burden in H1975 EGFR-mutated cell line but not in the A549 KRAS-mutated cell line.** Luciferase intensity relative to the onset of Omomyc expression is displayed (y axis) for mice inoculated with A549 (A) and mice inoculated with H1975 (B). X axis indicates week of treatment (where “-” indicates “weeks before treatment onset”). Mice treated with doxycycline are shown in red (7 and 6 for A549 and H1975 respectively), while control mice treated with sucrose are shown in black (7 for each A549 and H1975 cohorts). Means and standard deviations are represented for each treatment group in each time point. Student’s T-test was performed between group at each week;  $p < 0.05$  (\*).

Given the striking difference between the behavior of A549 cells *in vitro* and *in vivo*, we decided to check whether the outgrowing tumor cells in mice (visualized by the proliferation marker Ki67) still expressed Omomyc. Confocal images showed a heterogeneous expression of Omomyc across the tumor tissue (Figure 37). However, there was a clear mutual exclusion of cells expressing Omomyc and Ki67, suggesting that A549 cells indeed still respond to Omomyc *in vivo*, but those cells that have low or no expression levels of Omomyc manage to outgrow, masking its therapeutic impact.

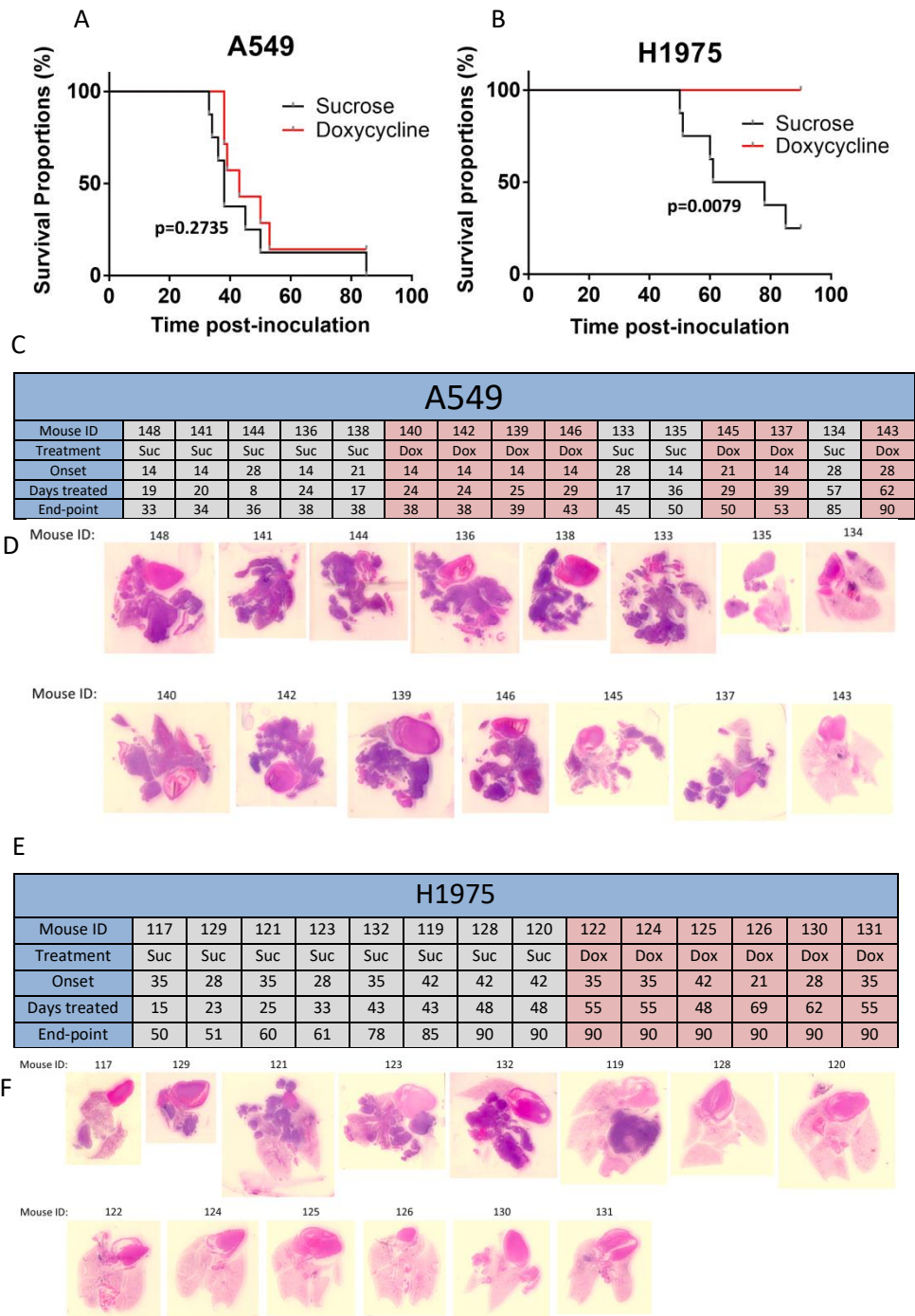


**Figure 36: Omomyc expression confers a survival advantage to mice inoculated with H1975 EGFR-mutated but not to mice inoculated with A549 KRAS-mutated cells.** Survival proportion of mice inoculated with A549 (A) and H1975 (B) grouped by treatment with doxycycline (red line) or sucrose



(black line). Statistical significance of the survival proportions were calculated using the Long-Rank (Mantel-Cox) test. *P*-values (*p*) are represented in the figures. (C) Table of A549-inoculated mice displaying information of mouse identification (ID), treatment received, day post-inoculation when treatment started (treatment onset), number of days during which treatment was received (days treated) and day post-inoculation of euthanasia (end-point). (D) Lung and heart tissue sections of the mice at the moment of euthanasia. (E) and (F) are equivalent to (C) and (D) for the H1975 cohort.

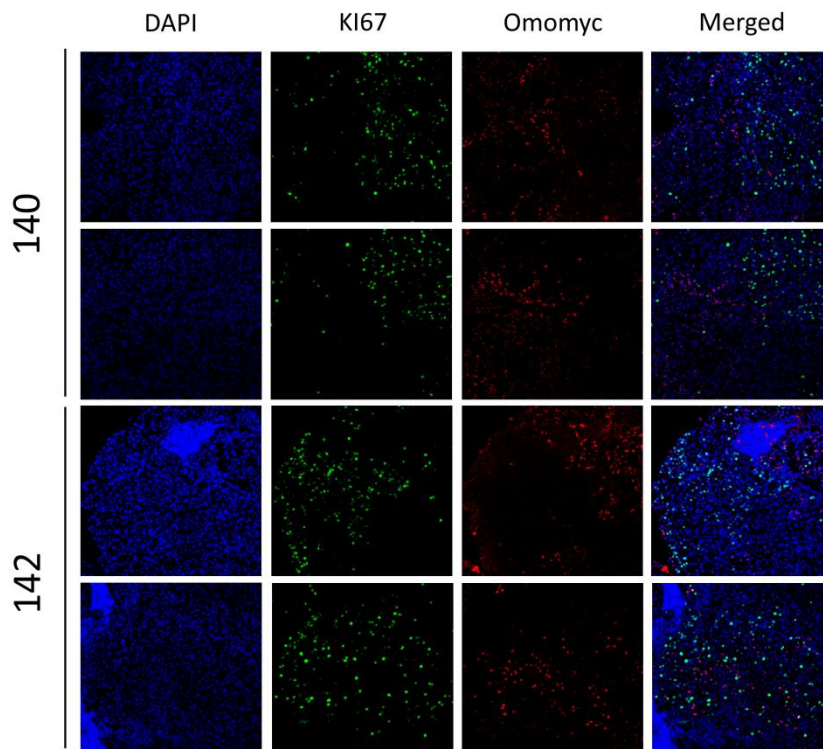


**Figure 37: Omomyc expression reduces the proliferation of A549 in vivo.** Confocal images of Omomyc and KI67 co-staining of animals 140 and 142 euthanized 38 days post-inoculation that expressed Omomyc-RFP for 2 weeks. KI67 (green) and Omomyc-RFP (red) are mutually exclusive.

#### 4.2.2. Validation of Omomyc as cell-penetrating peptide that inhibits Myc

Omomyc has so far been used as a transgene to demonstrate that Myc inhibition would represent a feasible therapeutic approach in cancer. However, for the first time, we have recently produced the Omomyc peptide

itself as a potential drug that could be used as a clinical Myc inhibitor. Therefore, to characterize it and test its efficacy, the Omomyc peptide was expressed in bacteria, purified and used as therapeutic agent (see materials and methods).

To investigate the potential of the Omomyc peptide to spontaneously enter cells, A549 and H1975 were treated with 0.5 $\mu$ M, 1 $\mu$ M, 5 $\mu$ M and 20 $\mu$ M of Omomyc labelled with AlexaFluor488 at the cysteine present at the C'-terminus (Omomyc-AF488) for 15 minutes. Before the analysis, cells were pre-treated with 0.25% of trypsin for 30 minutes to remove the peptide bound to the outer part of the cell membrane. Flow cytometry showed a dose-dependent entrance of the peptide, detectable even at 0.5 $\mu$ M (Figure 38A). Confocal images of A549 and H1975 treated with 5 $\mu$ M were acquired to determine the subcellular localization of the peptide. After 4 hours of treatment (in medium without FBS to limit protein precipitation and background), Omomyc displayed high signal within the cells and was partially located in the nuclei of cells (Figure 38B). The punctate cytoplasmic staining may correspond to an endosomal location. As a consequence of this entry, there was a reduced number of both A549 and H1975 cells after 5 days of treatment with the peptide compared to untreated cells, for which we determined an IC50s of 14 and 12.75 $\mu$ M respectively (Figure 38C). These results demonstrate that the Omomyc peptide behaves as a cell penetrating peptide (from now on the Omomyc peptide will be identified as Omomyc<sup>CPP</sup>) and displays anti-tumorigenic potential.

To confirm directly that the peptide is able to inhibit Myc function, ChIP-sequencing analysis was performed in A549 after 48 hours of treatment (20 $\mu$ M). Analysis of Myc DNA occupancy revealed that the peptide is able to reduce the binding of Myc on target genes (Figure 38D). Importantly, this happens while Myc protein levels remain unaffected (Figure 38E), implying that Myc is actively displaced from its target genes, in line with Omomyc's mode of action.

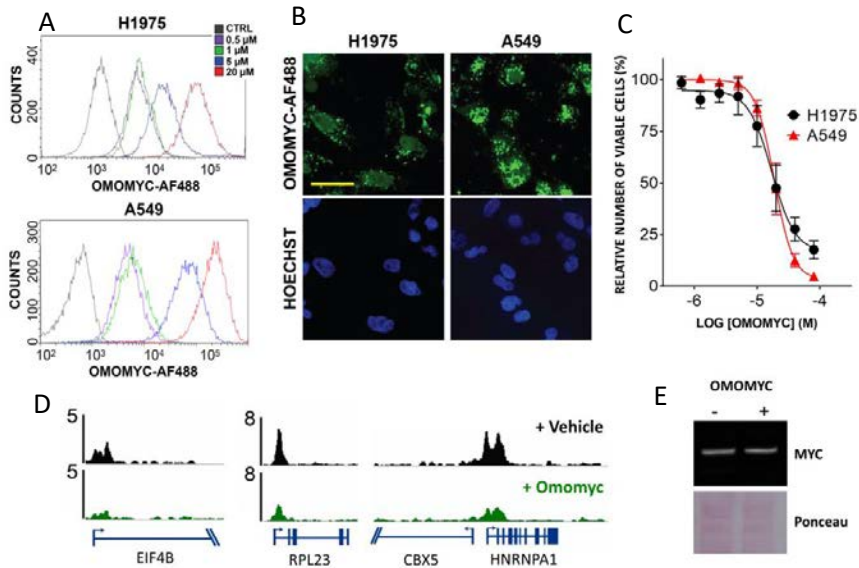


**Figure 38: The Omomyc peptide (*Omomyc<sup>CPP</sup>*) enters cells, partially localizes in the nuclei and acts as a Myc inhibitor that shows anti-tumorigenic potential.** (A) Flow cytometry analysis of control cells (CTRL) and cells treated with 0.5, 1, 5 and 20  $\mu\text{M}$  of Omomyc-AF488 for 15 minutes and detached with 0.25% of trypsin to remove membrane-bound peptide. (B) A549 and H1975 were treated with 5  $\mu\text{M}$  of Omomyc-AF488 for 4 hours in FBS-free medium and stained with Hoechst before capturing images by confocal microscopy. (C) A549 and H1975 were treated with the Omomyc peptide at concentrations from 300nM to 40  $\mu\text{M}$ . Cell viability was determined using AlamarBlue (Thermo). (D) Myc ChIP-sequencing was performed on A549 cells treated for 48 hours with 20  $\mu\text{M}$  of Omomyc (green) or vehicle. Myc occupancy at selected typical Myc target proximal promoter regions is shown. Ribosomal protein L23 (RPL23), Chromobox protein homolog 5 (CBX5), Heterogeneous nuclear ribonucleoprotein A1 (HNRNPA1) and Eukaryotic translation initiation factor 4B (EIF4B). (E) Myc immunoblot (N-262) of A549 treated 48 hours at 20  $\mu\text{M}$  of *Omomyc<sup>CPP</sup>*. Ponceau S is shown as protein loading control. Vehicle and *Omomyc<sup>CPP</sup>* treatments are represented by (-) and (+) respectively. (A), (B) and (E) are representative images of 2 independent experiments. (C) shows means and standard deviation of 3 independent experiments. (D) was performed once in triplicates and average signals are shown.

#### 4.2.3. Biodistribution of Omomyc<sup>CPP</sup> *in vivo*

Omomyc<sup>CPP</sup> is able to penetrate cells and cause an anti-tumorigenic effect *in vitro* acting as a Myc inhibitor. For its potential use *in vivo*, we initially assessed whether Omomyc<sup>CPP</sup> was able to systemically distribute in a living animal. Omomyc<sup>CPP</sup> was first labelled with DFO to allow subsequent radioactive labelling with <sup>89</sup>Zr. The resulting Omomyc<sup>CPP</sup>-DFO-<sup>89</sup>Zr was then administered intravenously to nude mice bearing subcutaneous H1975 tumors, and mPET scan was performed after 72 hours. Radioactive signal detected from the different tissues, including the tumor, showed a predominant distribution of Omomyc<sup>CPP</sup> in kidney, liver and spleen (Figure 39). At 72h following administration, 0.3% of the injected dose of Omomyc<sup>CPP</sup>-DFO-<sup>89</sup>Zr per gram of tissue was localized in the tumor. Hence, this biodistribution indicates that systemic administration of Omomyc<sup>CPP</sup> reaches several tissues including subcutaneous tumors.

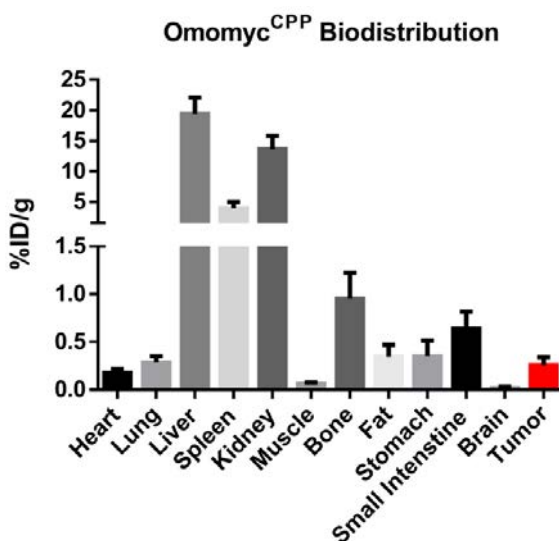


**Figure 39: Omomyc<sup>CPP</sup>-DFO-<sup>89</sup>Zr is present in subcutaneous tumors 72 hours after i.v. administration.** H1975 were subcutaneously inoculated in nude mice and 4.3 mg/kg of Omomyc<sup>CPP</sup>-DFO-<sup>89</sup>Zr systemically administered via tail vein injection once tumors were fully developed. Means of 5 mice and standard deviations are represented.

#### 4.2.4. In vivo efficacy of Omomyc<sup>CPP</sup>

Since i.v. administration of Omomyc<sup>CPP</sup> is able to reach subcutaneous tumors in vivo, as well as other tissues, we evaluated the therapeutic effect and the potential toxicity of Omomyc<sup>CPP</sup> administered by systemic treatment. Our previous data demonstrated the sensitivity of the H1975 cell line to Omomyc transgenic expression. Therefore, this cell line was selected to perform the first evaluation of Omomyc<sup>CPP</sup> in vivo efficacy following i.v. administration. H1975 were subcutaneously inoculated in nude mice and were allowed to reach 200 mm<sup>3</sup>. Animals were then treated i.v. with either the vehicle or a dose of 93.75mg/kg of Omomyc<sup>CPP</sup> 4 times per week (1101100) for 4 weeks. Weight and tumor volume were recorded twice per week. Both treated and control groups displayed stable weight during the treatment (Figure 40A) and physical evaluation of the mice did not reveal signs of side effects. Strikingly though, tumors displayed a significantly smaller volume in the treated group when compared to the control already at 15 days of treatment and this impairment of tumor growth continued until the experimental endpoint was reached at 26 days (Figure 40B).

To confirm that the Omomyc<sup>CPP</sup> reached the tumors, subcutaneous tumors of both experiments were collected, 24 hours after the last Omomyc<sup>CPP</sup> administration, and paraffin-embedded to perform double Ki67/Omomyc immunofluorescence. Confocal microscopy images of H1975 sections showed a heterogeneous distribution of Omomyc<sup>CPP</sup> within the tumors (Figure 41). Areas showing positive Omomyc and Ki67 signals correlated in the periphery, suggesting that highly-vascularized regions might receive more Omomyc<sup>CPP</sup> than poorly vascularized ones (e.g. core necrotic regions). Confocal images captured at higher magnification revealed a predominant cytoplasmic localization of Omomyc<sup>CPP</sup> (Figure 42). Together, these results show that while systemic Omomyc<sup>CPP</sup> represent already an effective and safe therapy, the therapeutic impact could still be increased by improving the biodistribution and the nuclear localization of the drug.

In this context, more investigation was conducted to, on one hand, assess whether increasing the dose of Omomyc<sup>CPP</sup> (alone and in combination with standard of care to assess whether there is synergy of the treatments) might increase the therapeutic index of the treatment, and, on the other hand, formulating a new Omomyc<sup>CPP</sup>-based drug that could improve both the biodistribution and the nuclear localization.

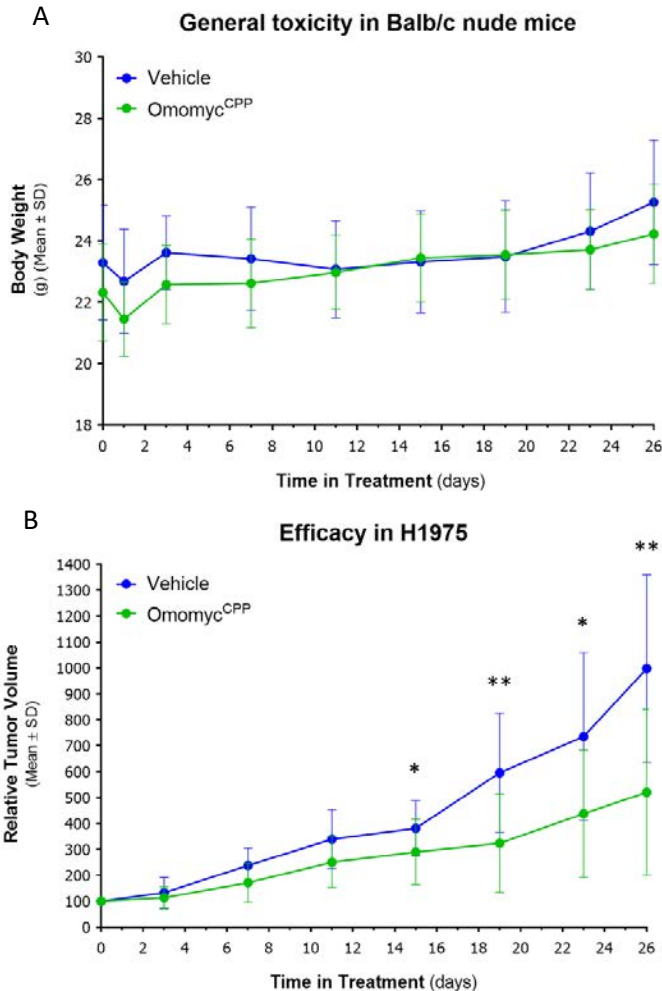


**Figure 40: 93.75mg/kg of Omomyc<sup>CPP</sup> administered i.v. does not cause toxicity to nude mice but reduces growth of H1975 subcutaneous tumors.** H1975 cells were subcutaneously inoculated in Balb/c nude mice and, when tumors reached 100-300mm<sup>3</sup>, one cohort was treated with Omomyc<sup>CPP</sup> for 26 days. (A) Weights of the animals (7 per group) were measured every 3-4 days. Means and standard deviations of the weights of each group are represented. No statistical significance was found in any of the time points. (B) Caliper measurements from 14 tumors per group were obtained twice per week to calculate tumor volume of animals inoculated with H1975. Volumes relative to the treatment onset were calculated for each tumor. Means and standard deviations are represented. Student's T-test between the groups at each time point was used to determine statistical significance;  $p < 0.05$  (\*)  $p < 0.01$  (\*\*).

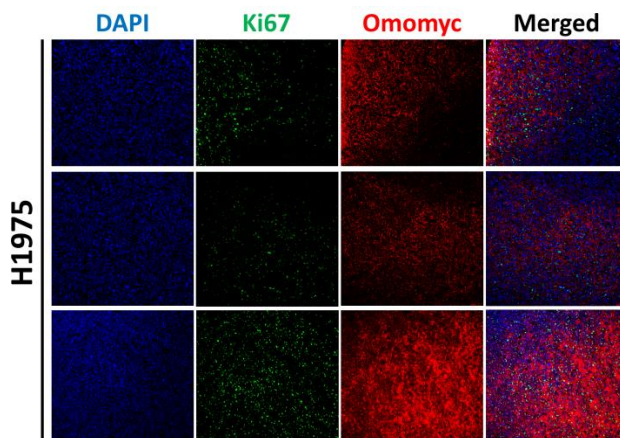


**Figure 41:** After i.v. administration, Omomyc<sup>CPP</sup> was detected in subcutaneous tumors of H1975 cells and correlated with Ki67 positive regions. Omomyc<sup>CPP</sup> was administered for 4 weeks at 93.75mg/kg. 24 hours before euthanasia the last dose was injected. Subcutaneous tumors were then resected and paraffin-embedded to perform IF. Ki67 was used as proliferation marker (green), Omomyc was detected using the Omomyc polyclonal antibody (red) and DNA stained with DAPI (blue). Confocal microscopy images were acquired setting the same parameter for all the images of each channel. Images show representative fields of 3 different samples using the 10x objective.

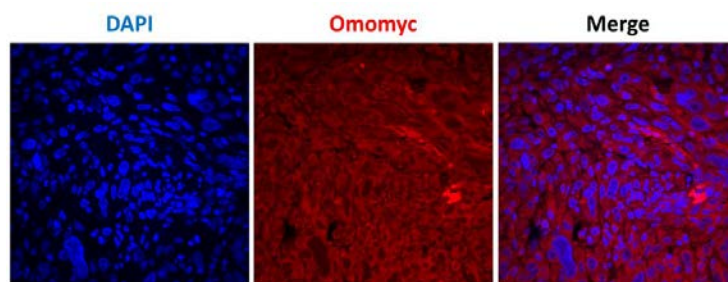


**Figure 42:** In vivo, Omomyc<sup>CPP</sup> localizes in the cytoplasm and, to a lesser extent, within the nuclei. Representative image of a region displaying Omomyc<sup>CPP</sup>-positive staining at 40x magnification is shown.

#### 4.2.5. Dose increase of Omomyc<sup>CPP</sup> and combination with paclitaxel

To assess whether increasing the dose of Omomyc<sup>CPP</sup> would cause an even more dramatic therapeutic impact in H1975, this cell line was inoculated into

nude mice that, once the tumors were established, were treated with 187.5mg/kg of Omomyc<sup>CPP</sup> following the same regimen previously used with a lower dose (1101100). In addition, to determine whether Omomyc<sup>CPP</sup> could synergize with standard chemotherapy, 2 more cohorts of mice were included in the study. One of these cohorts was treated with paclitaxel at 5mg/kg only twice a week (1001000) and the other one was treated with the combination of both therapies, Omomyc<sup>CPP</sup> and paclitaxel.

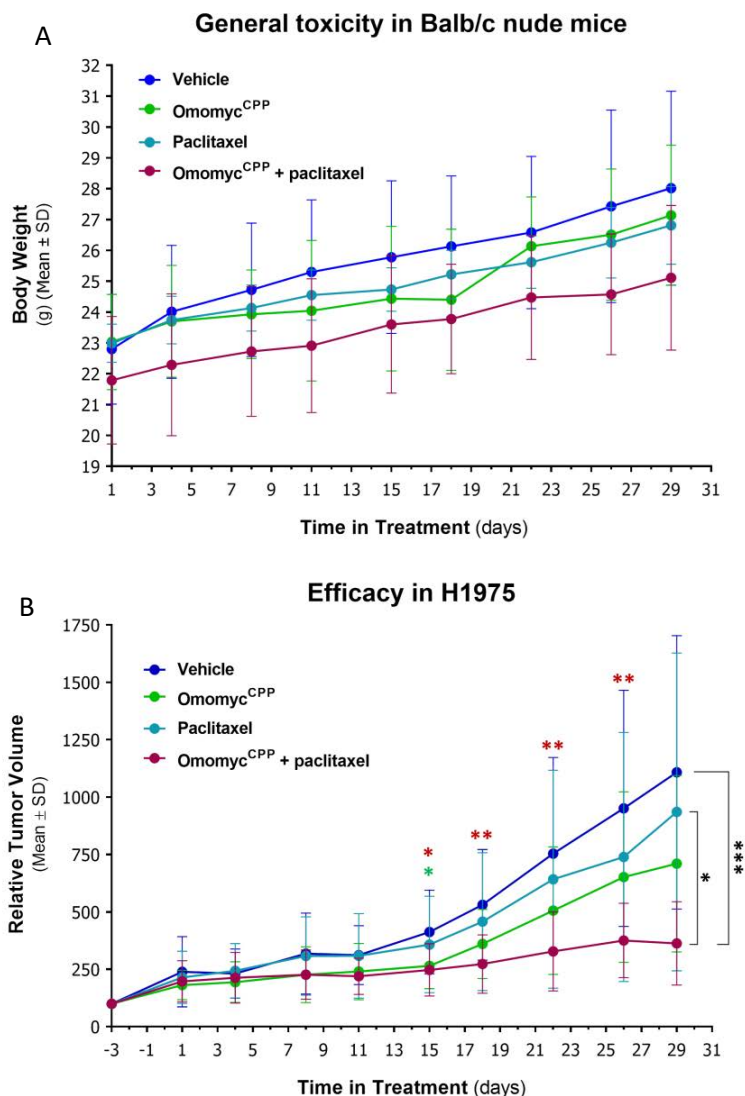


**Figure 43: Combining Omomyc<sup>CPP</sup> with standard chemotherapy (paclitaxel) represents a safe therapeutic option and displays increased efficacy compared to both monotherapies. H1975 cells were subcutaneously**



*inoculated in Balb/c nude mice and, when tumors reached 100-300mm<sup>3</sup>, animals were randomized and treated with Omomyc<sup>CPP</sup> (187.5mg/kg), paclitaxel (5mg/kg) or a combination of both for 26 days. (A) Weights of the animals (10 per group) were measured every 3-4 days. Means and standard deviations of the weights of each group are represented. (B) Caliper measurements from 20 tumors per group were obtained twice per week to calculate tumor volume. Volumes relative to the treatment onset were calculated for each tumor. Means and standard deviations are represented. One-way ANOVA (Bonferroni correction) between the 4 groups at each time point was used to determine statistical significance;  $p < 0.05$  (\*),  $p < 0.01$  (\*\*) and  $p < 0.001$  (\*\*\*). Statistical significance of middle time points was found between Omomyc<sup>CPP</sup> (at 15 days) and combination (at 15, 18, 22, 26 days) compared to the vehicle-treated cohort. At the endpoint, statistical significance of vehicle and paclitaxel groups vs the combination was also identified.*

The weight of the animals during the course of the treatment was used as read-out of general toxicity. Overall, weights were not significantly affected in any cohort during the 4-week treatment (Figure 43A). Moreover, the similar progressive gain-of-weight of all the groups revealed that the doses chosen for the treatments were not toxic for the mice. Interestingly, the increase of the Omomyc<sup>CPP</sup> dose did not show any improvement of the efficacy compared to the half-dose previously used, suggesting that both doses are within a plateau of therapeutic index with the formulation that was used. Importantly, when both treatments were combined, the effect on tumor growth was dramatic and the progression was significantly inhibited at all time-points from 15 to 29 days after treatment (Figure 43B). This result indicates that Omomyc<sup>CPP</sup> could synergize with standard chemotherapy to potentiate tumor response

#### 4.2.6. Formulation and in vitro validation of the first Omomyc-based liposomal nanoparticles

To potentially improve Omomyc<sup>CPP</sup> biodistribution, stability and integrity within the blood-stream, reduce its exposure to the immune system and achieve a better nuclear localization, we decided to test its encapsulation in liposomal nanoparticles. Thus, we established a collaboration with a laboratory that masters this expertise: the group of Dr. Vladimir Torchilin at

the Center for Pharmaceutical Biotechnology and Nanomedicine (Northeastern University, Boston, USA). I travelled to Boston and performed the initial experiments at their facilities for a period of 6 months to achieve the encapsulation and delivery of Omomyc<sup>CPP</sup>- liposomes.

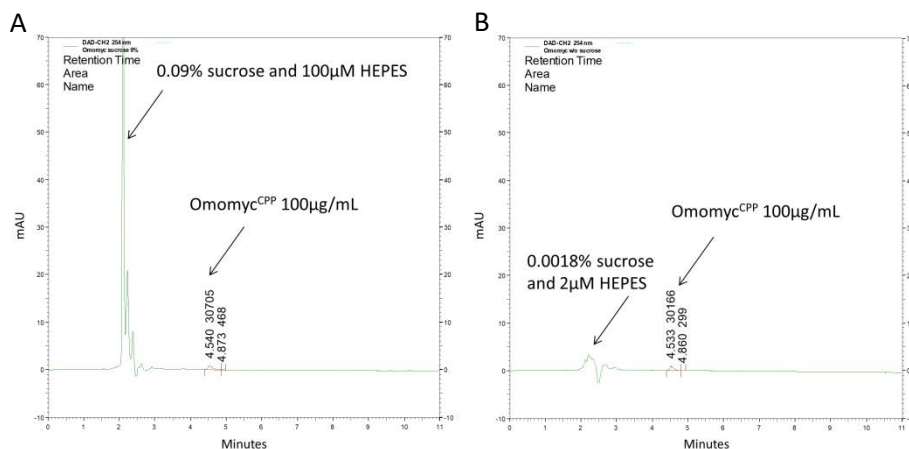


**Figure 44: Omomyc<sup>CPP</sup> shows an almost undetectable UV absorbance compared to the absorbance produced by the encapsulation buffer. UV absorbance of 100µg/mL of Omomyc<sup>CPP</sup> dissolved in encapsulation buffer (left panel) or 50-times dilutes encapsulation buffer (right panel). 50:50 water: acetonitrile was used as mobile phase. The experiment was performed once.**

To estimate liposomal encapsulation efficacy we evaluated whether encapsulated Omomyc<sup>CPP</sup> would be detected by reverse-phase chromatography using an UV/Vis detector. 3µL of Omomyc<sup>CPP</sup> at 10 µg/µL were dissolved 1:100 in acetonitrile:water 70:30 and loaded into a C18 column. 2 peaks of elution after 2 and 5 minutes were detected (Figure 44A). We hypothesized that the second peak, almost undetectable, corresponded to Omomyc<sup>CPP</sup>. To prove it, the HEPES/sucrose buffer was diluted 1:50 in a solution of Omomyc<sup>CPP</sup> in MQ H<sub>2</sub>O at 10µg/µL, thus maintaining the concentration of Omomyc<sup>CPP</sup> and diluting 50 times the HEPES/sucrose. The same parameters were applied to perform the chromatography. A notable decrease of the first peak was observed, confirming that the second one corresponded to Omomyc<sup>CPP</sup> (Figure 44B). At the concentration that we planned to encapsulate Omomyc<sup>CPP</sup>, detecting 100µg/µL will be equivalent to a 100% of encapsulation efficacy, and the signal obtained by the UV/Vis is almost undetectable compared to the buffer. To increase the detection of Omomyc<sup>CPP</sup> by HPLC, Omomyc<sup>CPP</sup> was covalently labelled with FITC at the C-

terminus cysteine (Omomyc<sup>CPP</sup>-FITC). Following a similar procedure, fluorescence detection of Omomyc<sup>CPP</sup>-FITC by HPLC displayed a strong signal and allowed quantification of Omomyc<sup>CPP</sup>-FITC within a linear range of stocks between 25 to 1.5 $\mu$ g/mL (Figure 45). Hence, 10% of Omomyc<sup>CPP</sup>-FITC was used as tracer along with 90% of unlabeled Omomyc<sup>CPP</sup> (hereafter, Omomyc<sup>CPP</sup>-FITC will refer to this 10:90 mixture) to characterize the liposome-mediated delivery of Omomyc<sup>CPP</sup>.

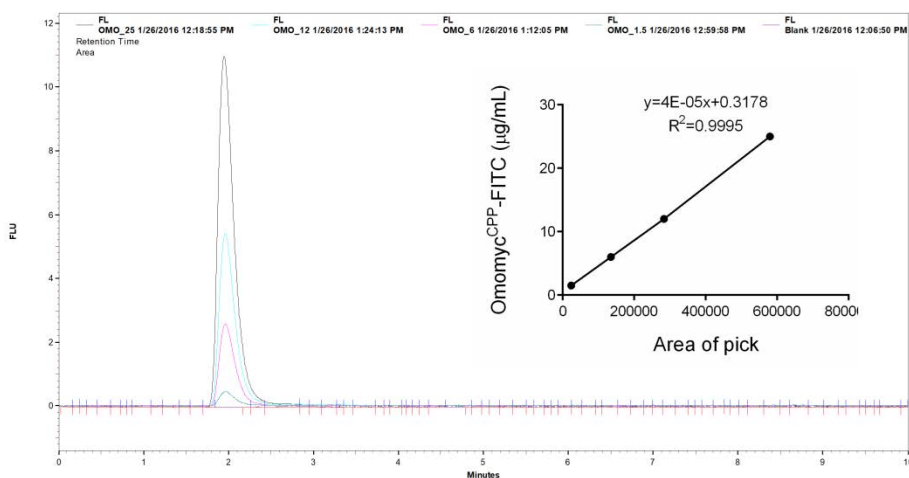


**Figure 45: Omomyc<sup>CPP</sup>-FITC can be detected up to 1.5 $\mu$ g/mL by fluorescence intensity.** Concentrations of Omomyc<sup>CPP</sup>-FITC of 25, 12, 6 and 1.5 $\mu$ g/mL were analyzed. Fluorescence intensity correlates with the concentration of Omomyc<sup>CPP</sup>-FITC within a linear range. 75:25 water: acetonitrile was used as mobile phase. The experiment was performed once.

Omomyc<sup>CPP</sup>-FITC was encapsulated in liposomes using an initial formulation of DPPC (56%), DOPS (12%), DOPE (10%), cholesterol (20%) and PEG-PE (2%). HPLC quantification of the FITC intensity exhibited an encapsulation efficacy of 30% (Table 2). To determine whether the Omomyc<sup>CPP</sup>-liposomes improve the delivery of Omomyc in vitro, U87-MG and A549 were treated with equivalent concentrations of free Omomyc<sup>CPP</sup>-FITC and Omomyc<sup>CPP</sup>-FITC-liposomes. Flow cytometry analysis of FITC intensity in U87-MG showed an increased entrance of Omomyc<sup>CPP</sup>-FITC when encapsulated in liposomes compared to the free Omomyc<sup>CPP</sup>-FITC (Figure 46A). Additionally, confocal images of Omomyc<sup>CPP</sup>-FITC inside A549 showed that the FITC signal was more intense when 0.5 $\mu$ M of Omomyc<sup>CPP</sup> was delivered by liposomes (Figure 46B).

| Sample   | Area   | SD     | Rel. Area (%) | Rel. SD (%) |
|----------|--------|--------|---------------|-------------|
| Initial  | 617169 | ±32848 | 100           | ±5.32       |
| Extruded | 546722 | ±25112 | 89            | ±4.07       |
| Purified | 175932 | ±9829  | 29            | ±1.59       |

**Table 2: Liposomes composed of DPPC (56%), DOPS (12%), DOPE (10%), cholesterol (20%) and PEG-PE (2%) encapsulate Omomyc<sup>CPP</sup>-FITC with an encapsulation efficacy of 29±1.59. Samples from the hydration solution (initial), after the extrusion (extruded) and after 3 hours of dialysis purification (purified). Mean area of the peaks (Area) and its standard deviation (SD) are described, along with the mean and standard deviation relative to the initial concentration (Rel. Area and Rel. SD respectively). 3 independent experiments were performed.**

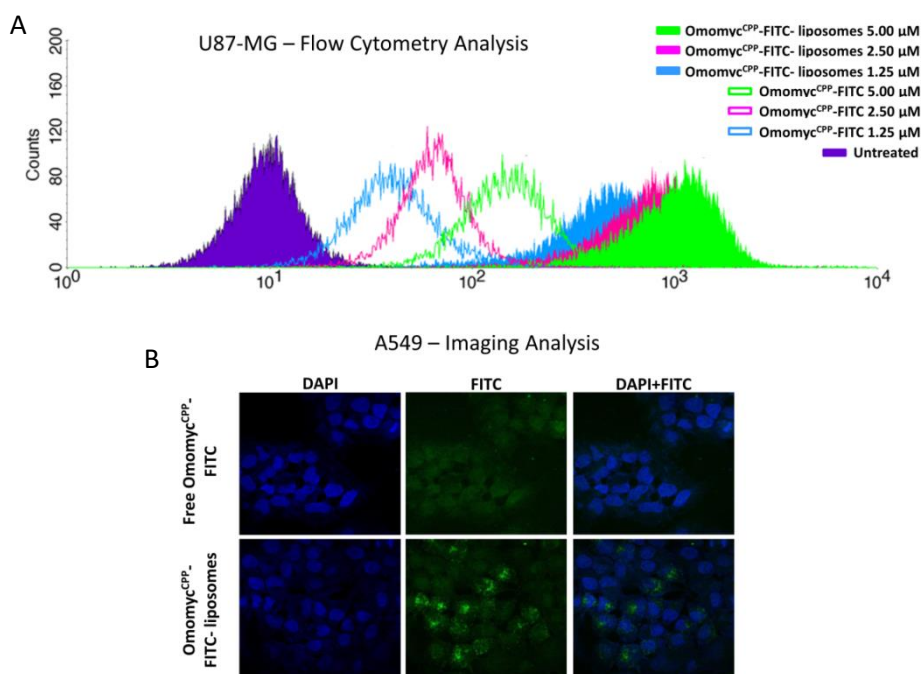


**Figure 46: Omomyc<sup>CPP</sup>-FITC encapsulated into liposomes is delivered more efficiently into cancer cells than the free Omomyc<sup>CPP</sup>-FITC. (A) Cell cytometry analysis of FITC intensity in U87-MG treated with either free or encapsulated Omomyc<sup>CPP</sup>-FITC inside liposomes for 24 hours at the specified**

concentrations. (B) Images of A549 cells treated for 24 hours with  $0.5\mu\text{M}$  of Omomyc<sup>CPP</sup>-FITC either free or encapsulated inside liposomes. Cells were fixed and permeabilized before incubation with DAPI. Confocal images were acquired at the same exposure settings. Images show one representative experiment out of 2 experiments performed.

To determine the predominant endocytic pathway that mediates the entrance of the Omomyc<sup>CPP</sup>-liposomes, both U87-MG and A549 were treated with  $1\mu\text{M}$  of Omomyc<sup>CPP</sup> encapsulated in rhodamine-PE-labelled liposomes. Different inhibitors were used to interfere with the main endocytic pathways: chlorpromazine (against clathrin), genistein (for caveolae) and cytochalasin D (for macropinocytosis). Quantification of rhodamine intensity demonstrated that in both cell lines caveolae-mediated endocytosis plays a prevalent role in the delivery of Omomyc<sup>CPP</sup>-liposomes (Figure 47). Moreover, macropinocytosis also seems to mediate the delivery of Omomyc<sup>CPP</sup>-liposomes into cells at least in U87-MG cells.

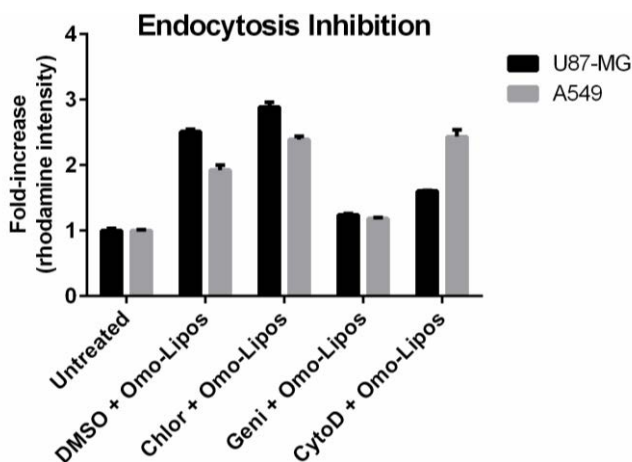


**Figure 47: Caveolae-mediated endocytosis represents the main endocytic pathway for the entry of the Omomyc<sup>CPP</sup>-liposomes in A549 and U87-MG. Additionally, macropinocytosis also mediates the entrance in U87-MG.** Omomyc<sup>CPP</sup> was encapsulated in rhodamine-labelled liposomes and cells were treated at  $1\text{mg/mL}$  of liposomes for 1 hour. Previously cells were exposed to each inhibitor for an hour. Rhodamine intensity is relative to untreated cells. DMSO was used as control treatment. Chlorpromazine (Chlor), genistein (Geni) and cytochalasin D (CytoD) were used as inhibitors of clathrin-, caveolae-mediated endocytosis and macropinocytosis respectively. The experiment was performed once.

To determine the subcellular localization of the Omomyc<sup>CPP</sup> delivered using labelled-liposomes, U87-MG were treated with encapsulated Omomyc<sup>CPP</sup>-FITC at 2 $\mu$ M and cells were fixed after 4 hours. Confocal imaging following DAPI staining revealed a predominant cytosolic localization (Figure 48). The high co-localization of Omomyc<sup>CPP</sup>-FITC and Rhodamine-PE, as well as the punctuated pattern observed, suggest an endosomal entrapment. Together, these results indicate that, while liposomal delivery enhances the entrance, it does not seem to trigger a good nuclear localization of Omomyc<sup>CPP</sup>.

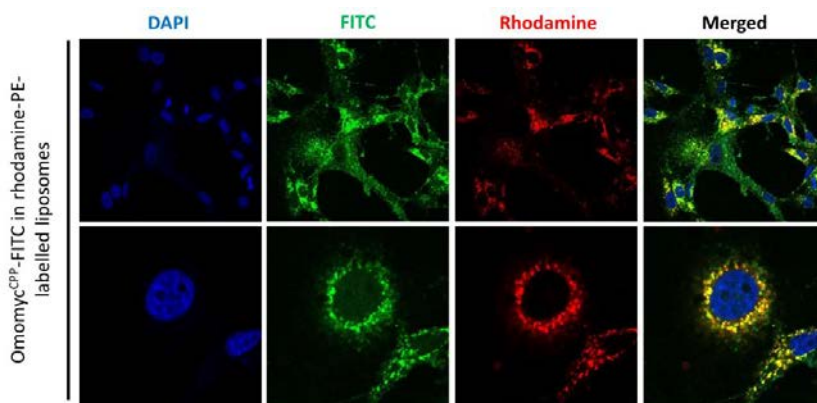


**Figure 48: Omomyc<sup>CPP</sup>-FITC presents a predominant cytoplasmic localization when delivered encapsulated into liposomes.** U87-MG cells were treated with 2 $\mu$ M of Omomyc<sup>CPP</sup>-FITC encapsulated into rhodamine-labelled liposomes for 24 hours. Cells were fixed and permeabilized before incubation with DAPI. Representative images of 2 independent experiments are shown.

#### 4.2.7. Optimization of Omomyc<sup>CPP</sup>-liposomes

To improve the endosomal escape of the Omomyc<sup>CPP</sup> as well as the encapsulation efficacy, different liposomal formulations were conceived and produced incorporating CHEMS and/or increasing the DOPE content. First, the z-potentials of empty formulations, a measure of the net charge of the nanoparticles, were examined. An increase of CHEMS/DOPE molar ratio provided negative z-potential to the liposomes, while an increase of DOTAP provided positive z-potential (Table 3A). Moreover, post-PEGylated liposomes presented lower z-potential compared to the non-PEGylated counterparts. All formulations displayed stability in solution, with the exception of formulation number 4 that resulted in aggregated liposomes after PEGylation. Second, these same formulations were used to encapsulate

Omomyc<sup>CPP</sup>-FITC and determine encapsulation efficacies. All formulations with molar ratios of CHEMS:DOPE of 10:10 or above produced a precipitate in the presence of Omomyc<sup>CPP</sup>-FITC, with the exception of the formulation presenting DOTAP (Table 3B). The 2 formulations below these molar ratios also formed stable nanoparticles. However, the encapsulation efficacies of the Omomyc<sup>CPP</sup>-FITC for these stable formulations were relatively low (10-15%).

A

| Formulation | Percentage of component |      |      |       |       | Before PEG |      | After PEG |      | EE |
|-------------|-------------------------|------|------|-------|-------|------------|------|-----------|------|----|
|             | ID                      | DPPC | DOPE | CHEMS | DOTAP | CHOL       | Size | ZP        | Size |    |
| Form. A     | 30                      | 35   | 35   | -     | -     | 160        | -42  | 170       | -40  | -  |
| Form. B     | 50                      | 25   | 25   | -     | -     | 160        | -42  | 160       | -40  | -  |
| Form. C     | 80                      | 10   | 10   | -     | -     | 200        | -31  | 200       | -43  | -  |
| Form. D     | 70                      | 10   | 10   | 10    | -     | 170        | 9.5  | 1000      | -12  | -  |
| Form. E     | 65                      | 5    | 5    | 5     | 20    | 170        | -3   | 170       | -24  | -  |
| Form. F     | 60                      | 5    | 5    | 10    | 20    | 150        | 35   | 150       | 13   | -  |

B

| Formulation | Percentage of component |      |      |       |       | Before PEG  |      | After PEG |      | EE |
|-------------|-------------------------|------|------|-------|-------|-------------|------|-----------|------|----|
|             | ID                      | DPPC | DOPE | CHEMS | DOTAP | CHOL        | Size | ZP        | Size |    |
| Form. A     | 30                      | 35   | 35   | -     | -     | Precipitate |      | -         | -    | -  |
| Form. B     | 50                      | 25   | 25   | -     | -     | Precipitate |      | -         | -    | -  |
| Form. C     | 80                      | 10   | 10   | -     | -     | Precipitate |      | -         | -    | -  |
| Form. D     | 70                      | 10   | 10   | 10    | -     | 180         | 25   | 160       | 9    | 15 |
| Form. E     | 65                      | 5    | 5    | 5     | 20    | 150         | 20   | 180       | 6    | 10 |
| Form. F     | 60                      | 5    | 5    | 10    | 20    | 150         | 28   | 150       | 10   | 10 |

C

| Formulation | Percentage of component |      |      |       |       |      | Before PEG |      | After PEG |      | EE    |
|-------------|-------------------------|------|------|-------|-------|------|------------|------|-----------|------|-------|
|             | ID                      | DPPC | DOPE | CHEMS | DOTAP | DOPS | CHOL       | Size | ZP        | Size |       |
| Form. G     | 45                      | 30   | -    | -     | 5     | 20   | 160        | -31  | 170       | -32  | 33-40 |
| Form. H     | 50                      | 30   | -    | -     | 20    | 20   | 140        | -30  | 150       | -32  | 26-35 |
| Form. I     | 65                      | 10   | 5    | -     | -     | 15   | 1000       | -5   | 160       | -10  | 46-50 |
| Form. J     | 60                      | 10   | 10   | 10    | -     | 10   | 160        | 20   | 170       | 15   | 10-15 |

**Table 3: Composition and characterization of size and z-potential (ZP) of the different formulations tested (A to J).** Form.: formulation; DPPC: 1,2-dipalmitoyl-sn-glycero-3-phosphocholine; DOPE: 1,2-dioleoyl-sn-glycero-3-phosphoethanolamine; CHEMS: cholesteryl hemisuccinate; DOTAP: 1,2-dioleoyl-3-trimethylammonium-propane; DOPS: 1,2-dioleoyl-sn-glycero-3-phospho-L-serine; CHOL: cholesterol. EE: Encapsulation efficacy. Size is measured in nanometers. Z-potential is measured in mV. Experiments of the

upper and middle table were performed once. Lower table shows 2 independent experiments performed.

In order to improve the encapsulation efficacy, in addition to a formulation similar to “D”, 3 formulations were tested, all of them with negative zeta-potential. Despite the negative charges of these new formulations, none of them precipitated. Interestingly, the encapsulation efficacy was dramatically increased by using CHEMS only up to 5% (Table 3C). The formulation that displayed the higher encapsulation efficacy (around 50%) formed aggregates after the liposomes were extruded through a 100nm membrane. These aggregates were however prevented upon liposomal PEGylation after the extrusion step (Figure 49). These series of observations indicate the formation of a complex between the negatively charged components of the liposomes and the positively charged Omomyc<sup>CPP</sup> at neutral pH.

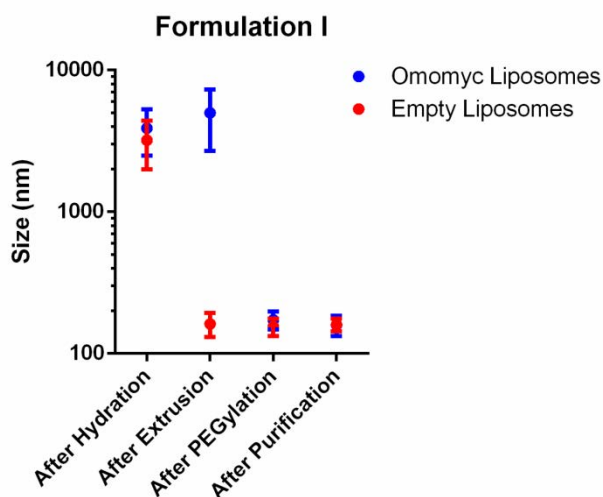


**Figure 49: Liposomes from formulation “I” aggregate after hydration with Omomyc<sup>CPP</sup> and extrusion, which is prevented by the PEGylation.** Graph shows size of liposomes (y axis, LOG10 scale) after different steps of the production of liposomes (x axis) for both Omomyc<sup>CPP</sup>-liposomes and empty liposomes. Graph shows means and standard deviation of one out of 3 independent experiments performed.

To assess the potential efficacy of the formulations G to J, A549 and U87-MG were treated with the same concentrations of liposomes following the encapsulation process. The reduction of cell viability after 3 days of



treatment was compared to the naked-peptide at concentrations of peptide equivalent to formulation “I” (assuming encapsulation efficacy of 50%): 12.5, 6.25, 3.13 and 1.56 $\mu$ M. Alamar Blue reading showed that formulation “J”, which encapsulated Omomyc with the lowest encapsulation efficacy (15%), displayed the lowest anti-tumorigenic efficacy and was comparable to a 3-fold higher concentration of naked-peptide (Figure 50). Consistently, formulation “I” showed both the highest encapsulation efficacy and effect on U87-MG and A549. Similarly to formulation “J”, the encapsulation of Omomyc<sup>CPP</sup> in formulation “I” improved 4 times the efficacy of the peptide in U87-MG and 3 times in A549. All Omomyc<sup>CPP</sup>-liposomal formulations seemed to be more effective in U87-MG than in A549. Given these results, formulation “I” was selected to look at the nuclear localization.

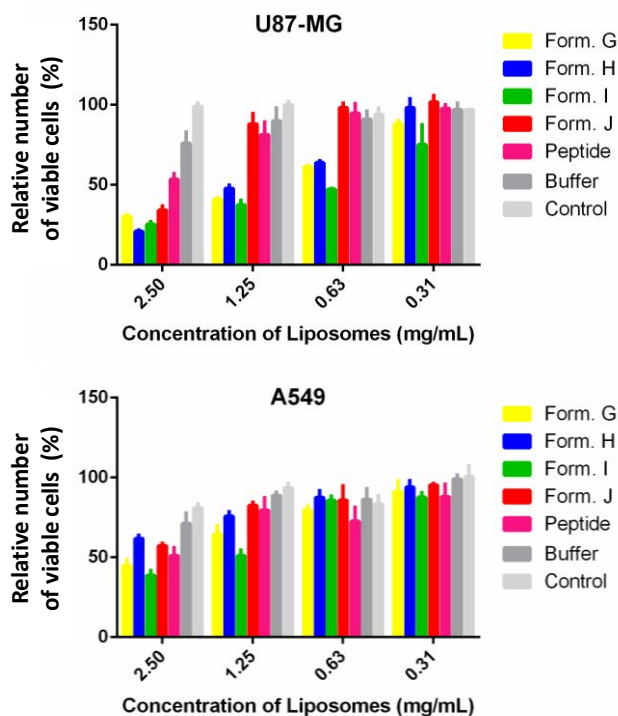


**Figure 50: Quantification of cell viability after 3 days of treatment shows that all 4 final formulations (table) reduce the number of U87-MG and A549 cells, and that formulation “I” is the most effective in both cell lines. Cells were treated with equivalent amount of liposomes (x axis) for each formulation. For each concentration of liposomes (2.50, 1.25, 0.63 and 0.31 mg/mL), concentrations of free Omomyc<sup>CPP</sup> were 12.5, 6.25, 3.13, 1.56 $\mu$ M**

respectively. Concentrations of for each formulation is dependent on their encapsulation efficacy (for "G": 10, 5, 2.5, 1.25 $\mu$ M; for "H": 8.75, 4.38, 2.19, 1.09 $\mu$ M; for "I": 12.5, 6.25, 3.13, 1.56 $\mu$ M; for "J": 3.75, 1.88, 0.94, 0.47 $\mu$ M). Encapsulation Buffer (Buffer) was used along with untreated cells (Control). Graphs represent means and standard deviation of one representative experiment out of 2 experiments performed.

Omomyc<sup>CPP</sup>-liposomes were prepared using formulation "I" and U87-MG cells were treated at a concentration of Omomyc<sup>CPP</sup> of 2 $\mu$ M. After 4 hours cells were fixed and immunofluorescence using an anti-Omomyc antibody was performed. Confocal images reveal a cytoplasmic and nuclear localization of Omomyc<sup>CPP</sup>, along with accumulations of peptide in specific regions within the cells (Figure 51). This formulation was also tested against U87-MG and A549. After 3-day treatment with Omomyc<sup>CPP</sup>-liposomes, wells presented fewer cells at concentrations up to 3.16 $\mu$ M in A549 and 1.56 $\mu$ M in U87-MG of Omomyc<sup>CPP</sup> compared to the cell number of untreated wells (Figure 52). The treatment with empty liposomes exhibited some degree of reduction in the final number of cells in both cell lines as well, although to a less extent compared to when Omomyc<sup>CPP</sup> was present.

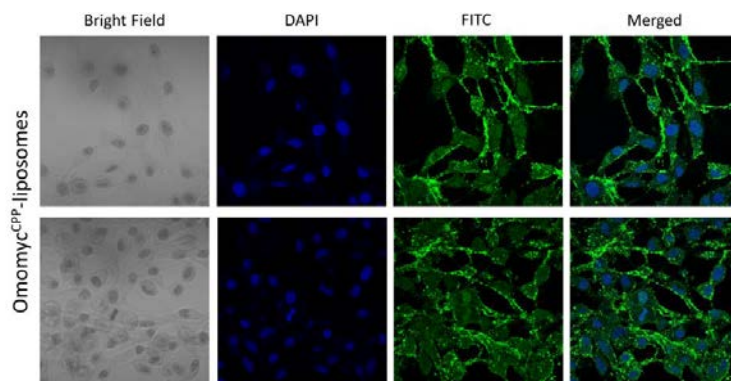


**Figure 51: Omomyc<sup>CPP</sup>-liposomes show intracellular localization, both cytoplasmic and nuclear.** U87-MG were treated with 2 $\mu$ M of Omomyc<sup>CPP</sup> encapsulated in formulation "I" for 4 hours. Cells were then fixed and permeabilized and Omomyc<sup>CPP</sup> was detected using an Omomyc-specific antibody. DNA was stained with DAPI. Representative images of one experiment out of 2 independent experiments performed are shown.

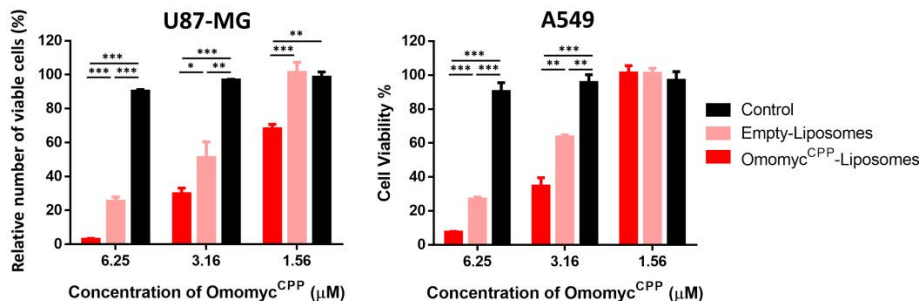


**Figure 52: Omomyc<sup>CPP</sup>-liposomes reduce the number of viable cells after 3 days, while empty liposomes also display some effect in cell number.** Cells were treated with either empty or Omomyc<sup>CPP</sup>-liposomes for 3 days and cell viability quantified using CellTiter-Blue. The number of viable cells relative to untreated control was calculated. Means and standard deviations of triplicates from a representative experiment out of 2 experiments performed are represented. One-way ANOVA was used to calculate statistical significance between the 3 groups at each concentration;  $p < 0.05$  (\*),  $p < 0.01$  (\*\*) and  $p < 0.001$  (\*\*\*).

#### 4.2.8. Proof-of-principle validation of Omomyc-derived mRNA delivery

Liposomal-mediated delivery of the Omomyc<sup>CPP</sup> increases the intracellular entrance of the peptide and displays partial nuclear localization. While these represent potentially interesting advances, an alternative method suitable for clinical application to potentiate the nuclear localization of Omomyc has also been considered and tested in preliminary experiments. Omomyc's modified-mRNA (Omomyc<sup>mRNA</sup>) has been obtained and lipofectamine used to transfect it inside cells. Then, the Omomyc antibody was used to determine if there was expression of the Omomyc protein and its subcellular localization. The Omomyc translated from the Omomyc<sup>mRNA</sup> presented a predominant nuclear localization (Figure 53). When 2 μM of Omomyc<sup>CPP</sup>-liposomes or 200 nM of Omomyc<sup>mRNA</sup> were compared directly, immunofluorescence showed more intense and nuclear staining in the cell transduced with the mRNA (Figure 54).

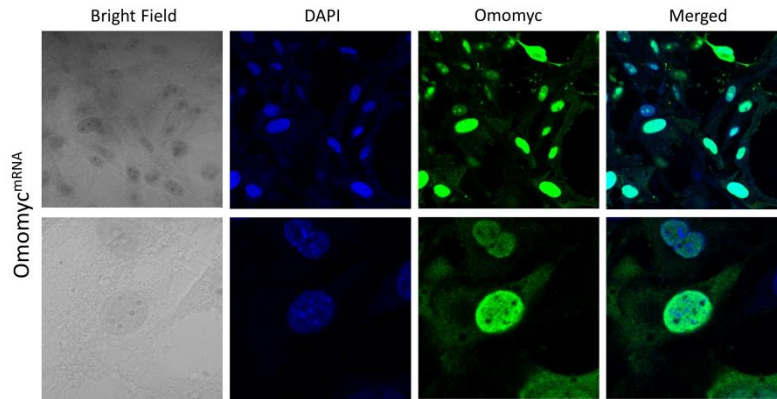


**Figure 53: Delivery of *Omomyc*<sup>mRNA</sup> is translated and the protein product localized mainly in the nuclei of cells.** 200nM of *Omomyc*<sup>mRNA</sup> were transfected using MessengerMax Lipofectamine. 24 hours after transfection cells were fixed and immunofluorescence against Omomyc was performed. Confocal images at 20x (upper row) and 40x (lower row) were acquired. Representative images of one experiment out of 2 experiments performed are shown.

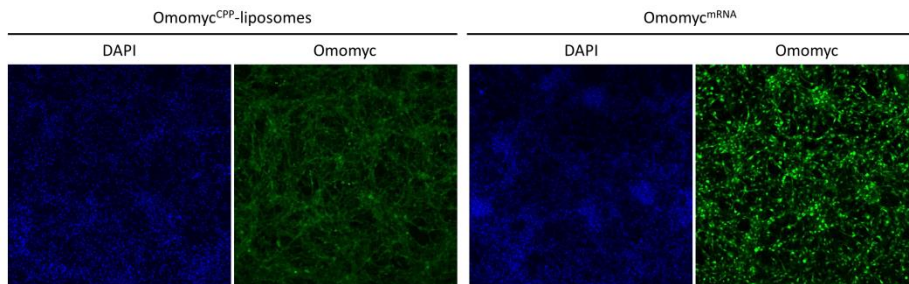


**Figure 54: 200nM of *Omomyc*<sup>mRNA</sup> produce more Omomyc than direct delivery of 2 $\mu$ M of *Omomyc*<sup>CPP</sup>-liposomes.** U87-MG cells were treated with either 2 $\mu$ M of *Omomyc*<sup>CPP</sup>-liposomes or 200nM of *Omomyc*<sup>mRNA</sup> using lipofectamine. 24 hours after the treatments cells were fixed and immunofluorescence against Omomyc was performed. Confocal images at 5x magnification were acquired maintaining the setting between images. The experiment was performed once.

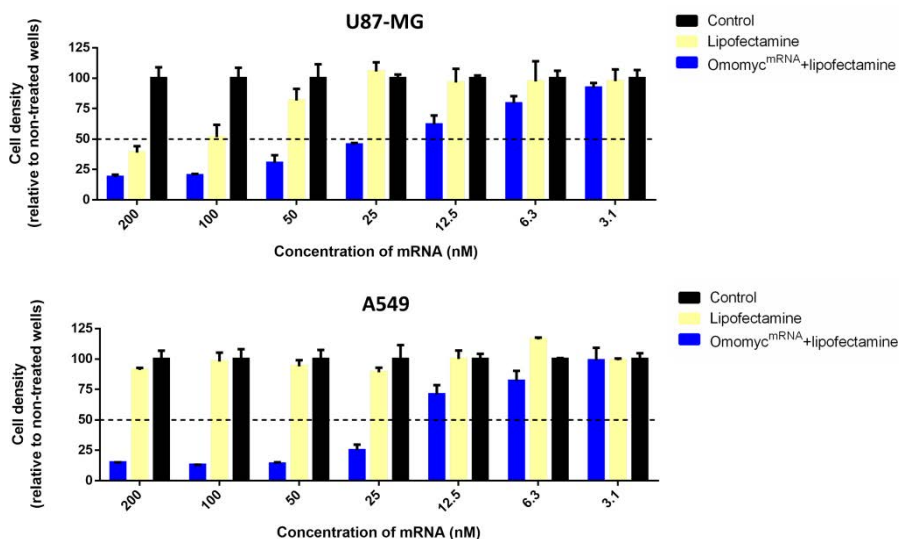


**Figure 55: Omomyc<sup>mRNA</sup> reduces the number of A549 and U87-MG cells after 3 days of treatment.** Cells were treated with 200 to 3.1nM of Omomyc<sup>mRNA</sup> previously mixed with MessengerMAX Lipofectamine (1.5 to 0.1 $\mu$ L respectively). Cells were transfected for 4 hours in FBS-free media and then replaced by fresh FBS-supplemented media for 3 days. Cell density was determined by crystal violet staining and absorbance quantified after dissolving it in acid acetic. Means and standard deviations of triplicates from one representative experiment out of 2 independent experiments are represented.

Hence, to assess whether Omomyc<sup>mRNA</sup> harbors anti-tumorigenic potential, U87-MG and A549 were treated with different concentrations of Omomyc<sup>mRNA</sup> or the corresponding amount of lipofectamine only. In both cell lines, Omomyc<sup>mRNA</sup> produced a decrease of cell viability at concentrations of mRNA up to 25nM, while addition of equivalent concentrations of lipofectamine produced toxicity at higher concentrations in U87-MG cells (Figure 55). These results suggest that Omomyc<sup>mRNA</sup> might be another useful strategy to effectively deliver Omomyc into the nuclei of cancer cells and achieve a therapeutic impact.

## 5. Discussion

---

### Section 1: Investigating Omomyc's fundamental mechanism of action in lung cancer

Myc is overexpressed and/or deregulated in the majority of human cancers. This oncogene controls several processes in normal cells that, when deregulated, contribute to the growth, maintenance and survival of tumors, acting as an engine of tumorigenesis. These reasons, among others, have raised Myc as one of the most interesting targets in oncology. However, pharmacological Myc inhibition has proven challenging and, to date, no Myc inhibitor has reached clinical application. Indeed, there are many considerations that position Myc as a potentially undruggable target. First, there are 3 different Myc family members described (c-Myc, N-Myc and L-Myc) that can replace each other in some contexts, therefore all of them must be blocked. Second, Myc acts in the nuclei of cells, so the drug against it must travel across the cell cytoplasm and efficiently translocate inside this organelle. Third, Myc is not an enzyme and displays no pocket or active site, the typical targets of traditional small molecule inhibitors. Last, Myc's critical role in normal tissue maintenance could lead to catastrophic side effects when Myc is inhibited systemically.

Despite all these preconceived notions, in 2008, Laura Soucek et al. inserted the Myc dominant negative called Omomyc as transgene in a mouse model of lung cancer and expressed it systemically [101]. These experiments proved that Myc inhibition could constitute an effective therapeutic strategy against tumors, while triggering only mild, well tolerated and fully reversible side effects in normal proliferating tissues. This discovery opened a new door to developing clinically-viable Myc inhibitors with the hope that they will be effective against tumors and present little toxicity. However, so far, no other Myc inhibitor has matched the expectations generated by Omomyc. Hence, we have proposed 2 research lines to take a step forward towards obtaining better Myc inhibitors. First, we wanted to investigate more in detail the source of Omomyc efficacy, to better understand its mechanism of action and potentially create drugs that can mimic the key features of Omomyc. Second, we have conceived for the first time the use of Omomyc itself as a

drug and tested different clinically-viable strategies in which Omomyc could be delivered to cancer cells.

To start, we aimed to identify the molecular alterations that predispose to either sensitivity or resistance to Omomyc expression. To do so, we selected a panel of lung cancer cell lines presenting different mutational profiles and expressed Omomyc by means of lentiviral transduction. It is worth noting that, in contrast to drugs, which can be used at a specific concentration against different cell lines, we could not control the expression levels of Omomyc across our panels of cells. Surprisingly, despite different levels of Omomyc expression, all the cell lines responded independently on the various mutational profiles they presented. This is consistent with a non-redundant role of Myc in cell proliferation and previous studies showing that Omomyc is effective in various mouse models regardless of their driving alterations [98, 102, 104-106, 159].

Interestingly, one independent study concluded instead that Omomyc would only be effective in cells expressing high levels of Myc [197]. However, our studies suggest instead that Omomyc's efficacy is independent of Myc expression levels. In fact, the same cell line that was identified as resistant to Omomyc expression in Fukazawa's study, H441, has shown susceptibility to treatment in our experiments.

On a different note, PC9, HCC827 and H1975 are the 3 cells line of our panel that harbor mutations in EGFR that lead to hyperactive EGFR signaling. In contrast, H292 presents wild type EGFR, but the receptor is constitutively active in this cell line, which is as sensitive to TKI as other EGFR mutants [198]. Intriguingly, these 4 cell lines showed a greater response to Omomyc when its expression levels are taken into account. More in detail, the quantification of SubG1 populations in different cell lines showed that the only cell lines with significant increases in cell death were the 2 EGFR-mutated cell lines tested, together with the KRAS-mutated Hop62 cell line that displayed the highest Omomyc levels of all.. These results imply that constitutively activated EGFR signaling might present a higher sensitivity to Omomyc. Thus, EGFR mutations could be used as a predictive marker of response to Omomyc-derived therapies. Further investigation is needed to explore the molecular bases of this observation.

Besides shedding light on EGFR hyperactivation and Omomyc sensitivity, we were interested in the reason why all cell lines analyzed, without exception, responded to Omomyc. We therefore aimed to find common events triggered by Omomyc in virtually all of them. The most evident common change produced by Omomyc was an increase in cell size. Intriguingly, again this growth was especially pronounced in the 2 EGFR mutated cell lines analyzed, which would potentially link this morphological change with the sensitivity to Omomyc. In this context, we also performed some experiments to determine whether there were consistent alterations in the metabolism and/or differentiation that could trigger the increase in size, for example by changes in glycolysis, lipid metabolism, senescence, stem cell markers and epithelial-to-mesenchymal transition. Unfortunately, the preliminary data showed no notable differences between Omomyc-expressing and control cells in any of these features. However, we believe that further studies in this phenomenon could help understanding the molecular events that are shared among different types of cancer.

In addition to the increase in cell size, one very interesting aspect we identified was the co-localization of Omomyc with condensed DNA during mitosis and the increase in Max protein levels, as communalities observed in all cell lines. Both events converged in the surprising and unexpected co-localization of Omomyc, Max and DNA during mitosis. This observation represents the first evidence of a gain-of-function of Omomyc, suggesting it may have additional effects within cancer cells aside from merely inhibiting Myc. This co-localization could also be related to the obstruction of a proficient cell division and triggering mitotic defects that we already observed, for example, in glioblastoma cells as a consequence of Omomyc expression [105]. Moreover, ChIP-sequencing analysis revealed that while Myc was largely displaced from DNA, Max was still mostly bound to it and was instead occupying new regions when Omomyc was expressed. A possible explanation for these results is the formation of Omomyc/Max dimers that could harbor a DNA specificity different from Myc/Max. The massive binding of Omomyc/Max on DNA (even visible by fluorescent microscopy when cells divide) may stabilize the dimer, which would explain the increased stability of Omomyc compared to Myc and of Max in the presence of Omomyc. Moreover, a higher DNA affinity could itself favor the formation of Omomyc/Max dimers compared to Myc/Max by when competing for binding Myc target genes. Hence, the net outcome of all these factors is a dramatic



inhibition of Myc binding to its DNA target sites-, while Max remains largely unaffected on those same sites. Thus, while it is true that Omomyc can dimerize with Myc, Max and with itself, , our experiments indicate an important contribution of Omomyc/Max heterodimers to the mechanism of action of Omomyc. Moreover, the unexpected binding of Max on genomic regions beyond Myc-related promoters upon Omomyc expression opens the possibility that Omomyc expression might also affect the binding of other transcription factors and/or the expression of Myc-unrelated part of the genome. This speculation will need to be studied in more detail.

Our observations suggest that the DNA binding ability of Omomyc/Max heterodimers potentially represents a key attribute of Omomyc. Thus, an Omomyc mutant that is not able to bind DNA should be much less effective than Omomyc. Such a mutant was described in [160], where the authors demonstrate that OmoHER (an Omomyc variant bearing 3 amino acidic mutations in the basic region) was not able to inhibit Myc binding to its target genes to the same extent that Omomyc does [160]. Consistent with this, in our hands, the efficacy of the mutant is largely impaired compared to Omomyc when we look at cell proliferation. However, in contrast to others [106, 160] and in light of our CHIP sequencing results, we hypothesize that it is also the inability to bind DNA of Omomyc/Max dimers, and not only of Omomyc/Omomyc homodimers, that would cause the reduced efficacy of OmoHER. Interestingly, while OmoHER has been described as unable to bind Myc target genes and we observed that it has little effect on cell proliferation, we showed that it is still able to co-localize with DNA in mitosis. Hence, we infer that OmoHER retains some of Omomyc's affinity toward DNA, but the 3 point mutations (H-E-R) impair the recognition of specific Myc-related DNA regions which, when inhibited, play a key role in mediating Omomyc's efficacy. Nevertheless, this supports that Omomyc/Max/DNA co-localization observed in mitosis does not seem to cause the reduction in cell proliferation observed as a consequence of Omomyc expression, since OmoHER's efficacy is vastly weaker than Omomyc's.

To complement these studies, we cloned the b-HLH-LZ domain of Myc ( $\Delta$ Myc) inside the pTRIPZ-RFP vector.  $\Delta$ Myc has been shown to dimerize with Max and bind to DNA as a heterodimer [63, 64]. However, since it lacks the transactivating domain of Myc, it does not recruit the co-factors necessary to activate target genes. Therefore,  $\Delta$ Myc binds to Max and forms a dimer that

acts as a competitor of Myc/Max on DNA, which is one of the known modes of action of Omomyc. On the other hand,  $\Delta$ Myc is neither able to bind to Myc nor to form homodimers (in contrast to Omomyc) due to the presence of repulsive interactions at the putative interface [99]. Interestingly, although  $\Delta$ Myc lacks 2 of Omomyc's main modes of action, its effect on cell proliferation was similar to Omomyc. In addition, we observed that  $\Delta$ Myc, like endogenous Myc, does not co-localize with DNA in mitosis. Therefore, it seems that the features that  $\Delta$ Myc lacks (homodimerization, sequestration of Myc and visible co-localization with DNA in mitosis) would not be essential events for an effective inhibition of cell proliferation at least in H1299. However, we cannot exclude the fact that these features of Omomyc might be contributing importantly to its anti-tumorigenic effect in other biological contexts (for example, in cancer cells harboring specific alterations, in tumors growing in a living organism or in cells with different levels or ratios of Myc and Max proteins). In fact, recent data generated using Omomyc in other cellular contexts, indicate that it inhibits Myc predominantly by forming homodimers that bind DNA [106, 160].

Actually, other publications support the importance of occupying DNA to inhibit Myc using HLH-LZ peptides including Omomyc [106, 160], Max\* [148] and ME47 [150]. Further investigation would be required to fully characterize whether the disruption of Myc/Max (by sequestering Myc and Max away from each other) would display less efficacy compared to directly inhibiting the DNA occupancy of Myc target genes, and how Myc inhibitors could better take advantage of endogenous Max to inhibit Myc's DNA occupancy more effectively. So far, our observations suggest that new peptidic drugs aimed at directly competing with Myc binding to DNA, rather than disrupting Myc/Max, might prove of good therapeutic value.

## Section 2: Transforming Omomyc from proof of principle to therapeutic strategy

In addition to unravelling the molecular mechanisms that lead to Omomyc's efficacy with the aim of designing better therapies, we have tested several Omomyc-based lead formulations to directly translate the Omomyc transgene into a pharmacological approach. Of note, the 91 amino acid peptide Omomyc has long been considered too bulky to be used as a drug. Interestingly though, Montagne et al. showed that Max\*, a b-HLH-LZ peptide that shares a high degree of homology with Omomyc, was able to spontaneously penetrate cells [148]. We therefore purified and tested the cell-penetrating potential of the Omomyc peptide in A549 and H1975 cells. Encouragingly, the Omomyc peptide was able to penetrate cells and partially locate in the nuclei (hence we called it Omomyc<sup>CPP</sup> for 'Omomyc cell-penetrating peptide'). Despite evidence of some endosomal retention, Omomyc<sup>CPP</sup> was able to reach its target and to inhibit cell proliferation and Myc occupancy on DNA. It is worth noting that this happened while Myc protein levels remained unaffected (at least in A549 cells), excluding any down-regulation of Myc expression due to off-target toxicity and, thus, indicating a proper Myc displacement from DNA. In vivo, the Omomyc<sup>CPP</sup> reached several organs following i.v. administration, including subcutaneous tumors generated using H1975 cells. Importantly, in this same model, i.v. administration of Omomyc<sup>CPP</sup> 4 times a week at 93.5kg/mg produced a notable reduction in the tumor growth and did not cause any visible sign of toxicity. Subsequent experiments demonstrated that a higher dose of Omomyc<sup>CPP</sup> (187.5mg/kg) does not cause a more pronounced therapeutic impact, which indicates that the responses we obtained have already reached a plateau at the lower dose. Thus, it is even possible that we could further reduce it, maintaining the same therapeutic impact, or even improving it.

In addition, we have shown that Omomyc<sup>CPP</sup> could be effectively combined with standard chemotherapy (paclitaxel) to boost the therapeutic response of the tumors without triggering further toxicity, valuable information for the future design of clinical trials.

Taken together, these results suggest that the Omomyc<sup>CPP</sup> can represent already a safe and promising therapeutic agent with an anti-tumorigenic

impact. Since we have demonstrated its efficacy through systemic administration, this approach could be used to treat cancers of several origins, including metastatic cancers. However, some aspects such as the nuclear localization or the biodistribution could still be improved to unleash the full therapeutic potential of Omomyc<sup>CPP</sup>. In addition, so far, immunocompromised animals have been used to test both efficacy and toxicity of the compound. However, in the presence of a fully competent immune system, it is possible that Omomyc<sup>CPP</sup> could become immunogenic and trigger a progressive immune response after continuous treatment that would reduce the efficacy over time. For these reasons, we decided to test the potential performance of the Omomyc<sup>CPP</sup> by encapsulating it inside liposomes.

Liposomes have already been used, among other purposes, to protect their cargos from degradation and from the immune system, to actively and passively target tumors and to improve the endosomal escape of drugs. We successfully produced the first Omomyc<sup>CPP</sup>-liposomes and demonstrated that liposomal delivery could improve even further the entrance of Omomyc<sup>CPP</sup> within cells. The caveolae-mediated endocytosis was identified as the main pathway used for the Omomyc<sup>CPP</sup>-liposomes uptake. This might represent some advantages compared the most common endocytic pathway, clathrin-mediated endocytosis. First, caveolae-mediated endocytosis can bypass the acidic and enzymatic degradation within lysosomes, which might increase the efficacy of delivering drugs [199]. And second, it has been shown that this pathway could represent a safe route to reach the nucleus [200]. We then incorporated CHEMS into the liposome composition, which can enhance endosomal escape, one of the main limiting factors in the delivery of DNA, RNA and peptides [201]. Moreover, CHEMS provide negative charges to the liposomes, which we thought might increase the encapsulation of the positively-charged peptide. These negative charges improved the encapsulation efficiency of the positively-charged Omomyc<sup>CPP</sup> at pH 7 to 50%. We demonstrated that, when CHEMS was incorporated, the liposomes aggregated only in the presence of Omomyc<sup>CPP</sup>, which indicates an interaction between the peptide and the phospholipid bilayer that may contribute to the increased encapsulation. This new liposomal formulation with CHEMS also displayed a higher nuclear localization of Omomyc<sup>CPP</sup> compared to the first formulation tested, although the experiments were not performed in parallel. Overall, this formulation is the one that performed

best in terms of encapsulation efficiency and reduction of cell viability, which was more pronounced than with the non-encapsulated Omomyc<sup>CPP</sup>. However, part of this improvement could be produced by the liposomes itself, since the empty formulation displayed some degree of toxicity (which was unexpected since this formulation has previously shown no toxicity in the Torchilin laboratory). Further investigation of this toxicity and attempts to reduce it with new formulations and improve Omomyc's biodistribution and efficacy in vivo will be needed in the near future. Moreover, given that Omomyc and paclitaxel have shown a higher therapeutic impact than both monotherapies, co-delivery of Omomyc and chemotherapeutic agents in the same liposomes is currently being investigated.

To complement our studies with the peptide, we investigated a third and completely different approach to deliver Omomyc into cancer cells: delivering Omomyc modified-mRNA (Omomyc<sup>mRNA</sup>). The most direct translation of the Omomyc proof-of-principle transgene into a clinical application would be its delivery of DNA (gene therapy). Virus-mediated gene transfer has shown good transfection efficiencies but has raised serious safety concerns. The use of plasmid DNA, conversely, is considered safer but has displayed much lower transfection efficiency [202]. Just recently, mRNA-based gene transfer has been proposed as a promising new strategy for gene therapy [203]. Limitations of the use of mRNA in vivo as therapeutic agent have been circumvented by modifications in the nucleotides that assemble the single-stranded mRNA. Replacing only 25% of uridines and cytidines with 2-thiouridines and 5-methyl-cytidines, respectively, synergistically decrease mRNA immunogenicity and increase stability in mice [204]. mRNA delivery has been even applied already in the clinic as means of exploiting the antiviral defenses of the host for cancer immunotherapy [205]. Thus, the delivery of an Omomyc<sup>mRNA</sup>, if effective, could be potentially pushed into clinical trials.

Given the potential use of Omomyc<sup>mRNA</sup> as a new therapeutic approach, we wanted to assess whether its delivery could improve the nuclear localization of Omomyc and the therapeutic potential that it would have in cancer cells. As expected, the delivery of Omomyc<sup>mRNA</sup> produced an Omomyc protein that was almost completely nuclear. The successful delivery of one molecule of mRNA could potentially trigger the expression of tens, hundreds or thousands of protein products, depending on the mRNA stability.

Consistently, although the delivery systems are different, the treatment of cells with 10 times fewer molecules of Omomyc<sup>mRNA</sup> compared to Omomyc<sup>CPP</sup>-liposomes produced a higher Omomyc presence inside cells. Our preliminary data show a strong impact of Omomyc<sup>mRNA</sup> on cell proliferation, thus demonstrating that the delivery of Omomyc<sup>mRNA</sup> could represent a promising complementary therapeutic strategy to the use of the Omomyc<sup>CPP</sup>. Future experiments in this research line are aimed at identifying suitable nanocarriers for the *in vivo* delivery of our mRNAs to cancer cells and the preclinical validation of intranasal and intravenous delivery to mouse models of lung cancer.

In summary, these 3 research lines led to the identification of 3 potential clinically-viable therapeutic strategies to deliver Omomyc into cancer cells. Each of these strategies covers potential deficiencies of the others. The free-Omomyc<sup>CPP</sup> is to date the most advanced and the one that has been tested *in vivo*, showing efficacy. The production of free-Omomyc<sup>CPP</sup> as a final drug is the simplest of the 3 and is being further tested *in vivo* with the aim of starting clinical trials in the near future.

The biodistribution and stability of the Omomyc<sup>CPP</sup> could be improved by its encapsulation as Omomyc<sup>CPP</sup>-liposomes. In addition, in the case of an immune response of the host against Omomyc<sup>CPP</sup>, the PEGylated liposomal membrane would minimize or completely prevent that response. These liposomes represent also a more flexible approach, since their outer part can be decorated to target the drug to tumor cells, maintaining the active component intact. Therefore, since Omomyc has already shown efficacy in different tumor types, this approach would allow us to actively target different cancers. However, the production of the Omomyc<sup>CPP</sup>-liposomes represents a longer and more complex process. In addition, the liposome itself could be a source of toxicity that would limit the maximum tolerated dose of the treatment.

Finally, the use of Omomyc<sup>mRNA</sup> has shown higher nuclear localization of Omomyc compared to the other 2 peptide strategies. In the last years, there has been an improvement in the delivery of RNA in general (especially siRNA and microRNA) and this knowledge can be applied to the delivery of mRNA too. This strategy represents the least advanced of the 3 approaches, yet it is also the most versatile. Virtually any Omomyc variant (even those that cannot be easily produced or purified as peptides) could be delivered using

the same strategy. Similarly to Omomyc<sup>CPP</sup>-liposomes, Omomyc<sup>mRNA</sup> nanoparticles could be decorated to improve tumor-targeting using ligands or antibodies against cell-surface tumor markers. While this active targeting approach may improve the pharmacokinetics of the encapsulated molecule, it may also present an important limitation. Although Omomyc has demonstrated to be effective against several different cancers, tumors could evolve and develop resistance once the targeted molecule is eliminated from its surface. Another potential limitation is the higher instability of mRNAs compared to proteins and peptides. Thus, their need for a nanocarrier would represent additional steps and complexity in the production procedure and a source of potential in vivo toxicity. Subsequent experiments, especially those in vivo, will help us determining which of these strategies can be the most promising or how they can complement each other to effectively treat cancer in patients.

In combination, results from the 2 sections gathered in the present thesis have significantly contributed – and will continue to contribute – to generating new Omomyc variants (produced as peptides and/or mRNAs), rationally conceived based on a better understanding of Omomyc's mechanism of action. A good example of this is represented by a patent we have filed to protect the use of an Omomyc variant that showed higher efficacy in vitro (P13088EP00).

In addition, these results have contributed to generating novel therapeutic options that have been already incorporated in the portfolio of PEPTOMYC S.L., a VHIO spin-off company from our laboratory that develops Omomyc-based drugs, to further boost the therapeutic arsenal for the treatment of cancer patients.

## 6. Conclusions

---

### Section 1:

1. The pTRIPZ Omomyc-RFP doxycycline inducible vector can be used as a tool to study the Omomyc-based Myc inhibition mechanism of action.
2. Omomyc expression is effective in various lung cancer cell lines, regardless of their mutational profile.
3. Omomyc expression consistently causes an increase in Max protein levels and its co-localization with DNA, which is visible when DNA condenses during cell division.
4. Omomyc expression displaces Myc from chromatin, but not Max .
5. The dimerization to Max and DNA occupancy as Omomyc/Max dimers provides a key contribution to Omomyc's anti-tumorigenic potential.

### Section 2:

6. The Omomyc<sup>CPP</sup> spontaneously penetrates cells, reduces Myc's DNA occupancy and displays anti-tumorigenic effects in A549 and H1957.
7. Intravenous administration of Omomyc<sup>CPP</sup> (up to 187.5mg/Kg) is safe and reduces tumor growth of H1975 inoculated subcutaneously in nude mice.
8. Intravenous administration of Omomyc<sup>CPP</sup> in combination with paclitaxel presents a higher therapeutic potential compared to both monotherapies without displaying higher toxicity.
9. Omomyc<sup>CPP</sup> can be encapsulated into liposomes, which increase the cellular uptake and allow partial nuclear localization of the peptide in vitro.
10. Delivery of Omomyc's mRNA is translated into a nuclear Omomyc protein that displays efficacy in cancer cells.





## 7. References

---

1. WHO. (2015). GLOBOCAN 2012: Estimated Cancer Incidence, Mortality and Prevalence Worldwide in 2012. (World Health Organization).
2. Ferlay J SI, Ervik M, Dikshit R, Eser S, Mathers C et al. (2013). Cancer Incidence and Mortality Worldwide: IARC CancerBase No. 11. GLOBOCAN 2012 v10,.
3. ACS. (2018). Cancer Basics: Lifetime Risk of Developing or Dying From Cancer. (American Cancer Society)
4. Stewart BW WC, editors. . World cancer report 2014. Lyon: International Agency for Research on Cancer. 2014. doi:
5. Vogelstein B, Papadopoulos N, Velculescu VE, Zhou S, Diaz LA, Jr., Kinzler KW. Cancer genome landscapes. *Science*. 2013; 339: 1546-58. doi: 10.1126/science.1235122.
6. Hanahan D, Weinberg RA. Hallmarks of cancer: the next generation. *Cell*. 2011; 144: 646-74. doi: 10.1016/j.cell.2011.02.013.
7. Alexandrov LB, Nik-Zainal S, Wedge DC, Aparicio SA, Behjati S, Biankin AV, Bignell GR, Bolli N, Borg A, Borresen-Dale AL, Boyault S, Burkhardt B, Butler AP, et al. Signatures of mutational processes in human cancer. *Nature*. 2013; 500: 415-21. doi: 10.1038/nature12477.
8. Cusnir M, Cavalcante L. Inter-tumor heterogeneity. *Hum Vaccin Immunother*. 2012; 8: 1143-5. doi: 10.4161/hv.21203.
9. Fisher R, Pusztai L, Swanton C. Cancer heterogeneity: implications for targeted therapeutics. *Br J Cancer*. 2013; 108: 479-85. doi: 10.1038/bjc.2012.581.
10. Konig IR, Fuchs O, Hansen G, von Mutius E, Kopp MV. What is precision medicine? *Eur Respir J*. 2017; 50. doi: 10.1183/13993003.00391-2017.
11. Roden D, Tyndale R. Genomic Medicine, Precision Medicine, Personalized Medicine: What's in a Name? *Clin Pharmacol Ther*. 2013; 94: 169-72. doi: 10.1038/clpt.2013.101.
12. Kwak EL, Bang YJ, Camidge DR, Shaw AT, Solomon B, Maki RG, Ou SH, Dezube BJ, Janne PA, Costa DB, Varella-Garcia M, Kim WH, Lynch TJ, et al. Anaplastic lymphoma kinase inhibition in non-small-cell lung cancer. *N Engl J Med*. 2010; 363: 1693-703. doi: 10.1056/NEJMoa1006448.
13. Mok TS, Wu YL, Thongprasert S, Yang CH, Chu DT, Saijo N, Sunpaweravong P, Han B, Margono B, Ichinose Y, Nishiwaki Y, Ohe Y, Yang JJ,

- et al. Gefitinib or carboplatin-paclitaxel in pulmonary adenocarcinoma. *N Engl J Med*. 2009; 361: 947-57. doi: 10.1056/NEJMoa0810699.
14. Rosell R, Carcereny E, Gervais R, Vergnenegre A, Massuti B, Felip E, Palmero R, Garcia-Gomez R, Pallares C, Sanchez JM, Porta R, Cobo M, Garrido P, et al. Erlotinib versus standard chemotherapy as first-line treatment for European patients with advanced EGFR mutation-positive non-small-cell lung cancer (EURTAC): a multicentre, open-label, randomised phase 3 trial. *Lancet Oncol*. 2012; 13: 239-46. doi: 10.1016/s1470-2045(11)70393-x.
15. Sequist LV, Yang JC, Yamamoto N, O'Byrne K, Hirsh V, Mok T, Geater SL, Orlov S, Tsai CM, Boyer M, Su WC, Bennouna J, Kato T, et al. Phase III study of afatinib or cisplatin plus pemetrexed in patients with metastatic lung adenocarcinoma with EGFR mutations. *J Clin Oncol*. 2013; 31: 3327-34. doi: 10.1200/jco.2012.44.2806.
16. Chan BA, Hughes BGM. Targeted therapy for non-small cell lung cancer: current standards and the promise of the future. *Transl Lung Cancer Res*. 2015; 4: 36-54. doi: 10.3978/j.issn.2218-6751.2014.05.01.
17. Lee CK, Brown C, Gralla RJ, Hirsh V, Thongprasert S, Tsai CM, Tan EH, Ho JC, Chu da T, Zaatar A, Osorio Sanchez JA, Vu VV, Au JS, et al. Impact of EGFR inhibitor in non-small cell lung cancer on progression-free and overall survival: a meta-analysis. *J Natl Cancer Inst*. 2013; 105: 595-605. doi: 10.1093/jnci/djt072.
18. Zhao D, Chen X, Qin N, Su D, Zhou L, Zhang Q, Li X, Zhang X, Jin M, Wang J. The prognostic role of EGFR-TKIs for patients with advanced non-small cell lung cancer. *Sci Rep*. 2017; 7. doi: 10.1038/srep40374.
19. Yang JC, Wu YL, Schuler M, Sebastian M, Popat S, Yamamoto N, Zhou C, Hu CP, O'Byrne K, Feng J, Lu S, Huang Y, Geater SL, et al. Afatinib versus cisplatin-based chemotherapy for EGFR mutation-positive lung adenocarcinoma (LUX-Lung 3 and LUX-Lung 6): analysis of overall survival data from two randomised, phase 3 trials. *Lancet Oncol*. 2015; 16: 141-51. doi: 10.1016/s1470-2045(14)71173-8.
20. Lin JZ, Long JY, Wang AQ, Zheng Y, Zhao HT. Precision medicine: In need of guidance and surveillance. *World J Gastroenterol*. 2017; 23: 5045-50. doi: 10.3748/wjg.v23.i28.5045.
21. Dienstmann R, Serpico D, Rodon J, Saura C, Macarulla T, Elez E, Alsina M, Capdevila J, Perez-Garcia J, Sanchez-Olle G, Aura C, Prudkin L, Landolfi S, et al. Molecular profiling of patients with colorectal cancer and matched targeted therapy in phase I clinical trials. *Mol Cancer Ther*. 2012; 11: 2062-71. doi: 10.1158/1535-7163.mct-12-0290.

22. De Mattos-Arruda L, Oliveira M, Navarro A, Vilaro M, Nuciforo P, Vivancos A, Seoane J, Rodon J, Cortes J, Saura C. (2013). Molecular profiling of advanced breast cancer patients and benefit obtained from matched targeted therapy in early phase clinical trials. *EUROPEAN JOURNAL OF CANCER: ELSEVIER SCI LTD THE BOULEVARD, LANGFORD LANE, KIDLINGTON, OXFORD OX5 1GB, OXON, ENGLAND*), pp. S418-S.
23. Morgillo F, Della Corte CM, Fasano M, Ciardiello F. Mechanisms of resistance to EGFR-targeted drugs: lung cancer. *ESMO Open*. 2016; 1. doi: 10.1136/esmoopen-2016-000060.
24. Prahallad A, Sun C, Huang S, Di Nicolantonio F, Salazar R, Zecchin D, Beijersbergen RL, Bardelli A, Bernards R. Unresponsiveness of colon cancer to BRAF(V600E) inhibition through feedback activation of EGFR. *Nature*. 2012; 483: 100-3. doi: 10.1038/nature10868.
25. Desai J, Markman B, Ananda S, Tebbutt NC, Michael M, Solomon BJ, McArthur GA, Tie J, Gibbs P, Ritchie D, Koldej R, Herschtal A, Columbus R, et al. A phase I/II trial of combined BRAF and EGFR inhibition in patients (pts) with BRAF V600E mutated (BRAFM) metastatic colorectal (mCRC): The EVICT (Erlotinib and Vemurafenib in Combination Trial) study. *Journal of Clinical Oncology*. 2017; 35: 3557-. doi: 10.1200/JCO.2017.35.15\_suppl.3557.
26. Janku F. Tumor heterogeneity in the clinic: is it a real problem? *Ther Adv Med Oncol*. 2014; 6: 43-51. doi: 10.1177/1758834013517414.
27. Lavi O. Redundancy: a critical obstacle to improving cancer therapy. *Cancer Res*. 2015; 75: 808-12. doi: 10.1158/0008-5472.can-14-3256.
28. Li YH, Yu CY, Li XX, Zhang P, Tang J, Yang Q, Fu T, Zhang X, Cui X, Tu G, Zhang Y, Li S, Yang F, et al. Therapeutic target database update 2018: enriched resource for facilitating bench-to-clinic research of targeted therapeutics. *Nucleic Acids Res*. 2018; 46: D1121-D7. doi: 10.1093/nar/gkx1076.
29. Bull SC, Doig AJ. Properties of Protein Drug Target Classes. *PLoS One*. 2015; 10. doi: 10.1371/journal.pone.0117955.
30. Munagala R, Aqil F, Gupta RC. Promising molecular targeted therapies in breast cancer. *Indian J Pharmacol*. 2011; 43: 236-45. doi: 10.4103/0253-7613.81497.
31. Sodir NM, Evan GI. Finding cancer's weakest link. *Oncotarget*. 2011; 2: 1307-13. doi:
32. Gashaw I, Ellinghaus P, Sommer A, Asadullah K. What makes a good drug target? *Drug Discov Today*. 2011; 16: 1037-43. doi: 10.1016/j.drudis.2011.09.007.

33. Sheiness D, Bishop JM. DNA and RNA from Uninfected Vertebrate Cells Contain Nucleotide Sequences Related to the Putative Transforming Gene of Avian Myelocytomatosis Virus. *J Virol.* 1979; 31: 514-21. doi:
34. Dalla-Favera R, Bregni M, Erikson J, Patterson D, Gallo RC, Croce CM. Human c-myc onc gene is located on the region of chromosome 8 that is translocated in Burkitt lymphoma cells. *Proc Natl Acad Sci U S A.* 1982; 79: 7824-7. doi:
35. Kalkat M, De Melo J, Hickman KA, Lourenco C, Redel C, Resetca D, Tamachi A, Tu WB, Penn LZ. MYC Deregulation in Primary Human Cancers. *Genes (Basel).* 2017; 8. doi: 10.3390/genes8060151.
36. Dang CV, Reddy EP, Shokat KM, Soucek L. Drugging the 'undruggable' cancer targets. *Nat Rev Cancer.* 2017; 17: 502-8. doi: 10.1038/nrc.2017.36.
37. Dang CV, O'Donnell KA, Zeller KI, Nguyen T, Osthus RC, Li F. The c-Myc target gene network. *Semin Cancer Biol.* 2006; 16: 253-64. doi: 10.1016/j.semancer.2006.07.014.
38. Sears R, Nuckolls F, Haura E, Taya Y, Tamai K, Nevins JR. Multiple Ras-dependent phosphorylation pathways regulate Myc protein stability. *Genes Dev.* 2000; 14: 2501-14. doi:
39. Zhu J, Blenis J, Yuan J. Activation of PI3K/Akt and MAPK pathways regulates Myc-mediated transcription by phosphorylating and promoting the degradation of Mad1. *Proc Natl Acad Sci U S A.* 2008; 105: 6584-9. doi: 10.1073/pnas.0802785105.
40. Lord JD, McIntosh BC, Greenberg PD, Nelson BH. The IL-2 receptor promotes lymphocyte proliferation and induction of the c-myc, bcl-2, and bcl-x genes through the trans-activation domain of Stat5. *J Immunol.* 2000; 164: 2533-41. doi:
41. Dubik D, Dembinski TC, Shiu RP. Stimulation of c-myc oncogene expression associated with estrogen-induced proliferation of human breast cancer cells. *Cancer Res.* 1987; 47: 6517-21. doi:
42. Yagi K, Furuhashi M, Aoki H, Goto D, Kuwano H, Sugamura K, Miyazono K, Kato M. c-myc is a downstream target of the Smad pathway. *J Biol Chem.* 2002; 277: 854-61. doi: 10.1074/jbc.M104170200.
43. Rennoll S, Yochum G. Regulation of MYC gene expression by aberrant Wnt/beta-catenin signaling in colorectal cancer. *World J Biol Chem.* 2015; 6: 290-300. doi: 10.4331/wjbc.v6.i4.290.
44. Welcker M, Orian A, Jin J, Grim JE, Harper JW, Eisenman RN, Clurman BE. The Fbw7 tumor suppressor regulates glycogen synthase kinase 3

- phosphorylation-dependent c-Myc protein degradation. *Proc Natl Acad Sci U S A*. 2004; 101: 9085-90. doi: 10.1073/pnas.0402770101.
45. Palomero T, Lim WK, Odom DT, Sulis ML, Real PJ, Margolin A, Barnes KC, O'Neil J, Neuberger D, Weng AP, Aster JC, Sigaux F, Soulier J, et al. NOTCH1 directly regulates c-MYC and activates a feed-forward-loop transcriptional network promoting leukemic cell growth. *Proc Natl Acad Sci U S A*. 2006; 103: 18261-6. doi: 10.1073/pnas.0606108103.
46. Kim HH, Kuwano Y, Srikantan S, Lee EK, Martindale JL, Gorospe M. HuR recruits let-7/RISC to repress c-Myc expression. *Genes Dev*. 2009; 23: 1743-8. doi: 10.1101/gad.1812509.
47. Lal A, Navarro F, Maher C, Maliszewski LE, Yan N, O'Day E, Chowdhury D, Dykxhoorn DM, Tsai P, Hofman O, Becker KG, Gorospe M, Hide W, et al. miR-24 inhibits cell proliferation by suppressing expression of E2F2, MYC and other cell cycle regulatory genes by binding to "seedless" 3'UTR microRNA recognition elements. *Mol Cell*. 2009; 35: 610-25. doi: 10.1016/j.molcel.2009.08.020.
48. Wang W, Liao P, Shen M, Chen T, Chen Y, Li Y, Lin X, Ge X, Wang P. SCP1 regulates c-Myc stability and functions through dephosphorylating c-Myc Ser62. *Oncogene*. 2016; 35: 491-500. doi: 10.1038/onc.2015.106.
49. Vervoorts J, Lüscher-Firzlaff JM, Rottmann S, Lilischkis R, Walsemann G, Dohmann K, Austen M, Lüscher B. Stimulation of c-MYC transcriptional activity and acetylation by recruitment of the cofactor CBP. *EMBO Rep*. 2003; 4: 484-90. doi: 10.1038/sj.embor.embor821.
50. Fujii M, Lyakh LA, Bracken CP, Fukuoka J, Hayakawa M, Tsukiyama T, Soll SJ, Harris M, Rocha S, Roche KC, Tominaga S, Jen J, Perkins ND, et al. SNIP1 is a candidate modifier of the transcriptional activity of c-Myc on E box-dependent target genes. *Mol Cell*. 2006; 24: 771-83. doi: 10.1016/j.molcel.2006.11.006.
51. Hung CL, Wang LY, Yu YL, Chen HW, Srivastava S, Petrovics G, Kung HJ. A long noncoding RNA connects c-Myc to tumor metabolism. *Proc Natl Acad Sci U S A*. 2014; 111: 18697-702. doi: 10.1073/pnas.1415669112.
52. Grandori C, Cowley SM, James LP, Eisenman RN. The Myc/Max/Mad network and the transcriptional control of cell behavior. *Annu Rev Cell Dev Biol*. 2000; 16: 653-99. doi: 10.1146/annurev.cellbio.16.1.653.
53. Evan GI, Wyllie AH, Gilbert CS, Littlewood TD, Land H, Brooks M, Waters CM, Penn LZ, Hancock DC. Induction of apoptosis in fibroblasts by c-myc protein. *Cell*. 1992; 69: 119-28. doi:
54. Lowe SW, Cepero E, Evan G. Intrinsic tumour suppression. *Nature*. 2004; 432: 307-15. doi: 10.1038/nature03098.

55. Bouchard C, Marquardt J, Brás A, Medema RH, Eilers M. Myc-induced proliferation and transformation require Akt-mediated phosphorylation of FoxO proteins. *Embo j.* 2004; 23: 2830-40. doi: 10.1038/sj.emboj.7600279.
56. Pelengaris S, Khan M, Evan GI. Suppression of Myc-induced apoptosis in beta cells exposes multiple oncogenic properties of Myc and triggers carcinogenic progression. *Cell.* 2002; 109: 321-34. doi:
57. Welm AL, Kim S, Welm BE, Bishop JM. MET and MYC cooperate in mammary tumorigenesis. *Proc Natl Acad Sci U S A.* 2005; 102: 4324-9. doi: 10.1073/pnas.0500470102.
58. Jacobs JJJ, Scheijen B, Voncken JW, Kieboom K, Berns A, van Lohuizen M. Bmi-1 collaborates with c-Myc in tumorigenesis by inhibiting c-Myc-induced apoptosis via INK4a/ARF. *Genes Dev.* 1999; 13: 2678-90. doi:
59. Conacci-Sorrell M, McFerrin L, Eisenman RN. An overview of MYC and its interactome. *Cold Spring Harb Perspect Med.* 2014; 4: a014357. doi: 10.1101/cshperspect.a014357.
60. Dang CV, Lee WM. Identification of the human c-myc protein nuclear translocation signal. *Mol Cell Biol.* 1988; 8: 4048-54. doi:
61. Kato GJ, Barrett J, Villa-Garcia M, Dang CV. An amino-terminal c-myc domain required for neoplastic transformation activates transcription. *Mol Cell Biol.* 1990; 10: 5914-20. doi:
62. Cowling VH, Chandriani S, Whitfield ML, Cole MD. A conserved Myc protein domain, MBIV, regulates DNA binding, apoptosis, transformation, and G2 arrest. *Mol Cell Biol.* 2006; 26: 4226-39. doi: 10.1128/mcb.01959-05.
63. Blackwell TK, Huang J, Ma A, Kretzner L, Alt FW, Eisenman RN, Weintraub H. Binding of myc proteins to canonical and noncanonical DNA sequences. *Mol Cell Biol.* 1993; 13: 5216-24. doi:
64. Rishi V, Vinson C. Dominant-negative mutants of helix-loop-helix proteins: transcriptional inhibition. *Methods Enzymol.* 2003; 370: 454-66. doi: 10.1016/s0076-6879(03)70039-1.
65. Liu X, Tesfai J, Evrard YA, Dent SY, Martinez E. c-Myc transformation domain recruits the human STAGA complex and requires TRRAP and GCN5 acetylase activity for transcription activation. *J Biol Chem.* 2003; 278: 20405-12. doi: 10.1074/jbc.M211795200.
66. Fladvad M, Zhou K, Moshref A, Pursglove S, Safsten P, Sunnerhagen M. N and C-terminal sub-regions in the c-Myc transactivation region and their joint role in creating versatility in folding and binding. *J Mol Biol.* 2005; 346: 175-89. doi: 10.1016/j.jmb.2004.11.029.

67. Rottmann S, Luscher B. The Mad side of the Max network: antagonizing the function of Myc and more. *Curr Top Microbiol Immunol.* 2006; 302: 63-122. doi:
68. Gupta S, Seth A, Davis RJ. Transactivation of gene expression by Myc is inhibited by mutation at the phosphorylation sites Thr-58 and Ser-62. *Proc Natl Acad Sci U S A.* 1993; 90: 3216-20. doi:
69. Sears RC. The life cycle of C-myc: from synthesis to degradation. *Cell Cycle.* 2004; 3: 1133-7. doi:
70. McMahon SB, Van Buskirk HA, Dugan KA, Copeland TD, Cole MD. The novel ATM-related protein TRRAP is an essential cofactor for the c-Myc and E2F oncoproteins. *Cell.* 1998; 94: 363-74. doi:
71. Gargano B, Amente S, Majello B, Lania L. P-TEFb is a crucial co-factor for Myc transactivation. *Cell Cycle.* 2007; 6: 2031-7. doi: 10.4161/cc.6.16.4554.
72. Wu SY, Lee AY, Lai HT, Zhang H, Chiang CM. Phospho switch triggers Brd4 chromatin binding and activator recruitment for gene-specific targeting. *Mol Cell.* 2013; 49: 843-57. doi: 10.1016/j.molcel.2012.12.006.
73. Kurland JF, Tansey WP. Myc-mediated transcriptional repression by recruitment of histone deacetylase. *Cancer Res.* 2008; 68: 3624-9. doi: 10.1158/0008-5472.can-07-6552.
74. Thomas LR, Wang Q, Grieb BC, Phan J, Foshage AM, Sun Q, Olejniczak ET, Clark T, Dey S, Lorey S, Alicie B, Howard GC, Cawthon B, et al. Interaction with WDR5 promotes target gene recognition and tumorigenesis by MYC. *Mol Cell.* 2015; 58: 440-52. doi: 10.1016/j.molcel.2015.02.028.
75. Chang TC, Yu D, Lee YS, Wentzel EA, Arking DE, West KM, Dang CV, Thomas-Tikhonenko A, Mendell JT. Widespread microRNA repression by Myc contributes to tumorigenesis. *Nat Genet.* 2008; 40: 43-50. doi: 10.1038/ng.2007.30.
76. Schneider A, Peukert K, Eilers M, Hanel F. Association of Myc with the zinc-finger protein Miz-1 defines a novel pathway for gene regulation by Myc. *Curr Top Microbiol Immunol.* 1997; 224: 137-46. doi:
77. Seoane J, Pouponnot C, Staller P, Schader M, Eilers M, Massague J. TGFbeta influences Myc, Miz-1 and Smad to control the CDK inhibitor p15INK4b. *Nat Cell Biol.* 2001; 3: 400-8. doi: 10.1038/35070086.
78. O'Donnell KA, Wentzel EA, Zeller KI, Dang CV, Mendell JT. c-Myc-regulated microRNAs modulate E2F1 expression. *Nature.* 2005; 435: 839-43. doi: 10.1038/nature03677.



79. Ribon V, Leff T, Saltiel AR. c-Myc does not require max for transcriptional activity in PC-12 cells. *Mol Cell Neurosci*. 1994; 5: 277-82. doi: 10.1006/mcne.1994.1032.
80. Steiger D, Furrer M, Schwinkendorf D, Gallant P. Max-independent functions of Myc in *Drosophila melanogaster*. *Nat Genet*. 2008; 40: 1084-91. doi: 10.1038/ng.178.
81. Schaefer IM, Wang Y, Liang CW, Bahri N, Quattrone A, Doyle L, Marino-Enriquez A, Lauria A, Zhu M, Debiec-Rychter M, Grunewald S, Hechtman JF, Dufresne A, et al. MAX inactivation is an early event in GIST development that regulates p16 and cell proliferation. *Nat Commun*. 2017; 8: 14674. doi: 10.1038/ncomms14674.
82. Romero OA, Torres-Diz M, Pros E, Savola S, Gomez A, Moran S, Saez C, Iwakawa R, Villanueva A, Montuenga LM, Kohno T, Yokota J, Sanchez-Céspedes M. MAX inactivation in small cell lung cancer disrupts MYC-SWI/SNF programs and is synthetic lethal with BRG1. *Cancer Discov*. 2014; 4: 292-303. doi: 10.1158/2159-8290.cd-13-0799.
83. Menssen A, Hermeking H. Characterization of the c-MYC-regulated transcriptome by SAGE: identification and analysis of c-MYC target genes. *Proc Natl Acad Sci U S A*. 2002; 99: 6274-9. doi: 10.1073/pnas.082005599.
84. Fernandez PC, Frank SR, Wang L, Schroeder M, Liu S, Greene J, Cocito A, Amati B. Genomic targets of the human c-Myc protein. *Genes Dev*. 2003; 17: 1115-29. doi: 10.1101/gad.1067003.
85. Chappell J, Dalton S. Roles for MYC in the establishment and maintenance of pluripotency. *Cold Spring Harb Perspect Med*. 2013; 3: a014381. doi: 10.1101/cshperspect.a014381.
86. Whitfield JR, Soucek L. Tumor microenvironment: becoming sick of Myc. *Cell Mol Life Sci*. 2012; 69: 931-4. doi: 10.1007/s00018-011-0860-x.
87. Casey SC, Baylot V, Felsher DW. MYC: Master Regulator of Immune Privilege. *Trends Immunol*. 2017; 38: 298-305. doi: 10.1016/j.it.2017.01.002.
88. Davis AC, Wims M, Spotts GD, Hann SR, Bradley A. A null c-myc mutation causes lethality before 10.5 days of gestation in homozygotes and reduced fertility in heterozygous female mice. *Genes Dev*. 1993; 7: 671-82. doi:
89. Mateyak MK, Obaya AJ, Adachi S, Sedivy JM. Phenotypes of c-Myc-deficient rat fibroblasts isolated by targeted homologous recombination. *Cell Growth Differ*. 1997; 8: 1039-48. doi:

90. Gabay M, Li Y, Felsher DW. MYC activation is a hallmark of cancer initiation and maintenance. *Cold Spring Harb Perspect Med.* 2014; 4. doi: 10.1101/cshperspect.a014241.
91. Pelengaris S, Littlewood T, Khan M, Elia G, Evan G. Reversible activation of c-Myc in skin: induction of a complex neoplastic phenotype by a single oncogenic lesion. *Mol Cell.* 1999; 3: 565-77. doi:
92. Shachaf CM, Kopelman AM, Arvanitis C, Karlsson A, Beer S, Mandl S, Bachmann MH, Borowsky AD, Ruebner B, Cardiff RD, Yang Q, Bishop JM, Contag CH, et al. MYC inactivation uncovers pluripotent differentiation and tumour dormancy in hepatocellular cancer. *Nature.* 2004; 431: 1112-7. doi: 10.1038/nature03043.
93. Felsher DW, Bishop JM. Reversible tumorigenesis by MYC in hematopoietic lineages. *Mol Cell.* 1999; 4: 199-207. doi:
94. Jain M, Arvanitis C, Chu K, Dewey W, Leonhardt E, Trinh M, Sundberg CD, Bishop JM, Felsher DW. Sustained loss of a neoplastic phenotype by brief inactivation of MYC. *Science.* 2002; 297: 102-4. doi: 10.1126/science.1071489.
95. Arvanitis C, Felsher DW. Conditionally MYC: insights from novel transgenic models. *Cancer Lett.* 2005; 226: 95-9. doi: 10.1016/j.canlet.2004.10.043.
96. Sharma SV, Settleman J. Oncogene addiction: setting the stage for molecularly targeted cancer therapy. *Genes Dev.* 2007; 21: 3214-31. doi: 10.1101/gad.1609907.
97. Jackson EL, Willis N, Mercer K, Bronson RT, Crowley D, Montoya R, Jacks T, Tuveson DA. Analysis of lung tumor initiation and progression using conditional expression of oncogenic K-ras. *Genes Dev.* 2001; 15: 3243-8. doi: 10.1101/gad.943001.
98. Soucek L, Nasi S, Evan GI. Omomyc expression in skin prevents Myc-induced papillomatosis. *Cell Death Differ.* 2004; 11: 1038-45. doi: 10.1038/sj.cdd.4401443.
99. Soucek L, Helmer-Citterich M, Sacco A, Jucker R, Cesareni G, Nasi S. Design and properties of a Myc derivative that efficiently homodimerizes. *Oncogene.* 1998; 17: 2463-72. doi: 10.1038/sj.onc.1202199.
100. Soucek L, Jucker R, Panacchia L, Ricordy R, Tato F, Nasi S. Omomyc, a potential Myc dominant negative, enhances Myc-induced apoptosis. *Cancer Res.* 2002; 62: 3507-10. doi:

101. Soucek L, Whitfield J, Martins CP, Finch AJ, Murphy DJ, Sodir NM, Karnezis AN, Swigart LB, Nasi S, Evan GI. Modelling Myc inhibition as a cancer therapy. *Nature*. 2008; 455: 679-83. doi: 10.1038/nature07260.
102. Soucek L, Whitfield JR, Sodir NM, Masso-Valles D, Serrano E, Karnezis AN, Swigart LB, Evan GI. Inhibition of Myc family proteins eradicates KRas-driven lung cancer in mice. *Genes Dev*. 2013; 27: 504-13. doi: 10.1101/gad.205542.112.
103. Ahuja D, Saenz-Robles MT, Pipas JM. SV40 large T antigen targets multiple cellular pathways to elicit cellular transformation. *Oncogene*. 2005; 24: 7729-45. doi: 10.1038/sj.onc.1209046.
104. Sodir NM, Swigart LB, Karnezis AN, Hanahan D, Evan GI, Soucek L. Endogenous Myc maintains the tumor microenvironment. *Genes Dev*. 2011; 25: 907-16. doi: 10.1101/gad.2038411.
105. Annibali D, Whitfield JR, Favuzzi E, Jauset T, Serrano E, Cuartas I, Redondo-Campos S, Folch G, Gonzalez-Junca A, Sodir NM, Masso-Valles D, Beaulieu ME, Swigart LB, et al. Myc inhibition is effective against glioma and reveals a role for Myc in proficient mitosis. *Nat Commun*. 2014; 5: 4632. doi: 10.1038/ncomms5632.
106. Galardi S, Savino M, Scagnoli F, Pellegatta S, Pisati F, Zambelli F, Illi B, Annibali D, Beji S, Orecchini E, Alberelli MA, Apicella C, Fontanella RA, et al. Resetting cancer stem cell regulatory nodes upon MYC inhibition. *EMBO Rep*. 2016; 17: 1872-89. doi: 10.15252/embr.201541489.
107. Yan C, Higgins PJ. Drugging the undruggable: transcription therapy for cancer. *Biochim Biophys Acta*. 2013; 1835: 76-85. doi: 10.1016/j.bbcan.2012.11.002.
108. Arkin MR, Tang Y, Wells JA. Small-molecule inhibitors of protein-protein interactions: progressing towards the reality. *Chem Biol*. 2014; 21: 1102-14. doi: 10.1016/j.chembiol.2014.09.001.
109. Whitfield JR, Beaulieu ME, Soucek L. Strategies to Inhibit Myc and Their Clinical Applicability. *Front Cell Dev Biol*. 2017; 5. doi: 10.3389/fcell.2017.00010.
110. Wu P, Ma DL, Leung CH, Yan SC, Zhu N, Abagyan R, Che CM. Stabilization of G-quadruplex DNA with platinum(II) Schiff base complexes: luminescent probe and down-regulation of c-myc oncogene expression. *Chemistry*. 2009; 15: 13008-21. doi: 10.1002/chem.200901943.
111. Brown RV, Danford FL, Gokhale V, Hurley LH, Brooks TA. Demonstration that drug-targeted down-regulation of MYC in non-Hodgkins lymphoma is directly mediated through the promoter G-quadruplex. *J Biol Chem*. 2011; 286: 41018-27. doi: 10.1074/jbc.M111.274720.

112. Prochownik EV, Kukowska J, Rodgers C. c-myc antisense transcripts accelerate differentiation and inhibit G1 progression in murine erythroleukemia cells. *Mol Cell Biol.* 1988; 8: 3683-95. doi:
113. Sklar MD, Thompson E, Welsh MJ, Liebert M, Harney J, Grossman HB, Smith M, Prochownik EV. Depletion of c-myc with specific antisense sequences reverses the transformed phenotype in ras oncogene-transformed NIH 3T3 cells. *Mol Cell Biol.* 1991; 11: 3699-710. doi:
114. Moreno PM, Pego AP. Therapeutic antisense oligonucleotides against cancer: hurdling to the clinic. *Front Chem.* 2014; 2: 87. doi: 10.3389/fchem.2014.00087.
115. Wang H, Mannava S, Grachtchouk V, Zhuang D, Soengas MS, Gudkov AV, Prochownik EV, Nikiforov MA. c-Myc depletion inhibits proliferation of human tumor cells at various stages of the cell cycle. *Oncogene.* 2008; 27: 1905-15. doi: 10.1038/sj.onc.1210823.
116. Fukuhara H, Ino Y, Todo T. Oncolytic virus therapy: A new era of cancer treatment at dawn. *Cancer Sci.* 2016; 107: 1373-9. doi: 10.1111/cas.13027.
117. Li Y, Zhang B, Zhang H, Zhu X, Feng D, Zhang D, Zhuo B, Li L, Zheng J. Oncolytic adenovirus armed with shRNA targeting MYCN gene inhibits neuroblastoma cell proliferation and in vivo xenograft tumor growth. *J Cancer Res Clin Oncol.* 2013; 139: 933-41. doi: 10.1007/s00432-013-1406-4.
118. Fletcher S, Prochownik EV. Small-Molecule Inhibitors of the Myc Oncoprotein. *Biochim Biophys Acta.* 2015; 1849: 525-43. doi: 10.1016/j.bbagr.2014.03.005.
119. Delmore JE, Issa GC, Lemieux ME, Rahl PB, Shi J, Jacobs HM, Kastiris E, Gilpatrick T, Paranal RM, Qi J, Chesi M, Schinzel A, McKeown MR, et al. BET bromodomain inhibition as a therapeutic strategy to target c-Myc. *Cell.* 2011; 146: 904-17. doi: 10.1016/j.cell.2011.08.017.
120. Mertz JA, Conery AR, Bryant BM, Sandy P, Balasubramanian S, Mele DA, Bergeron L, Sims RJ. Targeting MYC dependence in cancer by inhibiting BET bromodomains. *Proc Natl Acad Sci U S A.* 2011; 108: 16669-74. doi: 10.1073/pnas.1108190108.
121. Lockwood WW, Zejnullahu K, Bradner JE, Varmus H. Sensitivity of human lung adenocarcinoma cell lines to targeted inhibition of BET epigenetic signaling proteins. *Proc Natl Acad Sci U S A.* 2012; 109: 19408-13. doi: 10.1073/pnas.1216363109.
122. Sahai V, Kumar K, Knab LM, Chow CR, Raza SS, Bentrem DJ, Ebine K, Munshi HG. BET bromodomain inhibitors block growth of pancreatic cancer

- cells in three-dimensional collagen. *Mol Cancer Ther.* 2014; 13: 1907-17. doi: 10.1158/1535-7163.mct-13-0925.
123. Baker EK, Taylor S, Gupte A, Sharp PP, Walia M, Walsh NC, Zannettino ACW, Chalk AM, Burns CJ, Walkley CR. BET inhibitors induce apoptosis through a MYC independent mechanism and synergise with CDK inhibitors to kill osteosarcoma cells. *Sci Rep.* 2015; 5. doi: 10.1038/srep10120.
124. Ambrosini G, Sawle AD, Musi E, Schwartz GK. BRD4-targeted therapy induces Myc-independent cytotoxicity in Gnaq/11-mutant uveal melanoma cells. *Oncotarget.* 2015; 6: 33397-409. doi: 10.18632/oncotarget.5179.
125. Hogg SJ, Vervoort SJ, Deswal S, Ott CJ, Li J, Cluse LA, Beavis PA, Darcy PK, Martin BP, Spencer A, Traunbauer AK, Sadovnik I, Bauer K, et al. BET-Bromodomain Inhibitors Engage the Host Immune System and Regulate Expression of the Immune Checkpoint Ligand PD-L1. *Cell Rep.* 2017; 18: 2162-74. doi: 10.1016/j.celrep.2017.02.011.
126. Yao W, Yue P, Khuri FR, Sun SY. The BET bromodomain inhibitor, JQ1, facilitates c-FLIP degradation and enhances TRAIL-induced apoptosis independent of BRD4 and c-Myc inhibition. *Oncotarget.* 2015; 6: 34669-79. doi:
127. Bid HK, Phelps DA, Xiaio L, Guttridge DC, Lin J, London C, Baker LH, Mo X, Houghton PJ. The Bromodomain BET inhibitor JQ1 Suppresses Tumor Angiogenesis in Models of Childhood Sarcoma. *Mol Cancer Ther.* 2016; 15: 1018-28. doi: 10.1158/1535-7163.mct-15-0567.
128. Andrieu G, Belkina AC, Denis GV. Clinical trials for BET inhibitors run ahead of the science. *Drug Discov Today Technol.* 2016; 19: 45-50. doi: 10.1016/j.ddtec.2016.06.004.
129. Kwiatkowski N, Zhang T, Rahl PB, Abraham BJ, Reddy J, Ficarro SB, Dastur A, Amzallag A, Ramaswamy S, Tesar B, Jenkins CE, Hannett NM, McMillin D, et al. Targeting transcription regulation in cancer with a covalent CDK7 inhibitor. *Nature.* 2014; 511: 616-20. doi: 10.1038/nature13393.
130. Onuma K, Aga Y, Ogi S, Matsushita T, Sunamoto H, Ogawa A, Tokunaga Y, Ushiyama S. Preclinical in vitro and in vivo study of UD-017, a novel highly selective and orally available CDK7 inhibitor, in a variety of cancers. *Journal of Clinical Oncology.* 2017; 35: e14086-e. doi: 10.1200/JCO.2017.35.15\_suppl.e14086.
131. Cayrol F, Praditsuktavorn P, Fernando TM, Kwiatkowski N, Marullo R, Calvo-Vidal MN, Phillip J, Pera B, Yang SN, Takpradit K, Roman L, Gaudiano M, Crescenzo R, et al. THZ1 targeting CDK7 suppresses STAT transcriptional

activity and sensitizes T-cell lymphomas to BCL2 inhibitors. *Nature Communications*. 2017; 8: 14290. doi: 10.1038/ncomms14290.

132. Chesler L, Schlieve C, Goldenberg DD, Kenney A, Kim G, McMillan A, Matthay KK, Rowitch D, Weiss WA. Inhibition of Phosphatidylinositol 3-Kinase Destabilizes Mycn Protein and Blocks Malignant Progression in Neuroblastoma. *Cancer Res*. 2006; 66: 8139-46. doi: 10.1158/0008-5472.can-05-2769.

133. Roohi A, Hojjat-Farsangi M. Recent advances in targeting mTOR signaling pathway using small molecule inhibitors. *J Drug Target*. 2017; 25: 189-201. doi: 10.1080/1061186x.2016.1236112.

134. Wiegering A, Uthe FW, Jamieson T, Ruoss Y, Huttenrauch M, Kuspert M, Pfann C, Nixon C, Herold S, Walz S, Taranets L, Germer CT, Rosenwald A, et al. Targeting Translation Initiation Bypasses Signaling Crosstalk Mechanisms That Maintain High MYC Levels in Colorectal Cancer. *Cancer Discov*. 2015; 5: 768-81. doi: 10.1158/2159-8290.cd-14-1040.

135. Sun K, Atoyan R, Borek MA, Dellarocca S, Samson ME, Ma AW, Xu GX, Patterson T, Tuck DP, Viner JL, Fattaey A, Wang J. Dual HDAC and PI3K Inhibitor CUDC-907 Downregulates MYC and Suppresses Growth of MYC-dependent Cancers. *Mol Cancer Ther*. 2017; 16: 285-99. doi: 10.1158/1535-7163.mct-16-0390.

136. Oki Y, Kelly KR, Flinn I, Patel MR, Gharavi R, Ma A, Parker J, Hafeez A, Tuck D, Younes A. CUDC-907 in relapsed/refractory diffuse large B-cell lymphoma, including patients with MYC-alterations: results from an expanded phase I trial. *Haematologica*. 2017; 102: 1923-30. doi: 10.3324/haematol.2017.172882.

137. Sun XX, Sears RC, Dai MS. Deubiquitinating c-Myc: USP36 steps up in the nucleolus. *Cell Cycle*. 2015; 14: 3786-93. doi: 10.1080/15384101.2015.1093713.

138. Huang HL, Weng HY, Wang LQ, Yu CH, Huang QJ, Zhao PP, Wen JZ, Zhou H, Qu LH. Triggering Fbw7-mediated proteasomal degradation of c-Myc by oridonin induces cell growth inhibition and apoptosis. *Mol Cancer Ther*. 2012; 11: 1155-65. doi: 10.1158/1535-7163.mct-12-0066.

139. Marqus S, Pirogova E, Piva TJ. Evaluation of the use of therapeutic peptides for cancer treatment. *J Biomed Sci*. 2017; 24: 21. doi: 10.1186/s12929-017-0328-x.

140. Blanco-Miguez A, Gutierrez-Jacome A, Perez-Perez M, Perez-Rodriguez G, Catalan-Garcia S, Fdez-Riverola F, Lourenco A, Sanchez B. From amino acid sequence to bioactivity: The biomedical potential of antitumor peptides. *Protein Sci*. 2016; 25: 1084-95. doi: 10.1002/pro.2927.

141. Draeger LJ, Mullen GP. Interaction of the bHLH-zip domain of c-Myc with H1-type peptides. Characterization of helicity in the H1 peptides by NMR. *J Biol Chem.* 1994; 269: 1785-93. doi:
142. Blackwell TK, Kretzner L, Blackwood EM, Eisenman RN, Weintraub H. Sequence-specific DNA binding by the c-Myc protein. *Science.* 1990; 250: 1149-51. doi:
143. Derossi D, Joliot AH, Chassaing G, Prochiantz A. The third helix of the Antennapedia homeodomain translocates through biological membranes. *J Biol Chem.* 1994; 269: 10444-50. doi:
144. Giorello L, Clerico L, Pescarolo MP, Vikhanskaya F, Salmona M, Colella G, Bruno S, Mancuso T, Bagnasco L, Russo P, Parodi S. Inhibition of cancer cell growth and c-Myc transcriptional activity by a c-Myc helix 1-type peptide fused to an internalization sequence. *Cancer Res.* 1998; 58: 3654-9. doi:
145. Bidwell GL, Davis AN, Raucher D. Targeting a c-Myc inhibitory polypeptide to specific intracellular compartments using cell penetrating peptides. *Journal of Controlled Release.* 2009; 135: 2-10. doi: <https://doi.org/10.1016/j.jconrel.2008.11.015>.
146. Li L, Sun W, Zhang Z, Huang Y. Time-staggered delivery of docetaxel and H1-S6A,F8A peptide for sequential dual-strike chemotherapy through tumor priming and nuclear targeting. *Journal of Controlled Release.* 2016; 232: 62-74. doi: <https://doi.org/10.1016/j.jconrel.2016.04.021>.
147. Bidwell GL, 3rd, Perkins E, Hughes J, Khan M, James JR, Raucher D. Thermally targeted delivery of a c-Myc inhibitory polypeptide inhibits tumor progression and extends survival in a rat glioma model. *PLoS One.* 2013; 8: e55104. doi: 10.1371/journal.pone.0055104.
148. Montagne M, Beaudoin N, Fortin D, Lavoie CL, Klinck R, Lavigne P. The Max b-HLH-LZ can transduce into cells and inhibit c-Myc transcriptional activities. *PLoS One.* 2012; 7: e32172. doi: 10.1371/journal.pone.0032172.
149. Jouaux EM, Schmidtkunz K, Muller KM, Arndt KM. Targeting the c-Myc coiled coil with interfering peptides. *J Pept Sci.* 2008; 14: 1022-31. doi: 10.1002/psc.1038.
150. Lustig LC, Dingar D, Tu WB, Lourenco C, Kalkat M, Inamoto I, Ponzielli R, Chan WCW, Shin JA, Penn LZ. Inhibiting MYC binding to the E-box DNA motif by ME47 decreases tumour xenograft growth. *Oncogene.* 2017; 36: 6830-7. doi: 10.1038/onc.2017.275.
151. Hurst HC. Transcription factors 1: bZIP proteins. *Protein Profile.* 1995; 2: 101-68. doi:

152. Landschulz WH, Johnson PF, McKnight SL. The leucine zipper: a hypothetical structure common to a new class of DNA binding proteins. *Science*. 1988; 240: 1759-64. doi:
153. Lavigne P, Kondejewski LH, Houston ME, Jr., Sonnichsen FD, Lix B, Skyes BD, Hodges RS, Kay CM. Preferential heterodimeric parallel coiled-coil formation by synthetic Max and c-Myc leucine zippers: a description of putative electrostatic interactions responsible for the specificity of heterodimerization. *J Mol Biol*. 1995; 254: 505-20. doi:
154. Lavigne P, Crump MP, Gagne SM, Hodges RS, Kay CM, Sykes BD. Insights into the mechanism of heterodimerization from the 1H-NMR solution structure of the c-Myc-Max heterodimeric leucine zipper. *J Mol Biol*. 1998; 281: 165-81. doi: 10.1006/jmbi.1998.1914.
155. Guo J, Li T, Schipper J, Nilson KA, Fordjour FK, Cooper JJ, Gordan R, Price DH. Sequence specificity incompletely defines the genome-wide occupancy of Myc. *Genome Biol*. 2014; 15: 482. doi: 10.1186/s13059-014-0482-3.
156. Sauve S, Naud JF, Lavigne P. The mechanism of discrimination between cognate and non-specific DNA by dimeric b/HLH/LZ transcription factors. *J Mol Biol*. 2007; 365: 1163-75. doi: 10.1016/j.jmb.2006.10.044.
157. Ferre-D'Amare AR, Prendergast GC, Ziff EB, Burley SK. Recognition by Max of its cognate DNA through a dimeric b/HLH/Z domain. *Nature*. 1993; 363: 38-45. doi: 10.1038/363038a0.
158. Savino M, Annibali D, Carucci N, Favuzzi E, Cole MD, Evan GI, Soucek L, Nasi S. The action mechanism of the Myc inhibitor termed Omomyc may give clues on how to target Myc for cancer therapy. *PLoS One*. 2011; 6: e22284. doi: 10.1371/journal.pone.0022284.
159. Fiorentino FP, Tokgün E, Solé-Sánchez S, Giampaolo S, Tokgün O, Jauset T, Kohno T, Perucho M, Soucek L, Yokota J. Growth suppression by MYC inhibition in small cell lung cancer cells with TP53 and RB1 inactivation. *Oncotarget*. 2016; 7: 31014-28. doi: 10.18632/oncotarget.8826.
160. Jung LA, Gebhardt A, Koelmel W, Ade CP, Walz S, Kuper J, von Eyss B, Letschert S, Redel C, d'Artista L, Biankin A, Zender L, Sauer M, et al. OmoMYC blunts promoter invasion by oncogenic MYC to inhibit gene expression characteristic of MYC-dependent tumors. *Oncogene*. 2017; 36: 1911-24. doi: 10.1038/onc.2016.354.
161. von Eyss B, Eilers M. Addicted to Myc—but why? *Genes Dev*. 2011; 25: 895-7. doi: 10.1101/gad.2053311.



162. Fosgerau K, Hoffmann T. Peptide therapeutics: current status and future directions. *Drug Discovery Today*. 2015; 20: 122-8. doi: <https://doi.org/10.1016/j.drudis.2014.10.003>.
163. Morris MC, Depollier J, Mery J, Heitz F, Divita G. A peptide carrier for the delivery of biologically active proteins into mammalian cells. *Nat Biotechnol*. 2001; 19: 1173-6. doi: 10.1038/nbt1201-1173.
164. Patel LN, Wang J, Kim KJ, Borok Z, Crandall E, Shen WC. Conjugation with Cationic Cell-Penetrating Peptide Increases Pulmonary Absorption of Insulin. *Mol Pharm*. 2009; 6: 492-503. doi: 10.1021/mp800174g.
165. Kristensen M, Birch D, Mørck Nielsen H. Applications and Challenges for Use of Cell-Penetrating Peptides as Delivery Vectors for Peptide and Protein Cargos. *Int J Mol Sci*. 2016; 17. doi: 10.3390/ijms17020185.
166. Suhorutsenko J, Eriste E, Copolovici D-M, Langel Ü. Human Protein 53-Derived Cell-Penetrating Peptides. *International Journal of Peptide Research and Therapeutics*. 2012; 18: 291-7. doi: 10.1007/s10989-012-9302-3.
167. Meloni BP, Craig AJ, Milech N, Hopkins RM, Watt PM, Knuckey NW. The neuroprotective efficacy of cell-penetrating peptides TAT, penetratin, Arg-9, and Pep-1 in glutamic acid, kainic acid, and in vitro ischemia injury models using primary cortical neuronal cultures. *Cell Mol Neurobiol*. 2014; 34: 173-81. doi: 10.1007/s10571-013-9999-3.
168. Snyder EL, Meade BR, Saenz CC, Dowdy SF. Treatment of terminal peritoneal carcinomatosis by a transducible p53-activating peptide. *PLoS Biol*. 2004; 2: E36. doi: 10.1371/journal.pbio.0020036.
169. Meyer-Losic F, Nicolazzi C, Quinonero J, Ribes F, Michel M, Dubois V, de Coupade C, Boukaissi M, Chene AS, Tranchant I, Arranz V, Zoubaa I, Fruchart JS, et al. DTS-108, a novel peptidic prodrug of SN38: in vivo efficacy and toxicokinetic studies. *Clin Cancer Res*. 2008; 14: 2145-53. doi: 10.1158/1078-0432.ccr-07-4580.
170. Michiue H, Eguchi A, Scadeng M, Dowdy SF. Induction of in vivo synthetic lethal RNAi responses to treat glioblastoma. *Cancer Biol Ther*. 2009; 8: 2306-13. doi:
171. Guidotti G, Brambilla L, Rossi D. Cell-Penetrating Peptides: From Basic Research to Clinics. *Trends Pharmacol Sci*. 2017; 38: 406-24. doi: 10.1016/j.tips.2017.01.003.
172. Jia L, Gorman GS, Coward LU, Noker PE, McCormick D, Horn TL, Harder JB, Muzzio M, Prabhakar B, Ganesh B, Das Gupta TK, Beattie CW. Preclinical pharmacokinetics, metabolism, and toxicity of azurin-p28

- (NSC745104) a peptide inhibitor of p53 ubiquitination. *Cancer Chemother Pharmacol.* 2011; 68: 513-24. doi: 10.1007/s00280-010-1518-3.
173. Warso MA, Richards JM, Mehta D, Christov K, Schaeffer C, Rae Bressler L, Yamada T, Majumdar D, Kennedy SA, Beattie CW, Das Gupta TK. A first-in-class, first-in-human, phase I trial of p28, a non-HDM2-mediated peptide inhibitor of p53 ubiquitination in patients with advanced solid tumours. *Br J Cancer.* 2013; 108: 1061-70. doi: 10.1038/bjc.2013.74.
174. Pisal DS, Kosloski MP, Balu-Iyer SV. DELIVERY OF THERAPEUTIC PROTEINS. *J Pharm Sci.* 2010; 99: 2557-75. doi: 10.1002/jps.22054.
175. Adjei IM, Sharma B, Labhasetwar V. Nanoparticles: cellular uptake and cytotoxicity. *Adv Exp Med Biol.* 2014; 811: 73-91. doi: 10.1007/978-94-017-8739-0\_5.
176. Chazov EI, Mazaev AV, Torchilin VP, Smirnov VN. [Use of immobilized enzymes in clinical practice]. *Klin Med (Mosk).* 1980; 58: 51-5. doi:
177. Kim A, Yun MO, Oh YK, Ahn WS, Kim CK. Pharmacodynamics of insulin in polyethylene glycol-coated liposomes. *Int J Pharm.* 1999; 180: 75-81. doi:
178. Kanaoka E, Takahashi K, Yoshikawa T, Jizomoto H, Nishihara Y, Hirano K. A novel and simple type of liposome carrier for recombinant interleukin-2. *J Pharm Pharmacol.* 2001; 53: 295-302. doi:
179. Li H, Song JH, Park JS, Han K. Polyethylene glycol-coated liposomes for oral delivery of recombinant human epidermal growth factor. *Int J Pharm.* 2003; 258: 11-9. doi:
180. van Slooten ML, Storm G, Zoephel A, Kupcu Z, Boerman O, Crommelin DJ, Wagner E, Kircheis R. Liposomes containing interferon-gamma as adjuvant in tumor cell vaccines. *Pharm Res.* 2000; 17: 42-8. doi:
181. Israelachvili JN, Marcelja S, Horn RG. Physical principles of membrane organization. *Q Rev Biophys.* 1980; 13: 121-200. doi:
182. Iwanaga K, Ono S, Narioka K, Kakemi M, Morimoto K, Yamashita S, Namba Y, Oku N. Application of surface-coated liposomes for oral delivery of peptide: effects of coating the liposome's surface on the GI transit of insulin. *J Pharm Sci.* 1999; 88: 248-52. doi: 10.1021/js980235x.
183. Park JW, Kirpotin DB, Hong K, Shalaby R, Shao Y, Nielsen UB, Marks JD, Papahadjopoulos D, Benz CC. Tumor targeting using anti-her2 immunoliposomes. *J Control Release.* 2001; 74: 95-113. doi:
184. Ishida O, Maruyama K, Tanahashi H, Iwatsuru M, Sasaki K, Eriguchi M, Yanagie H. Liposomes bearing polyethyleneglycol-coupled transferrin

with intracellular targeting property to the solid tumors in vivo. *Pharm Res.* 2001; 18: 1042-8. doi:

185. Vaupel P, Kallinowski F, Okunieff P. Blood flow, oxygen and nutrient supply, and metabolic microenvironment of human tumors: a review. *Cancer Res.* 1989; 49: 6449-65. doi:

186. Drummond DC, Zignani M, Leroux J. Current status of pH-sensitive liposomes in drug delivery. *Prog Lipid Res.* 2000; 39: 409-60. doi:

187. Hafez IM, Ansell S, Cullis PR. Tunable pH-sensitive liposomes composed of mixtures of cationic and anionic lipids. *Biophysical Journal.* 2000; 79: 1438-46. doi:

188. Harrington KJ, Lewanski CR, Northcote AD, Whittaker J, Wellbank H, Vile RG, Peters AM, Stewart JS. Phase I-II study of pegylated liposomal cisplatin (SPI-077) in patients with inoperable head and neck cancer. *Ann Oncol.* 2001; 12: 493-6. doi:

189. Bandak S, Goren D, Horowitz A, Tzemach D, Gabizon A. Pharmacological studies of cisplatin encapsulated in long-circulating liposomes in mouse tumor models. *Anticancer Drugs.* 1999; 10: 911-20. doi:

190. Carvalho Junior AD, Vieira FP, Melo VJ, Lopes MT, Silveira JN, Ramaldes GA, Garnier-Suillerot A, Pereira-Maia EC, Oliveira MC. Preparation and cytotoxicity of cisplatin-containing liposomes. *Braz J Med Biol Res.* 2007; 40: 1149-57. doi:

191. Leite EA, Giuberti Cdos S, Wainstein AJ, Wainstein AP, Coelho LG, Lana AM, Savassi-Rocha PR, De Oliveira MC. Acute toxicity of long-circulating and pH-sensitive liposomes containing cisplatin in mice after intraperitoneal administration. *Life Sci.* 2009; 84: 641-9. doi: 10.1016/j.lfs.2009.02.002.

192. Fortin-Ripoche JP, Martina MS, Gazeau F, Menager C, Wilhelm C, Bacri JC, Lesieur S, Clement O. Magnetic targeting of magnetoliposomes to solid tumors with MR imaging monitoring in mice: feasibility. *Radiology.* 2006; 239: 415-24. doi: 10.1148/radiol.2392042110.

193. Barenholz Y. Doxil(R)--the first FDA-approved nano-drug: lessons learned. *J Control Release.* 2012; 160: 117-34. doi: 10.1016/j.jconrel.2012.03.020.

194. McDuff FO, Naud JF, Montagne M, Sauve S, Lavigne P. The Max homodimeric b-HLH-LZ significantly interferes with the specific heterodimerization between the c-Myc and Max b-HLH-LZ in absence of DNA: a quantitative analysis. *J Mol Recognit.* 2009; 22: 261-9. doi: 10.1002/jmr.938.

195. Pattni BS, Chupin VV, Torchilin VP. New Developments in Liposomal Drug Delivery. *Chem Rev.* 2015; 115: 10938-66. doi: 10.1021/acs.chemrev.5b00046.
196. Nagamachi Y, Tani M, Shimizu K, Tsuda H, Niitsu Y, Yokota J. Orthotopic growth and metastasis of human non-small cell lung carcinoma cell injected into the pleural cavity of nude mice. *Cancer Lett.* 1998; 127: 203-9. doi:
197. Fukazawa T, Maeda Y, Matsuoka J, Yamatsuji T, Shigemitsu K, Morita I, Faiola F, Durbin ML, Soucek L, Naomoto Y. Inhibition of Myc effectively targets KRAS mutation-positive lung cancer expressing high levels of Myc. *Anticancer Res.* 2010; 30: 4193-200. doi:
198. Gao W, Wang M, Wang L, Lu H, Wu S, Dai B, Ou Z, Zhang L, Heymach JV, Gold KA, Minna J, Roth JA, Hofstetter WL, et al. Selective Antitumor Activity of Ibrutinib in EGFR-Mutant Non-Small Cell Lung Cancer Cells. *JNCI Journal of the National Cancer Institute.* 2014; 106: dju204. doi: 10.1093/jnci/dju204.
199. Carver LA, Schnitzer JE. Caveolae: mining little caves for new cancer targets. *Nat Rev Cancer.* 2003; 3: 571-81. doi: 10.1038/nrc1146.
200. Reilly MJ, Larsen JD, Sullivan MO. Polyplexes traffic through caveolae to the Golgi and endoplasmic reticulum en route to the nucleus. *Mol Pharm.* 2012; 9: 1280-90. doi: 10.1021/mp200583d.
201. Lonn P, Kacsinta AD, Cui XS, Hamil AS, Kaulich M, Gogoi K, Dowdy SF. Enhancing Endosomal Escape for Intracellular Delivery of Macromolecular Biologic Therapeutics. *Sci Rep.* 2016; 6: 32301. doi: 10.1038/srep32301.
202. Das SK, Menezes ME, Bhatia S, Wang X-Y, Emdad L, Sarkar D, Fisher PB. Gene Therapies for Cancer: Strategies, Challenges and Successes. *Journal of cellular physiology.* 2015; 230: 259-71. doi: 10.1002/jcp.24791.
203. Youn H, Chung JK. Modified mRNA as an alternative to plasmid DNA (pDNA) for transcript replacement and vaccination therapy. *Expert Opin Biol Ther.* 2015; 15: 1337-48. doi: 10.1517/14712598.2015.1057563.
204. Kormann MS, Hasenpusch G, Aneja MK, Nica G, Flemmer AW, Herber-Jonat S, Huppmann M, Mays LE, Illenyi M, Schams A, Griese M, Bittmann I, Handgretinger R, et al. Expression of therapeutic proteins after delivery of chemically modified mRNA in mice. *Nat Biotechnol.* 2011; 29: 154-7. doi: 10.1038/nbt.1733.
205. Kranz LM, Diken M, Haas H, Kreiter S, Loquai C, Reuter KC, Meng M, Fritz D, Vascotto F, Hefesha H, Grunwitz C, Vormehr M, Husemann Y, et al. Systemic RNA delivery to dendritic cells exploits antiviral defence for cancer immunotherapy. *Nature.* 2016; 534: 396-401. doi: 10.1038/nature18300.



---